PHASE NOISE REDUCTION IN A MULTIPHASE OSCILLATOR

by

Antonie Craig Alberts

Submitted in partial fulfilment of the requirements for the degree

Master of Engineering (Microelectronic Engineering)

in the

Department of Electrical, Electronic and Computer Engineering
Faculty of Engineering, Built Environment and Information Technology

UNIVERSITY OF PRETORIA

August 2017

SUMMARY

PHASE NOISE REDUCTION IN A MULTIPHASE OSCILLATOR

by

Antonie Craig Alberts

Promoter: Prof. S. Sinha

Department: Electrical, Electronic and Computer Engineering

University: University of Pretoria

Degree: Master of Engineering (Microelectronic Engineering)

Keywords: SiGe, voltage-controlled oscillator, multiphase oscillator, phase noise, phase noise reduction, passive sub-harmonic mixer.

Oscillators are ubiquitous to radio frequency circuits, where frequency translations and channel selection play a central role in the analogue communications channel. Oscillators also form part of digital systems as a time reference. Typical heterodyne receivers require an intermediate frequency channel. The associated oscillators and variable filters can only be centred perfectly at a single frequency, and degrade performance at the boundaries of the channel. These circuits also require image-rejecting filters and phase-locked loops in order to enable down-conversion. The penalties for these components are increased circuit area and power consumption. A direct down-conversion circuit will reduce the number of components in the system. A requirement added by the structural change is a passive sub-harmonic mixer. Quadrature oscillators may be achieved by cross-coupling two nominally identical *LC* differential voltage-controlled oscillators. Because of the widespread use of voltage-controlled oscillators in wireless communication systems, the development of comprehensive nonlinear analysis is pertinent in theory and applications. A key characteristic that defines the performance of an oscillator is the phase noise measurement. The voltage-controlled oscillator is also a key component in phase-locked loops, as it contributes to most of the out-of-band phase noise, as well as a significant portion of in-band noise. Current state-of-the-art modulation techniques, implemented at 60 GHz, such as quadrature amplitude modulation, and orthogonal frequency domain multiplexing,

require phase noise specifications superior to 90 dBc/Hz at a 1 MHz offset. It has been shown that owing to the timing of the current injection, the Colpitts oscillator tends to outperform other oscillator structures in terms of phase noise performance. The Colpitts oscillator has a major flaw in that the start-up gain must be relatively high in comparison to the cross-coupled oscillator. The oscillation amplitude cannot be extended as in the cross-coupled case. The oscillator's bias current generally limits the oscillation amplitude. The phase noise is defined by a stochastic differential equation, which can be used to predict the system's phase noise performance. The characteristics of the oscillator can then be defined using the trajectory. The model projects the noise components of the oscillator onto the trajectory, and then translates the noise into the resulting phase and amplitude shift. The phase noise performance of an oscillator may be improved by altering the shape of the trajectory. The trajectory of the oscillator is separated into slow and fast transients. Improving the shape of the oscillator's slow manifold may improve its phase noise performance, and improving the loaded quality factor of the tank circuit may be shown to directly improve upon close-in phase noise.

The approach followed describes oscillator behaviour from a circuit-level analysis. The derived equations do not have a closed form solution, but are reformulated using harmonic balance techniques to yield approximate solutions. The results from this closed form approximation are very close to both the numerical solutions of the differential equations, as well as the Simulation Program with Integrated Circuit Emphasis solutions for the same circuits. The derived equations are able to predict the amplitude and frequency in the single-phase example accurately, and are extended to provide a numerical platform for defining the amplitude and frequency of a multiphase oscillator. The analysis identifies various circuit components that influence the oscillator's phase noise performance. A circuit-level modification is then identified, enabling the decoupling of some of the factors and their interactions. This study demonstrates that the phase noise performance of a Colpitts oscillator may be significantly improved by making the proposed changes to the oscillator. The oscillator's figure of merit is improved even further. When a given oscillator is set at its optimum phase noise level, the collector current will account for approximately 85% of the phase noise; with the approach in this work, the average collector current is reduced and phase noise performance is improved. The key focus of the work was to identify circuit level changes to an oscillator's structure that could be improved or changed to achieve better phase noise performance. The objective was not to improve passive components, but rather to identify how the noise-to-phase noise transfer function could be improved. The

work successfully determines what can be altered in an oscillator that will yield improved phase noise performance by altering the phase noise transfer function. The concept is introduced on a differential oscillator and then extended to the multiphase oscillator. The impulse sensitivity function of the modified multiphase oscillator is improved by altering the typical feedback structure of the oscillator. The multiphase oscillator in this work is improved from -106 dBc/Hz to -113 dBc/Hz when considering the phase noise contribution from the tank circuits' bias current alone. This is achieved by uniquely altering the feedback method of the oscillator. This change alters the noise-to-phase noise properties of the oscillator, reducing phase noise. The improvement in the phase noise does not account for further improvements the modification would incorporate in the oscillator's limit cycle. For a given tank circuit, supply current and voltage, compared to an optimised Colpitts oscillator, the modifications to the feedback structure proposed in this work would further improve the figure of merit by 9 dB. This is not considering the change in the power consumption, which would yield a further improvement in the figure of merit by 7 dB. This is achieved by relaxing the required start-up current of the oscillator and effecting an improvement in the impulse sensitivity function. Future research could include further modelling of the phase shift in the feedback network, including the transmission lines in the feedback networks using the harmonic balance technique in a numerical form. The feedback technique can also be modified to be applicable to single and differential oscillators.

ACKNOWLEDGEMENTS

The author would like thank some of the people who were involved during the research phase leading to the completion of this dissertation.

- my supervisor, Professor Saurabh Sinha, for his support and availability during the entire process;
- SAAB Electronic Defence Systems, for enabling the measurements relating to this work;
- the National Research Foundation and The Department of Science and Technology, South Africa, for funding:
    - NRF funding was granted for measurement equipment – a millimetre-wave vector network analyser (under grant ID: 72321) and wafer-prober (under grant ID: 78580); and
    - NRF funding (under grant ID: 72321) also allowed collaboration with Professor Luca Larcher from Università degli studi di Modena e Reggio Emilia, Italy;
- the MOSIS Educational Program, for prototyping; and
- GEW Technologies (Pty) Ltd (previously known as Grintek Ewation) for partial sponsorship/studentship.

LIST OF ABBREVIATIONS

AC	Alternating current
ADE	Analogue design environment
CMOS	Complementary metal oxide semiconductor
DC	Direct current
DRC	Design rule check
EDA	Electronic design automation
EDS	Electronic defence systems
FoM	Figure of merit
GDS	Graphic data system
IBM	International business machines
IC	Integrated circuit
IF	Intermediate frequency
ISF	Impulse sensitivity function
LTI	Linear time invariant
LO	Local oscillator
LVS	Layout versus schematic
mm-wave	Millimetre-wave
NLTV	Non-linear time variant
NMF	Noise modulation function
NRF	National Research Foundation
MOS	Metal oxide semiconductor
MPW	Multi-project wafer
PCB	Printed circuit board
PDF	Probability density function

PSHM	Passive sub-harmonic mixer
MOSIS	Metal Oxide Semiconductor Implementation Service
MPF	Multi-project wafer
QVCO	Quadrature voltage-controlled oscillator
VCO	Voltage-controlled oscillator
Zero-IF	Zero intermediate frequency

TABLE OF CONTENTS

CHAPTER 1 INTRODUCTION

1.1 CHAPTER OVERVIEW

This dissertation investigates the possibility of improving the current state-of-the-art multiphase oscillators. This chapter outlines the background to the research and develops the research question. The work is justified through relevant objectives, which are outlined in order to define and defend the study's contribution to the existing body of knowledge.

1.1.1 Background to the research

In order to create a communication channel in the millimetre-wave (mm-wave) range successfully, certain foundation blocks are required. These include voltage-controlled oscillators (VCOs), mixers, buffers, and filters. The down-conversion of information in the band from 57-63 GHz is possible using a zero-intermediate frequency (zero-IF) receiver. Problems typically associated with a zero-IF receiver are the wandering and fixed direct current (DC) offsets that occur in the demodulation channel. These offsets tend to saturate filters in the down-conversion path, and prevent the successful implementation of zero-IF receivers. A solution to the wandering DC offsets is to use a passive sub-harmonic mixer (PSHM) that does not require a DC current, and that will not induce DC offsets.

The PSHM requires a four-phase oscillator to enable mixing. The larger the voltage swing, the greater the conversion efficiency. The oscillator's phase noise will directly influence the noise floor of the system, and specific phase noise requirements will be application-dependent. The goal of the research is to generate a four-phase oscillator capable of driving a PSHM, and improve its phase noise performance when compared to a current state-of-the-art configuration. The vector summation of the currents in the different tank circuits of the four-phase oscillator pulls the oscillation frequency away from the ideal tank oscillation frequency and degrades phase noise performance. The addition of the cross-coupled currents also introduces additional noise sources and further reduces the multiphase oscillator's phase noise performance.

A considerable amount of research has been conducted on methods to estimate the phase noise of an oscillator. The process is mathematically complex, and it introduces a layer of abstraction

between the circuit parameters and the amount by which a circuit designer could potentially improve the key performance characteristics. The current tools allow the designer to quantify the different circuit components' contributions to phase noise, but offer no indication of how to improve the metric. There is an approach to quantify oscillator phase noise [1] that solves the system using a linear time invariant (LTI) model in combination with a non-linear time variant (NLTV) model. This approach estimated the phase noise with moderate accuracy, but ultimately proved incomplete.

Despite the existing research on the quantification of phase noise, there are inadequate publications on the possible improvements to the oscillator's phase noise. The approach employed in this study aims to establish a connection between circuit parameters and phase noise.

1.1.2 Hypothesis and research questions

The primary objective of this work is presented as follows:

> *Determining which noise source component in an autonomous oscillator is responsible for the greatest contribution to phase noise.*

The phase noise is characterised for a single-phase oscillator. The characterisation aims to establish whether or not the factors influencing phase noise can be improved at a circuit structure level. Therefore, this study investigates whether or not a multiphase oscillator's phase noise is comparable to a single and differential oscillator, based on a review of the relevant literature, and a review of the various oscillator structures that have been previously implemented. The factors that directly result in phase noise performance are subsequently considered, and the key attributes are identified in order to establish an approach for generating a quadrature oscillator with improved phase noise performance and low power consumption.

Oscillator performance is important to any modulation and mixing system, and the tools that reduce the phase noise are invaluable. Chapter 2 presents a comparison of current single and differential oscillator topologies. Furthermore, this study presents an oscillator design that can be compared to state-of-the-art quadrature oscillators (Section 2.2.3).

Passive devices influence oscillator performance significantly, and therefore the technology in which the oscillator is manufactured has a strong influence on oscillator performance. For this reason, it is necessary to compare the quadrature oscillator to a similarly structured oscillator in the same process. The objective is to identify circuit parameters that can be targeted to improve phase noise, specifically targeted at a multiphase implementation.

An *LC* oscillator based on the Colpitts structure is investigated, as are the different noise effects that influence phase noise. The Colpitts structure extends to enable the generation of four phases. The various noise conversion mechanisms investigated are then used to modify the circuit's basic structure in order to improve the multiphase oscillator's phase noise performance.

Therefore, the study's hypothesis is formulated as follows:

> *If the circuit structure of an autonomous oscillator is altered to change the loading of the relative tank circuit and timing of current injection, then the phase noise performance can be improved, otherwise the achievable phase noise performance in any oscillator–single or multiphase–is simply a function of the oscillation frequency and quality of active and passive devices within the relative technology node.*

The research questions are addressed through the following process:

1. identification of the factors influencing phase noise performance;
2. alteration of the structures of both single and multiphase oscillators;
3. characterisation of the phase noise by the oscillators' relative figure of merit (FoM);
4. comparison of the alterations to the same underlying oscillator structure where no modifications are made (the test case is first demonstrated on a single-phase oscillator);
5. verification whether the same improvement will be translated to the multiphase oscillator, given that the single-phase oscillator's FoM is improved;
6. implementation of a single Colpitts oscillator in order to make comparisons between a basic oscillator and the methods implemented to achieve improved phase noise;
7. extension of the improvements identified in the modifications to the circuit to both a novel single-phase Colpitts oscillator and a novel quadrature Colpitts oscillator;
8. implementation of three oscillators in a 0.13 µm silicon-germanium (SiGe) bi-complementary metal oxide semiconductor (CMOS) process from International Business Machines (IBM); the first is a standard Colpitts oscillator, which forms the

basis for the comparison to the new novel oscillators, and the second and third oscillators are the modified single-phase oscillator and the modified quadrature oscillator, respectively; and

9. comparison of the measurements on the prototype to theoretical and simulated values r to verify whether the circuit performance has been improved.

1.1.3 Justification for the research

The different mechanisms that cause noise conversion to phase noise are qualitatively investigated to identify potential improvements to circuit structures that will enable phase noise reduction. The research identifies the components of an oscillator that are responsible for phase noise contributions. This allows for a general approach to be defined that will enable modifications to be made to standard oscillators, which will lead to greater performance. The work aims to identify procedural methods to help design more efficient oscillator circuits. Although several methods exist for the prediction and estimation of phase noise, it is possible to extend the effects into a procedural method for phase noise performance improvements.

There are existing models for predicting phase noise of varying complexity and accuracy. This study follows a mathematically rigorous approach, and demonstrates a novel multiphase oscillator as the output of the study, incorporating improvements identified in the literature review. A Colpitts oscillator is extended in order to enable the efficient generation of quadrature oscillations. The structure utilises super-harmonic and parallel coupling to generate the four-phase oscillator. The novel quadrature oscillator changes the feedback structure in order to reduce both the power consumption and phase noise of the quadrature oscillator.

The research methodology structures the approach of determining a hypothesis by investigating possible openings in the current body of knowledge, and providing adequate reasoning via justification of the identified research questions. The steps to define, model, and verify the proposed research are outlined below.

1.1.4 Research methodology

The research methodology employed in the study encourages the application of a systematic procedure. A typical scientific method is thus as follows:

1. existing theories and observations;
2. hypothesis;
3. prediction;
4. design, test, and new observations; this step will either validate the hypothesis or lead to further analysis of the existing theories and observations;
5. the hypothesis is confirmed if congruent results with existing theories and observations are achieved, but if this is not true, then the hypothesis must be rejected; and
6. the conclusion of the hypothesis then becomes part of the body of knowledge and takes its place in the existing theories and observations.

The hypothesis is formulated and validated based on the limitations or technological constraints. Technological developments are required to provide the same or better performance within the existing theories or observations from experiments. The system description is based on design concepts, and are employed to verify the modules that comprise the design hypothesis.

Figure 1.1 illustrates the scientific process followed during the research. This process involves the adjustment and redefinition of the hypothesis in order to establish a correlation between the predicted outcome and the existing theories; it also requires consistency during testing and observation. Competing theories were selected and compared, based on their performance for specific applications, focusing on mm-wave applications.

As indicated in Figure 1.1, this study demonstrates a thorough literature review of oscillator circuits and phase noise, including an investigation into the current state-of-the-art methods for phase noise performance. Furthermore, the various options currently available for multiphase oscillation generation were examined and factors that influence phase noise performance were identified. These oscillator structures were tested and modelled in MATLAB[1] and were then compared to the expected results and performance available in the existing body of knowledge concerning high-performance oscillators. The 130 nm process used for the designs had a unity gain frequency of 200 gigahertz (GHz) and modelling was done in Cadence Virtuoso, with component model libraries supplied by the vendor. The layout of the schematic circuit was performed in Cadence Layout Editor. Design rule checks (DRCs) and layout versus schematic

[1] MATLAB is a technical computing software package supplied by Mathworks (www.mathworks.com).

(LVS) tests confirmed that the layout and the schematic designs coincided and no design rules were broken, as specified by the 130 nm process.

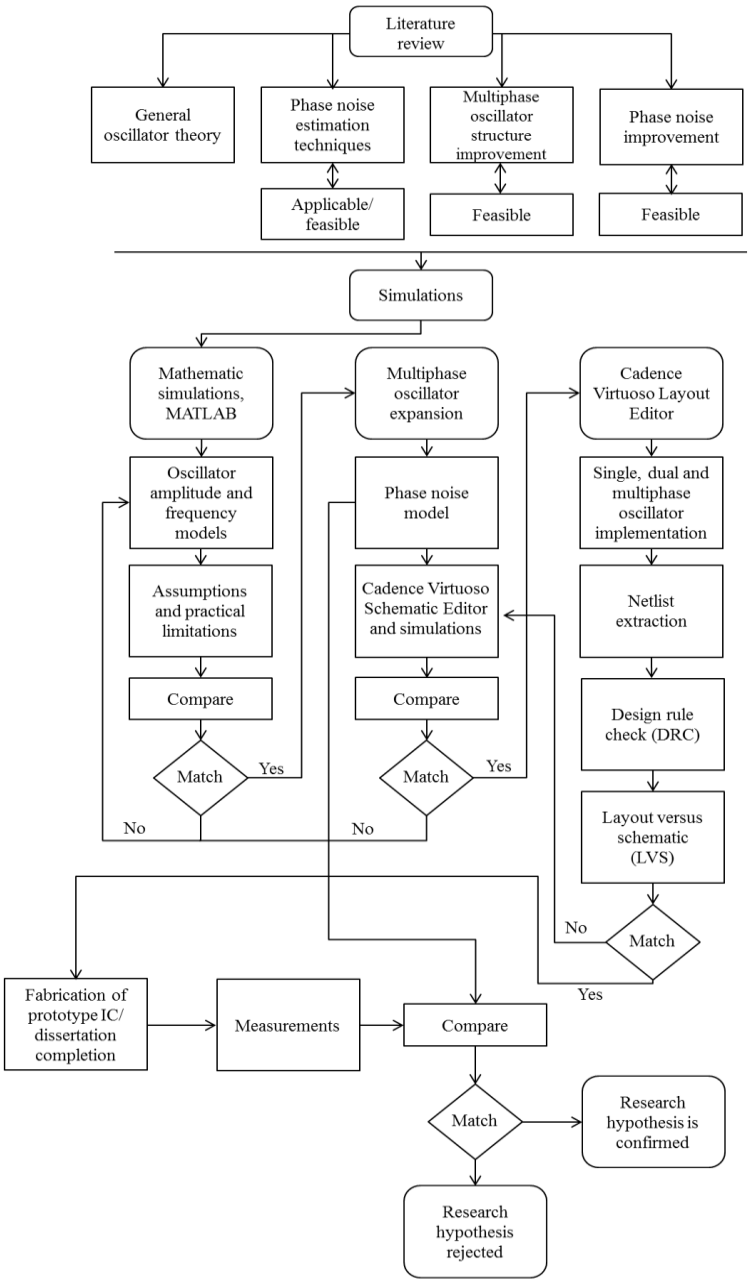

Figure 1.1. Research methodology followed for the proposed research.

The relevant, completed layouts could be submitted for fabrication in a 0.13 µm process in a multi-project wafer (MPW) project handled through the MOSIS Service[2], based on their output on a single graphic data system file. The prototype was subsequently delivered, mounted on a printed circuit board (PCB), and measured using the Anritsu MS 2668C spectrum analyser and the Anritsu 37397D vector network analyser connected to a probing station for on-wafer measurements. The measurement results were then compared to the schematic simulations, and the mathematical models and the accuracy of these models were verified.

1.1.5 Delimitations and assumptions

The delimitations applicable within the scope of work by the fabrication process used, the compact model approximations, and the key assumptions based on the literature review are provided hereunder:

1. scaling is directly proportional to high frequency, thus, by determining the effects of scaling, deductions are made for high-frequency operations;
2. the process technology places a limit on the design parameters (minimum transistor length, supply voltage, saturation velocity) and the operation ranges, and design parameters are specified by the foundry and restrict the designer;
3. compact models used for mm-wave frequencies are approximations, since there are no generalised models, and thus, the accuracy of measurements is limited by the best parameter fit of the compact models;
4. in other cases, parameters for design are extracted experimentally, but since no prior experiments have been performed, such design parameters are unknown and are approximated, where possible, based on findings in the literature.

1.1.6 Research contribution

This study focuses on phase noise in an oscillatory system and identifies several factors influencing phase noise performance. After isolating the factors that play the most significant roles in phase noise, a new structure for a multiphase oscillator was identified. This new structure takes advantage of the factors identified in the literature review. A MATLAB algorithm was developed to aid in determining component values during the design of a low

[2] Information on scheduled multi-wafer project runs from The MOSIS Service and is presented at www.mosis.com.

phase noise multiphase oscillator. The new structure alters the oscillator's feedback mechanism and yields improved power consumption and phase noise performance.

1.1.7 Publication from this research

The following publication has appeared in *The Microelectronics Journal* listed by Thomson Reuters Web of Knowledge (formerly ISI):

A.C. Alberts and S. Sinha, "A modified multiphase oscillator with improved phase noise performance," *Microelectronics Journal* (Elsevier), Vol. 62, No. 4, pp. 21-29, Apr. 2017.

1.1.8 Outline of the dissertation

Chapter 1 – Introduction

The chapter introduces and contextualises the research problem and presents the study's hypothesis. The aim of the research is discussed, and the specific contributions are stated.

Chapter 2 – Literature Review

The literature review focuses on two main components that include noise contributions and the relationship to phase noise, oscillator structures, quadrature oscillator structures, and their influence on achievable phase noise performance. A thorough description and comparison of possible oscillator architectures are presented. The mechanism through which noise is converted to phase noise is examined and two approaches are discussed. The phase and amplitude mismatches of a quadrature oscillator are also studied, and the effect of the coupling of oscillators is investigated.

Chapter 3 – Methodology

This chapter discusses the manner in which the hypothesis was approached and verified. The methodology investigates solutions to the research problem based on the identified deficiencies in conventional oscillator structures.

Chapter 4 – Oscillator Design and Simulation

This chapter discusses the design method for the various oscillator structures, and progresses through each stage to demonstrate the oscillator's key aspects. The main performance characteristics and interactions are demonstrated using a mathematical flow. The final demonstration is the modified multiphase oscillator and its key performance characteristics.

Chapter 5 – Measurements and Results

This chapter presents the outcomes of a discussion of the oscillator and the measurements.

Chapter 6 – Conclusion

This chapter demonstrates that the key concepts that are presented are consistent with the theory, as illustrated by the numerical simulations demonstrated in the work. The study concludes that it is possible to remove some of the inherent limitations on phase noise performance of an oscillator by removing the link between tank voltage swing and feedback network.

1.1.9 Conclusion

This study investigates Colpitts and cross-coupled oscillators in order to measure their performance. It is likely that the varactors' quality factor and tuning range will strongly influence circuit performance; however, the amplitude-to-phase modulation caused by the varactor's voltage-dependent capacitance, is not considered in this work. Similarly, passive component improvement is not considered.

A general multiphase oscillator was investigated and the key performance-affecting parameters were established. The Colpitts structure is extended to enable the generation of four phases and then the feedback structure is changed to improve phase noise over a basic Colpitts oscillator. This study illustrates that the expected phase noise of a single oscillator is superior to its quadrature counterpart. It has been established that through the proposed modifications to the single-phase oscillator structure, the phase noise performance can be greater than for a simple single-phase oscillator that does not include the circuit modifications. The study further demonstrates that the oscillator's basic structure has a significant impact on phase noise performance, and the quadrature oscillator design was implemented in order to exploit this fact.

CHAPTER 2 LITERATURE REVIEW

2.1 CHAPTER OVERVIEW

This chapter presents a review of the relevant research in order to expand upon the research problem. The different aspects regarding oscillators are investigated and the focus is to determine the key factors influencing phase noise performance in an oscillatory system. The aspects of the oscillator are examined to determine the feasibility of improvement to the multiphase oscillator's phase noise performance. Finally, this chapter reviews current state-of-the-art oscillators and the best methods for predicting phase noise performance.

2.2 INTRODUCTION

Oscillators, more specifically voltage-controlled oscillators, are at the centre of any communication channel. There are three different wireless receiver architectures, namely:

1. direct down-conversion;
2. low-intermediate frequency (IF); and
3. superheterodyne.

The oscillator is part of all three architectures, and cannot be removed from the receiver. Figure 2.1 shows a simplified example of a typical IF receiver block diagram [2].

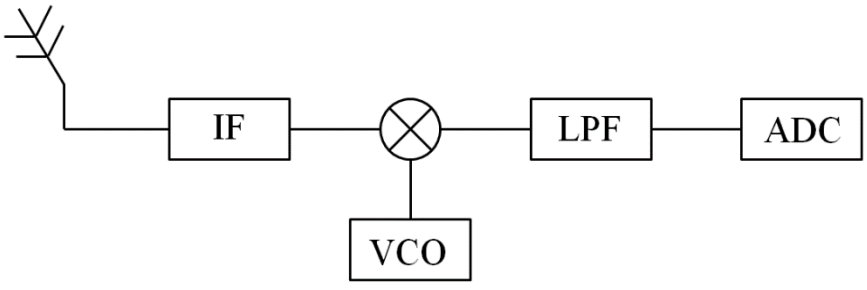

Figure 2.1. Typical IF receiver block diagram, republished with permission from IEEE [2].

In Figure 2.1, the IF is converted to baseband by convolving the received signal with a sinusoidal signal that is at the centre of the information spectrum. The result is a conversion to baseband and a vestigial copy of the information spectrum at a higher frequency. The baseband signal is lowpass filtered to remove the copy of the information signal at a higher frequency, and is then sampled by an analogue to digital converter. Figure 2.2 shows how the convolution with a sinusoid may be used to shift the centre frequency of a data signal.

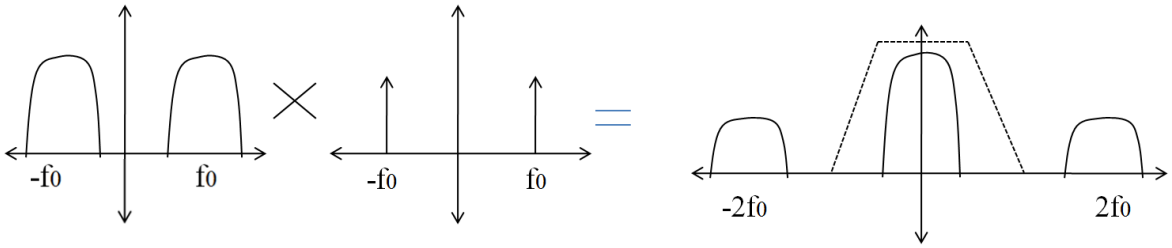

Figure 2.2. Noise current impulse injected at maximum tank voltage and at the zero crossing of the tank voltage; republished with permission from IEEE [3].

Figure 2.2 shows how the convolution of the frequency domain is equivalent to multiplication in the time domain. The single mixing local oscillator (LO) direct down-conversion receiver suffers from wandering DC offsets and intermodulation from LO leakage [2]. In order to overcome the problems associated with a zero IF receiver, PSHMs are used, and these require a quadrature voltage-controlled oscillator (QVCO). The oscillator's phase noise defines the receiver's performance. For a quadrature oscillator to perform orthogonal frequency domain modulation at a carrier frequency of 60 GHz, a phase noise of at least -90 dBc/Hz at a 1 MHz offset is required [3].

2.2.1 Noise sources

It is necessary to investigate and explain the noise phenomena associated with semi-conductor devices. The noise is a direct result of active and passive devices. It should be noted that external noise contributions are not considered. The noise floor represents the lower limit of the size of

the electrical signal that can be amplified by the circuit without significant degradation in signal quality. The different noise mechanisms contribute to the oscillator's phase noise in a combination of different effects.

2.2.1.1 Shot noise

Shot noise is associated with DC flow, and is present in diodes, metal oxide semiconductor (MOS) transistors, and bipolar transistors. The DC flow is caused by electrons and holes drifting across a highly positively and negatively doped Silicon junction (*p-n)* junction. The carriers cross the junction when the potential energy of the electron or hole is greater than the junction's built-in potential. After the carriers drift across the junction they diffuse away as minority carriers. Although the DC flow appears to be constant, it actually comprises a series of random events defined by the carriers crossing the *p-n* junction.

Given a DC flow, and the drain current I_D, there will be random fluctuations, I, around the mean value. These fluctuations are referred to as the shot noise, and are described by the mean-squared variation about the average value. The average value is given in the equation below (2.1):

$$\overline{i^2} = \overline{(I - I_D)^2} \tag{2.1}$$

$$= \lim_{T\to\infty} \frac{1}{T} \int_0^T (I - I_D)^2 dt . \tag{2.2}$$

If the current is defined in terms of its average value I_D, and the current is described in terms of random independent pulses, then the resulting noise current has a mean-squared value given by (2.3) [4],

$$\overline{i^2} = 2qI_D\Delta f \ , \tag{2.3}$$

where q is the electron charge, 1.6×10^{-19} C, and Δf is the bandwidth in hertz.

2.2.1.2 Thermal noise

Thermal noise is related to the random thermal motion of electrons and is not related to the DC flow. Thermal noise is directly proportional to absolute temperature, and as the temperature approaches zero, so does the thermal noise. In a resistor *R*, the thermal noise can be described as either a series voltage generator or parallel current generator, as given in (2.4) and (2.5):

$$\overline{v^2} = 4KTR\Delta f \,, \tag{2.4}$$

$$\overline{i^2} = \frac{4KT}{R}\Delta f \,, \tag{2.5}$$

where $KT = 1.66 \times 10^{-20}$ V-C at room temperature [4].

2.2.1.3 Flicker noise

Flicker noise is associated with the DC flow in active devices, as well as some passive devices such as carbon resistors. Flicker noise is a result of traps caused by contamination and crystal defects. The traps capture and release carriers in a random fashion. This source of noise results in energy that is concentrated at a low frequency. The noise spectral density drops off at a rate of 1/*f*. The effects of flicker noise are most significant at low frequencies, but can be seen even in the megahertz range in certain devices.

$$\overline{i^2} = K_1 \frac{I^a}{f^b}\Delta f \,, \tag{2.6}$$

where *I* is the DC, K_1 is a constant that is defined by the specific process, *a* is a constant in the range of 0.5 to 2, and *b* is a constant that is approximately 1, Δf is the bandwidth in hertz. Flicker noise is of particular concern to the "close in" phase noise of an oscillator. The phase noise is mixed up to the carrier, as "close in" noise, owing to large signal effects [4].

2.2.1.4 Other sources of noise

Popcorn, or burst noise, is a low-frequency noise that is associated with heavy metal contamination. Avalanche noise results from avalanche breakdown, when a *p-n* junction goes into reverse breakdown. Avalanche breakdown will occur if the collector emitter voltage exceeds the breakdown voltage [4].

2.2.1.5 Phase noise

The output of an oscillator may be expressed by:

$$v_{OUT}(t) = A(t)\cos[\omega_0 t + \phi(t)], \tag{2.7}$$

where *A(t)* is the amplitude, ω_0 is the oscillation frequency, $\phi(t)$ is the random phase associated with the carrier.

Because of the time-varying nature of the amplitude and the oscillator's phase variations, the spectrum of the oscillator's output will not be a pure sinusoid, but will have sidebands close into the oscillation frequency. Short-term instability can be characterised in terms of single sideband noise spectral density. The unit of measurement is given in decibels below the carrier per hertz (dBc/Hz), and is defined by (2.8), [6]:

$$\mathcal{L}(\Delta\omega) = 10.\log\left[\frac{P_{\text{sideband}}(\omega_0 + \Delta\omega, 1\text{ Hz})}{P_{\text{carrier}}}\right], \tag{2.8}$$

where $P_{\text{sideband}}(\omega_0 + \Delta\omega, 1\text{ Hz})$ is the single sideband power at a frequency offset of $\Delta\omega$ from the carrier, with a measurement bandwidth of 1 Hz. The above definition of phase noise includes the effects of both phase and amplitude fluctuations [5]. The phase measure is convenient because of its ease of measurement. However, it does not differentiate between amplitude noise and phase noise. The natural amplitude limiting action of active devices in an oscillator leads to the ability to eliminate amplitude noise almost completely. The phase noise in a circuit will be dominant.

A semi-empirical [6] model that is proposed, known as the Leeson-Cutler phase noise model, is given in (2.9). The model is based on an LTI assumption for tuned tank oscillators. The phase noise model is predicted as follows:

$$\mathcal{L}(\Delta\omega) = 10\log\left[\frac{2FkT}{P_s}\left[1+\left(\frac{\omega_0}{2Q_L\Delta\omega}\right)^2\right]\left(1+\frac{\Delta\omega_{f^3}}{|\Delta\omega|}\right)\right], \tag{2.9}$$

where F is an empirical parameter, which is often referred to as "device excess noise number", and k is Boltzmann's constant, T is the absolute temperature, P_s is the average power dissipated in the resistive part of the tank. ω_0 is the oscillation frequency and Q_L is the loaded quality factor of the tank. $\Delta\omega$ is the offset from the carrier and $\Delta\omega_{f^3}$ is the corner between the $1/f^2$ and $1/f^3$ regions. The active device noise figure and the $1/f^2$ corner frequency are generally difficult to calculate, and are usually fitted afterwards [6].

In a different approach, the oscillator is modelled as a system with n inputs and two outputs, $A(t)$ and $\phi(t)$. Noise inputs are modelled as current sources at different nodes of the circuit. The noise currents are modelled as impulses into the circuit at different circuit nodes. Given a tank circuit, shown in Figure 2.3, the effects of injected noise at different points throughout the oscillation may be investigated. Figure 2.3 shows how the non-linear amplitude-limiting effects of the active device in the oscillation circuit tend to reduce amplitude disturbances within the tank circuit. However, the phase disturbances are not corrected by natural circuit action, and will persist as a phase shift in the oscillation frequency [6]. The sensitivity of the phase shifts to current impulses injected across the period of oscillation is defined as the impulse sensitivity function (ISF) [7].

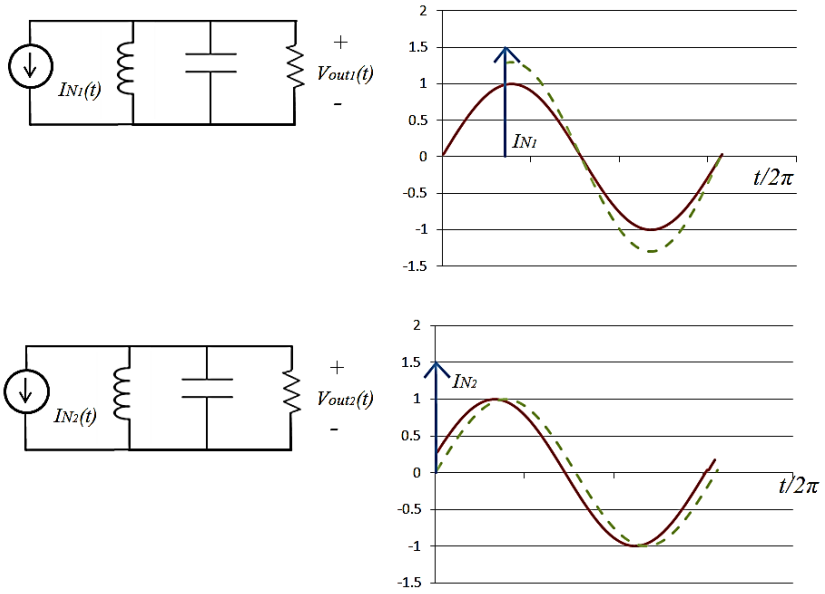

Figure 2.3. Noise current impulse injected at maximum tank voltage and at the zero crossing of the tank voltage; republished with permission from IEEE, [7].

The unit impulse response for the excess phase can be expressed as:

$$h_{\phi} = \frac{\Gamma(\omega_0 \tau)}{q_{\max}} u(t-\tau), \tag{2.10}$$

where q_{max} is the maximum charge displacement across the capacitor on the node, and $u(t)$ is the unit step function. $\Gamma(x)$ is the ISF. The excess phase is dimensionless and periodic over 2π. Since the ISF is periodic, it can be expanded as a Fourier series, [6] given in (2.11):

$$\Gamma(\omega_0 \tau) = \frac{c_0}{2} + \sum_{n=1}^{\infty} c_n \cos(n\omega_0 \tau + \theta_n), \tag{2.11}$$

where the coefficients c_n are real-valued coefficients, and θ_n is the phase noise of the n^{th} harmonic. Noise components are then mapped into their relative spectrum position by weighting the components by the relative ISF.

Thermal and flicker noise are converted into phase noise through different mechanisms. These include the ISF projections, as well as large signal-mixing effects that occur at the input of the oscillator's active device. The different noise conversion effects are demonstrated in Figure 2.4. Figure 2.4 shows how flicker noise and thermal noise are mixed through non-linear circuit effects and then shifted as close in phase noise through phase modulation [6].

The Colpitts oscillator has an ISF that is 90º out of phase with the tank voltage, and is an optimum ISF. The phase noise of an oscillator can be calculated using (2.12).

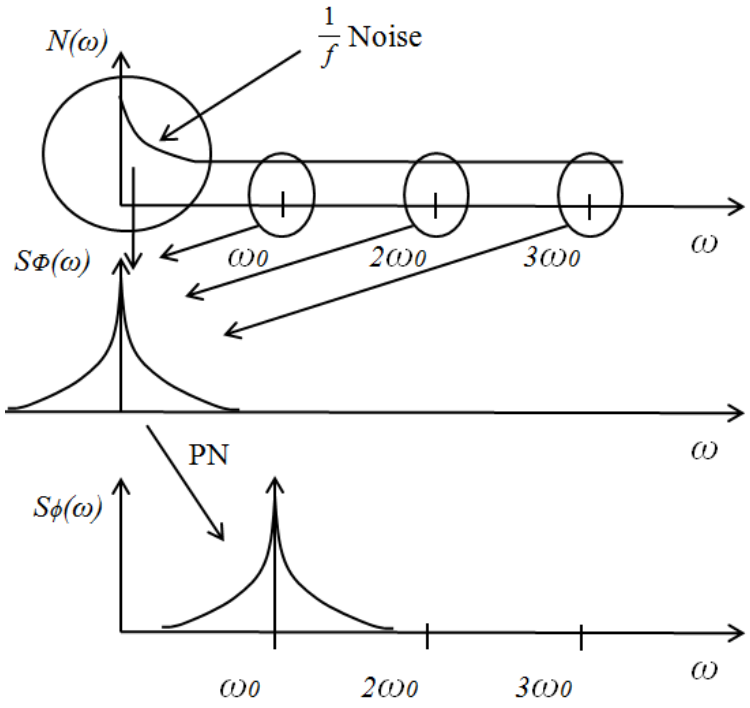

Figure 2.4. Conversion of noise to phase fluctuations and phase-noise sidebands; republished with permission from IEEE [6].

$$\mathcal{L}(\Delta\omega) = 10.\log\left[\frac{\Gamma_{\text{rms}}^2}{q_{\max}^2}.\frac{\overline{i_n^2}/\Delta f}{4\Delta\omega^2}\right], \tag{2.12}$$

where $\mathcal{L}(\Delta\omega)$ is the root mean squared (rms) value of $\Gamma(x)$, $\overline{i_n^2}/\Delta f$ is the summation of the different noise sources in the tank circuit. Equation (2.12) represents the phase noise spectrum of an arbitrary oscillator in the $1/f^2$ region.

Figure 2.5 shows a block diagram of an *LC*-oscillator. The oscillator is modelled as a non-linear limiting device in a positive feedback configuration with a tank circuit and a voltage divider.

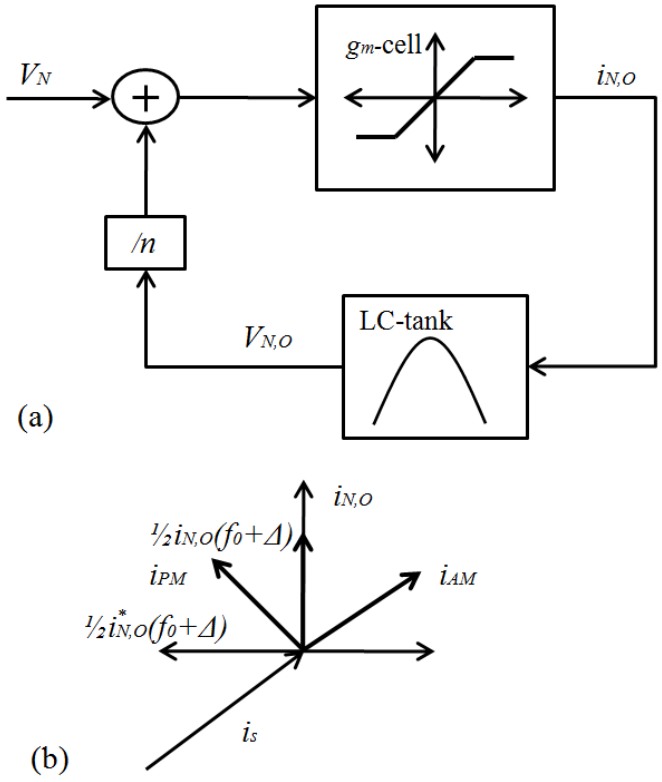

Figure 2.5: a) Oscillator positive-feedback model. (b) Phasor description of oscillator phase-noise model (counter-clockwise rotation); republished with permission of IEEE, [8].

In Figure 2.5 V_N, $i_{N,O}$, and $V_{N,O}$ are the Fourier amplitude components of noise signals at the inputs to the non-linear limiting device, resonator, and feedback divider, respectively. The amplitude of the signal current is $i_s = v_S / R_{TK}$ through the resonator, the phasor diagram in Figure 2.5 (b) illustrates the relationship between the noise component at a frequency $f_0 + \Delta$, and the oscillation signal at frequency f_0. v_S is the voltage across the tank circuit. Δ is the offset frequency. The oscillation current is given as i_s, with the noise component $i_{N,O}$ split into an in-phase i_{AM} and in-phase quadrature component i_{PM}. The phase-related noise power density relates to the single-sided phase noise at the output of the resonator at frequency $f_0 + \Delta$ as:

$$\mathcal{L}(\Delta\omega) = \frac{\left|Z(f_0 + \Delta)\right|^2 i_{PM,TOT}^2}{v_S^2/2}, \tag{2.13}$$

where $Z(f_0 + \Delta)$ is the tank impedance at an offset of Δ from the resonant frequency f_0, and $i_{PM,TOT}^2$ is the single-sided phase-related noise components [8]. The circuit representation of Figure 2.5 is shown in Figure 2.6. For the given *LC*-oscillator the different circuit parameters are defined by (2.14)-(2.18), [8]:

$$k = \frac{g_m}{2n}\frac{1}{G_{TK}}, \tag{2.14}$$

$$g_m = \frac{I_{TAIL}}{2V_T}, \tag{2.15}$$

$$n = 1 + \frac{C_A + C_\pi}{C_B}, \tag{2.16}$$

$$\omega_0 = \frac{1}{\sqrt{LC_{TOT}}}, \tag{2.17}$$

$$C_{TOT} = C + \frac{1}{2}\frac{(C_A + C_\pi)C_B}{C_A + C_\pi + C_B} \tag{2.18}$$

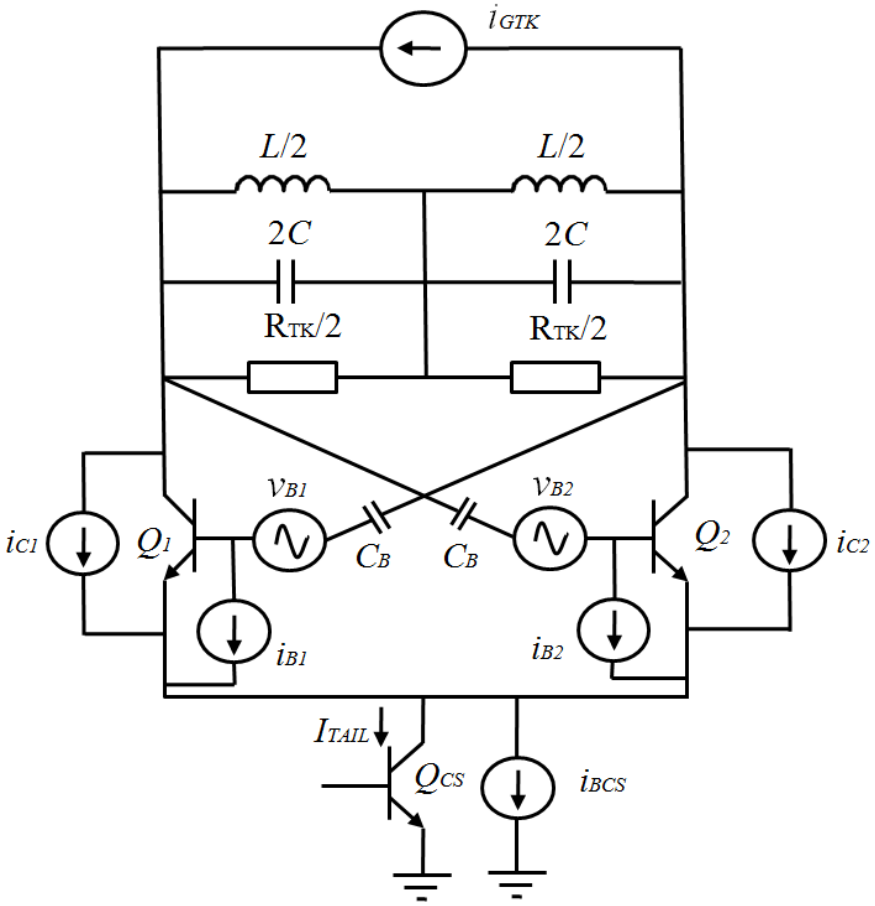

Figure 2.6. Bipolar LC-VCO and its main noise sources, republished with permission from IEEE, [8].

The noise components shown in Figure 2.6 are the double-sided noise power densities of the oscillator noise. The noise components are:

1 the tank conductance noise, $i_{GTK,}$
2 the tank conductance, $G_{TK;}$
3 the base resistance noise, given by $v_{B;}$
4 the collector-current shot noise i_C;
5 the base-current shot noise, denoted by i_B, and
6 the equivalent output current noise, i_{BCS}.

The noise components are defined by equations:

$$i_N^2\left(G_{TK}\right) = 2KTG_{TK}, \tag{2.19}$$

$$v_N^2\left(r_B\right) = 2KT_{r_B}, \tag{2.20}$$

$$i_N^2\left(I_C\right) = \frac{2KT_{g_m}}{2}, \tag{2.21}$$

$$i_N^2\left(I_B\right) = \frac{2KT_{g_m}}{2\beta}, \tag{2.22}$$

$$i_N^2\left(I_{BCS}\right) = 2KT\frac{g_{m,CS}}{2}\left[1+2r_{B,CS}g_{m,CS}\right] \tag{2.23}$$

where I_C is the collector current, I_B is the base current, β is the base current gain of the transistors in the g_m-cell. $g_{m,CS}$ is the transconductance, and $r_{B,CS}$ is the base resistance of Q_{CS}.

The voltage-to-current transfer characteristic of the transconductance stage is provided in (2.24) [8]:

$$i_{OUT}\left(t\right) = \frac{I_{TAIL}}{2}tanh\left(\frac{v_{S,B}}{2V_T}\right), \tag{2.24}$$

$v_{S,B}$ is the feedback voltage and V_T is the thermal voltage. I_{TAIL} is the average current through the transconductance stage. The transfer function is non-linear; in order to calculate the transconductance of the cell the Fourier coefficients of the current transfer are calculated. The Fourier components of the current through a differential pair can be calculated using (2.25).

$$a_n\left(x\right) = \frac{1}{\pi}\int_{-\pi}^{\pi}\left[\frac{1}{2}\tanh\left(\frac{x}{2}\cos\theta\right)\right]\cos n\theta\partial\theta, \tag{2.25}$$

where n represents the relative harmonic, x is the input voltage divided by the thermal voltage, and θ is an integration variable. Table 2.1 shows the harmonic components for the 1st, 3rd, and 5th harmonic components as a function of the input voltage and DC component [9].

Table 2.1. Tabulation of I_n/I_k vs. x for n = 1, 3, 5.

x	$a_1(x) = I_1/I_k$	$a_3(x) = I_3/I_k$	$a_5(x) = I_5/I_k$
0.0	0.0000	0.0000	0.0000
0.5	0.1231	—	—
1.0	0.2356	-0.0046	—
1.5	0.3305	-0.0136	—
2.0	0.4058	-0.0271	0.00226
2.5	0.4631	-0.0435	0.00226
3.0	0.5054	-0.0611	.0097
4.0	0.5586	—	—
5.0	0.5877	-0.1214	0.0355
7.0	0.6112	-0.1571	00575
10.0	0.6257	-0.1827	0.0831
∞	0.6366	-0.2122	0.1273

The noise sources from the tank circuit and active devices are modulated by the time-varying gain. This leads to noise folding. The noise sources are converted from a number of different frequencies, and are converted into phase noise around the oscillation frequency. The phase noise contribution from the tank circuit–prior to weighting from the tank impedance–is given as:

$$\mathcal{L}(R_{TK}) = \frac{4KTG_{TK}}{v_S^2} \quad . \tag{2.26}$$

The base thermal noise does not contribute significantly to phase noise in the voltage limiting regime [8].

The phase noise contribution due to the shot noise from the base and collector current is dominated by the collector current. Considering only the collector current, the phase noise contribution is given by (2.27).

$$\mathcal{L}(I_C) = \frac{KTG_{TK}n}{v_S^2} \tag{2.27}$$

If the phase noise contribution from the collector is analysed, it is noted that the magnitude of its contribution is independent of the small loop gain and power consumption, but is proportional to the capacitive divider ratio. The phase noise contribution due to the bias current is given by (2.28):

$$\mathcal{L}(I_{BCS}) = \frac{KTg_m(1+2r_Bg_m)}{v_S^2} \tag{2.28}$$

.

Equation (2.28) shows that to reduce the phase noise contribution, the base resistance and transconductance should be minimised.

If multiple tank circuits with the same oscillation frequency are coupled together, the phase noise can be reduced. If *N* oscillators are connected together, the impedance is reduced by a factor of *N*. The result of coupling the oscillators is that the phase noise is improved by 10log(*N*) dB at a given frequency offset. The penalty for using additional oscillators is an increase in both circuit size and in power consumption by a factor of *N* [10].

By analysing the different noise sources in terms of their contribution to the phase noise, several different improvements can be made in order to achieve the best possible phase noise These include:

- maximising the amplitude of the tank voltage;
- maximising the value of the loaded *Q;*
- maximising the feedback ratio *n*;
- minimising the base resistance of the coupled transistors;
- the ability to minimise the tank inductance for a given oscillation frequency to reduce the tank impedance at the oscillation frequency;
- having multiple cross-coupled tank circuits oscillating at the same frequency; and
- maximising the small loop gain.

The above observations for methods to improve phase noise are specific to *LC*-oscillators. Ring oscillators tend to exhibit poorer phase noise performance. This can be explained by the ISF that the ring oscillators exhibit [6]. Therefore, ring oscillators are not studied as an alternative to the structure of a low phase noise quadrature oscillator.

An oscillator's phase noise performance can be modified by changing different circuit parameters. The main factors that influence phase noise performance were introduced in section 2.2.5. It was noted that phase noise is proportional to the amplitude of the voltage developed across the tank circuit. Phase noise can also be reduced by using injection-locked coupling between identical oscillators [10]. To classify an oscillator, an FoM is defined and it takes into account the oscillator's centre frequency, the offset frequency at which the phase noise is measured at the offset frequency, and the power dissipated by the oscillator. The FoM is defined by (2.29):

$$\text{FOM} = \mathcal{L}(\Delta f) - 20\log\left(\frac{f_0}{\Delta f}\right) + 10\log\left(\frac{P_{DC}}{1\text{mW}}\right), \tag{2.29}$$

where $\mathcal{L}(\Delta f)$ is the phase noise measured at an offset frequency of Δf, f_0 is the centre frequency of the oscillator, and P_{DC} is the DC power dissipation of the oscillator circuit. The FoM defined in (2.29) does not account for the oscillator's tuning range and therefore an additional FoM is defined. The new FoM is given as (2.30):

$$\mathrm{FOM}_T = \mathrm{FOM} - 20\log\left(\frac{\mathrm{FTR}}{10\%}\right), \tag{2.30}$$

where FTR is the tuning range as a percentage relative to the centre frequency.

Another FoM that accounts for the active area of the oscillator core is given by (2.31):

$$\mathrm{FOM}_A = \mathrm{FOM} + 10\log\left(\frac{\mathrm{Area}}{1\mathrm{mm}^2}\right). \tag{2.31}$$

An oscillator's performance can be judged on the three FoMs and, if necessary, a weighted combination can be used, based on the importance of the different performance parameters [11].

2.2.2 Overview of current phase noise estimation techniques

In this section, existing noise analysis techniques for autonomous circuits are reviewed [12]. At this point it is noted that since an oscillator does not have a specific time reference, the oscillator's output cannot be cyclostationary by nature. The phase noise estimation is approached as the analysis of a non-autonomous circuit driven by a large periodic signal with phase noise as the solution of a stochastic differential equation. It has been shown that:

1 the output of a nonlinear non-autonomous system in the presence of a periodic input with Brownian motion phase deviation is asymptotically wide sense stationary;
2 the Lorentzian spectrum of the input signal and the characteristic Brownian motion input phase deviation process is preserved at the output of an oscillator; and
3 the noisy input is shown to contribute to a wide-band amplitude noise term at the output of the nonlinear circuit, and appears as a white noise source modulated by the time derivative of the system's steady-state response.

Up to this point, an oscillator's phase noise has been treated as an LTV system. The phase noise conversion function is considered over an oscillator's cycle. Several specific aspects of the characteristics of phase noise are subsequently considered. The oscillator is characterised by a set of first-order differential equations. The circuit nodes can be investigated using Kirchhoff's current and voltage laws to generate a system that meets the following requirements:

$$\dot{x} = f(x), \tag{2.32}$$

where $x \in \mathbb{R}^n$ and $f(\bullet): \mathbb{R}^n \to \mathbb{R}^n$ describes the system of differential equations that defines the oscillator. It is assumed that the system satisfies the conditions for the uniqueness of an initial value problem, as specified by the Picard-Lindelöf existence and uniqueness theorem. The solution to the system is assumed to be T-periodic. Small perturbations are then introduced into the system, and the changes to the stable limit cycle of the noiseless oscillator are considered. A small, state-dependent noise source defined by $b(\bullet): \mathbb{R} \to \mathbb{R}^p$, where $b(\bullet): \mathbb{R} \to \mathbb{R}^p$ and $b(\bullet): \mathbb{R} \to \mathbb{R}^p$ is the aggravator to the noiseless unperturbed oscillator and is defined as:

$$\dot{x} = f(x) + B(x)b(t). \tag{2.33}$$

Conventional perturbation theory would then assume that the error introduced from the random noise sources remains small. This is however not true for the case of an autonomous oscillator. If the solution to the oscillator is given as (2.33), then the perturbation causes the component $\varphi(t)$ to grow without bound, with a variance that increases linearly with time [12]. The fluctuation of the term $A(t)$ from (2.34) remains bounded with a small error around the constant oscillation amplitude. The results show that conventional perturbation methods fail to characterise phase noise in an autonomous system. To determine the phase noise of an oscillator, the stable noiseless solution of the system is considered. Floquet theory [13] is then directly

applicable to the problem. Referring to (2.33), the coefficient matrix is periodically time varying such that:

$$\begin{aligned} \dot{x} &= A(t)x, \quad x(t_0) = x_0 \\ A(t) &= A(t+T)\,\forall t \end{aligned} . \tag{2.34}$$

Defining $\Phi(t,t_0)$ as the state transition matrix for (2.33), it can be shown that it satisfies

$$\Phi(t,t_0) = \Phi(t+nT, t_0+nT)\,\forall t, t_0, \tag{2.35}$$

$$\Phi(t+nT,t_0) = \Phi(t,t_0)\Phi(t+nT,t_0)\,\forall t, t_0. \tag{2.36}$$

Then setting:

$$F = \frac{1}{T}\Phi(t+nT,t_0), \quad \Phi(t+nT,t_0) = \exp(FT), \tag{2.37}$$

it follows that:

$$\Phi(t,t_0) = P(t,t_0)\exp\left((t-t_0)F\right), \tag{2.38}$$

where $P(t,t_0)$ is both periodic and singular.

The eigenvalues of the state transition matrix determine the stability of the solution to the system (2.34). For the system to have a stable limit cycle, there must be an eigenvalue equal to one with the rest of the eigenvalues of the system having a real part that is less than 1.

It has been shown that the phase noise of the oscillator is not bounded about the system's stable limit cycle. A small bounded error described in (2.33) by the second term, results in phase noise that is not bounded, but rather continually increases. To calculate the phase noise, it is necessary

to perform a nonlinear perturbation analysis for phase deviation. Classical perturbation techniques fail to fully characterise the nature of phase noise. The noise component is separated into two parts. The small noise component is projected onto the vector, which is parallel to the oscillators' stable noiseless limit cycle, with a projection of the remaining noise component onto the vector that is perpendicular to the trajectory. Equation (2.33) can be rewritten as:

$$\dot{x} = f(x) + b_1(x,t) + b(x,t), \tag{2.39}$$

where $f(x) + b_1(x,t)$ solves the system for $x(t + \alpha(t))$; the term describes the phase deviation of the oscillator. The phase term is not bounded by the size of the perturbation, but is rather periodic in time, limited by the diameter of the limit cycle. The remaining term may be treated with conventional perturbation techniques and results in a bounded amplitude error. The amplitude deviation is described by taking the Taylor expansion of the solution for (2.32).

Given the above results, the phase noise can be derived by the stochastic differential equation given as follows:

$$\frac{d\alpha(t)}{dt} = v(t + \alpha(t)) D(x_s(t + \alpha(t))) b(t), \tag{2.40}$$

where *v(t)* is the Floquet basis vector as defined before, and $b(t)$ is a noise component that has a Gaussian distribution. The remaining term from (2.39) can be examined by continuing to assume the noise component is small, then the solution is given as $z(t) = x_p(t) + y(t)$, with $x_p(t) = x(t + \alpha(t))$. The phase noise of an autonomous system that is perturbed by noise components can now be derived.

It is assumed that all noise components are uncorrelated Gaussian random variables. This is a typically accurate assumption. There will be temperature-related noise correlation. The system is characterised by calculating the time-varying probability density function defined as $\alpha(t)$:

$$p_{\alpha(\eta,t)} = \frac{\partial\left[\alpha(t) \le \eta\right]}{\partial \eta} \forall t \ge 0. \tag{2.41}$$

The probability density function is a Gaussian random variable asymptotically with *t*. The result implies that the statistics of the system are fully characterised using only the mean and variance of the random variable. The phase deviation has a constant mean, and a variance that increases linearly with time. The time-varying PDF $p_{\alpha(\eta,t)}$ does not provide any correlation information between $\alpha(t)$ and $\alpha(t+\tau)$, which is needed for the evaluation of its spectral characteristics. The phase noise requires the calculation of the time-varying variance-covariance matrix, for the equation defined in (2.39), with the noise components being defined as Gaussian random variables.

The circuit equations defining the oscillator circuit need to be analysed to determine the components described above. In a seminal work [15], the time-varying autocorrelation function is derived from the system of equations defining the autonomous oscillator system. The work expands this solution by only considering nodes of the circuit that have capacitors to ground or inductors in the branches. The variance-covariance matrix then solves for the noise component that is perpendicular to the stable limit cycle of the oscillator. The solution is complete and can be expanded to consider higher order statistics of the system through the projection of the solution space onto the stable limit cycle. The solution requires the projection of the system with a Taylor series expansion of the perturbation. The level of expansion is defined by a solution to a differential equation. The correlation function for the phase variable is then defined as follows:

$$\mathrm{E}\left[\alpha(t)\alpha(t+\tau)\right] = m^2 + c\min(t, t+\tau). \tag{2.42}$$

The terms $\alpha(t_1)$ and $\alpha(t_2)$ become jointly Gaussian asymptotically [15] with time. At this point, it is pertinent to mention some of the properties of the differential stochastic equation.

2.2.2.1 The stochastic differential equation

(2.33) is re-evaluated setting the perturbation from an unknown deterministic value into a stochastic Weiner process. Then (2.33) can be expressed as [16]:

$$dX(t) = f(t, X(t)) + G(t, X(t))dW(t),\ X(t_0 = C),\ \mathrm{t}_0 \le t \le T < \infty, \tag{2.43}$$

or more commonly seen in its integral form:

$$X(t) = C + \int_{t_0}^{t} f(s, X(s))ds + \int_{t_0}^{t} G(a, X(a))dW(s)ds,\ \ \mathrm{t}_0 \le t \le T < \infty, \tag{2.44}$$

where $X(t)$ is a stochastic process defined on $[t_0, T]$ and $W(t)$ is a Wiener process. The functions $f(t, X(t))$ and $G(t, X(t))$ are assumed to be deterministic for fixed *t* and *x* [16].

This implies that the uncertainty is introduced by the variable $X(t)$. The stochastic integral is known as Itô's stochastic differential equation. There is another interpretation of this integral, introduced by Stratonovich [18]. This form is a more natural interpretation for the autonomous systems that are investigated, but will not be implemented because of the near impossibility to derive useful mathematical models.

Starting from (2.40), the partial differential equation known as the Fokker-Planck equation [18] is derived, for the probability density function (PDF) $p_{\alpha(\eta,t)}$.

$$\frac{\partial p_\alpha(\eta,t)}{\partial t} = -\frac{\partial}{\partial \eta}\left(\lambda p_\alpha(\eta,t)\frac{\partial v^T(t+\eta)}{\partial \eta}v(t+\eta)\right)+\frac{1}{2}\frac{\partial^2}{\partial \eta^2}\left(v^T(t+\eta)v(t+\tau)p_\alpha(\eta,t)\right) \qquad (2.45)$$

where $v^T(t) = v_1^T(t)D(x_s(t))$, and the value of η depends on, λ which in turn depends on the definition of the stochastic integral. The result is that $p_{\alpha(\eta,t)}$ becomes a Gaussian PDF asymptotically with linearly increasing variance. The characteristic function $F(\omega,t)$ of $\alpha(t)$ is defined by:

$$F(\omega,t) = \mathrm{E}\left[\exp\left(j\omega\alpha(t)\right)\right], \text{ or} \qquad (2.46)$$

$$F(\omega,t) = \int_{-\infty}^{\infty}\exp\left(j\omega\eta\right)p_\alpha(\eta,t)d\eta \qquad (2.47)$$

.

Then, since $v_1^T(\bullet)$ and $D(x(\bullet))$ are *T*-periodic in their arguments, $v^T(\bullet)$ is also periodic with period *T*. This enables the Fourier series expansion:

$$v^T(t) = \sum_{i=-\infty}^{\infty} V_i^T \exp\left(ji\omega_0 t\right),\ \omega_0 = \frac{2\pi}{T}, \qquad (2.48)$$

and finally:

$$\frac{\partial F(\omega,t)}{\partial t} = \sum_{i=-\infty}^{\infty}\sum_{k=-\infty}^{\infty} V_i^T V_k^* \exp\left(j\omega_0(i-k)t\right)\left(-\lambda\omega_0 i\omega - \frac{1}{2}\omega^2\right)F\left(\omega_0(i-k)+\omega,t\right) \qquad (2.49)$$

The differential equation for $F(\omega,t)$ then, has a solution that becomes the function of a Gaussian random variable asymptotically with time and

$$\lim_{t\to\infty} F(\omega,t) = \exp\left(j\omega\mu(t) - \frac{\omega^2\sigma^2(t)}{2} \right) \tag{2.50}$$

solves (2.49), with $\mu(t) = c$ being a constant and $\sigma^2(t) = ct$ and

$$c = \frac{1}{T}\int_0^T V^T(t)v(t)dt \tag{2.51}$$

.

The variance of this Gaussian random variable increases linearly with time. The statistics of the process that defines $\alpha(t)$ are then governed by:

$$\mathrm{E}\left[\alpha(t)\alpha(t+\tau)\right] = \begin{cases} \mathrm{E}\left(\alpha^2(t)\right) \; if \;\; \tau \geq 0 \\ \mathrm{E}\left(\alpha^2(t+\tau)\right) \; if \;\; \tau < 0 \end{cases} \tag{2.52}$$

.

Each noise can then be calculated to contribute varying amounts to the phase noise of the system. The following equation defines the noise contributions translation into phase noise:

$$c = \frac{1}{T} v_1^T(\tau) D\left(x_s(\tau)\right) D^T\left(x_s(\tau)\right) v_1(\tau) d\tau \tag{2.53}$$

,

where $D(\bullet) : \mathbb{R}^n \to \mathbb{R}^{n\times p}$ represents the modulation of the intensities of the noise sources with the large-signal state. (2.53) can be rewritten as:

$$c = \sum_{i=1}^{P} \left[\frac{1}{T} v_1^T(\tau) D_i(\tau) \right]^2 v_1(\tau) d\tau \tag{2.54}$$

,

where p is the number of noise sources within the system. A further useful extrapolation of (2.54) is then:

$$c_s^{(k)} = \frac{1}{T}\int_0^T \left[v_1^T(\tau) e_k \right]^2 d\tau \quad , \tag{2.55}$$

where $1 \le k \le n$ and e_k is the k^{th} unit vector. The term e_k represents the noise source added to the k^{th} circuit node.

The methods presented allow the system's phase noise to be fully characterised. To implement the above methods, (2.32)-(2.55), the algorithm below is considered. An algorithmic approach to calculating phase noise is presented [15].

1. compute the large-signal periodic steady-state solution $x_s(t)$ for $0 \le t \le T$ by numerically integrating the system given in (2.34);
2. compute the state-transition matrix $\Phi(T,0)$ by numerically integrating $\dot{Y} = A(t)Y,\ Y(0) = I_n$ from 0 to *T*, where $A(t)$ is the Jacobian and $\Phi(T,0) = Y(T)$;
3. compute $u_1(0)$ using $u_1(0) = \dot{x}(0)$;
4. $v_1(0)$ is an eigenvector of $\Phi^T(T,0)$ corresponding to the eigenvalue 1; to compute $v_1(0)$, first compute an eigenvector of $\Phi^T(T,0)$ corresponding to the eigenvalue 1, then scale this eigenvector so that $v_1(0)u_1(0) = 1$ is satisfied;
5. compute the periodic vector $v_1(t)$ for $0 \le t \le T$ by numerically solving the adjoint system $\dot{y} = -A^T(t)y$ using $v_1(0) = v_1(T)$ as the initial condition; and
6. calculate $c = \frac{1}{T}\int_0^T v_1^T(\tau) B\left(x(\tau)\right) B^T\left(x(\tau)\right) v_1(\tau)\, d\tau$.

A simple interpretation of the method presented above is that, given an autonomous system, there is a solution with a Floquet multiplier of 1, which corresponds to a steady-state solution. The perturbations in the form of noise are then subjected to the state transition matrix, where noise that is tangential to the stable limit cycle in the oscillator's hyperplane will result in the

deviations $\varphi(t)$, which will increase linearly with time. This is representative of the system not having a specific time reference. The noise that is not tangential to the stable limit cycle is projected onto the hyperplane that is perpendicular to the stable limit cycle, and corresponds to the remaining eigenvalues and the associated eigenvectors. These values will decay exponentially to the stable noiseless limit cycle with the corresponding exponential decay defined by the Floquet multipliers; see section A.4 for the translation of this algorithm to the relevant problem.

2.2.3 Oscillators

An oscillator's phase noise performance is strongly determined by its structure. Ring oscillators can be realised without the use of bulky inductors. Ring oscillators tend to yield poor phase noise figures and lower FoMs than *LC*-oscillators. The aim of the improvements to the oscillator is to maximise the general FoM, and therefore ring oscillators are not considered for the oscillator design.

2.2.3.1 Single-ended and differential oscillators

Oscillators have several different structures, and some of the more general cases are investigated below.

Figure 2.7 shows two cross-coupled *LC*-oscillators. Another example of a cross-coupled oscillator was discussed in section 2.2.5, and is shown in Figure 2.6. Figure 2.7 (b) shows a cross-coupled *LC*-oscillator with tail current-shaping filter [17].

In Figure 2.7 the tail current shaping filter improves the phase noise measurement by up to 6 dB. The active devices in the cross-coupled oscillator generate a negative transconductance and cancel out losses in the tank circuit. The oscillators in Figure 2.7 make use of both positive-channel metal-oxide semiconductor (PMOS) and negative-channel metal-oxide semiconductor (NMOS) devices, and this increases the negative transconductance value. However, the active devices also increase the noise contributions to the tank circuit. The oscillator can be realised without using both NMOS and PMOS cross-coupled transistors, and

can make use of either type [19]. Figure 2.8 shows a circuit diagram for a transformer feedback oscillator. Figure 2.8 demonstrates the oscillator's transformer coupling connections. The transformer has a higher quality factor than a single inductor. The tank voltage is also larger than the voltage in a simple cross-coupled oscillator, and in section 2.2.1.5 it was shown that larger tank voltages lead to phase noise improvements.

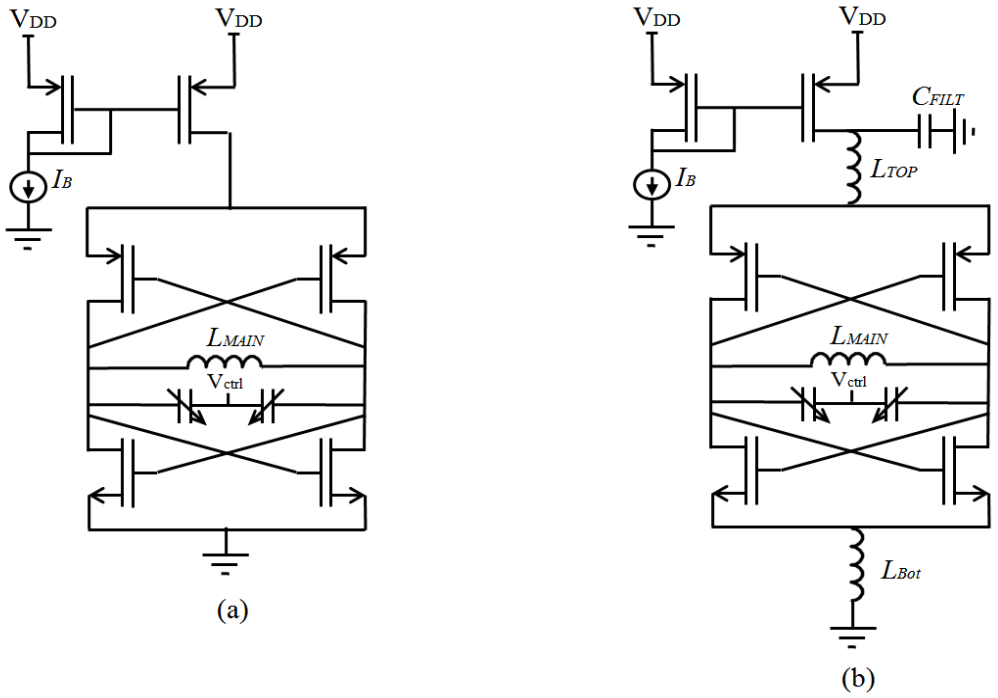

Figure 2.7. (a) Cross-coupled LC-oscillator, and (b) cross-coupled oscillator with tail current shaping filter, republished with permission from IEEE, [19].

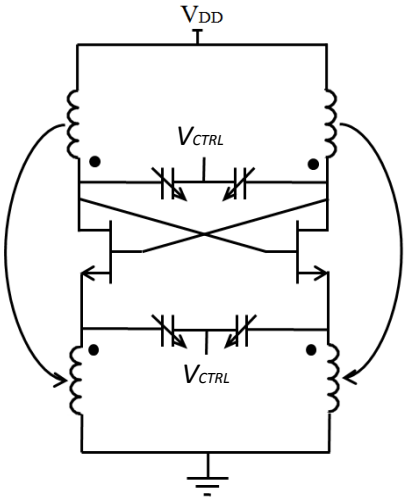

Figure 2.8. A simplified circuit schematic of a transformer-coupled oscillator, republished with permission from IEEE, [21].

The feedback structure of the transformer-coupled oscillator is similar to a Colpitts oscillator with a narrow tuning range, which also leads to an oscillator with good phase noise performance [20]. Furthermore, the transformer forces the oscillator's output signal to injection lock to the oscillator itself, as presented in [21]. Figure 2.9 shows a transformer-coupled Colpitts structure [23].

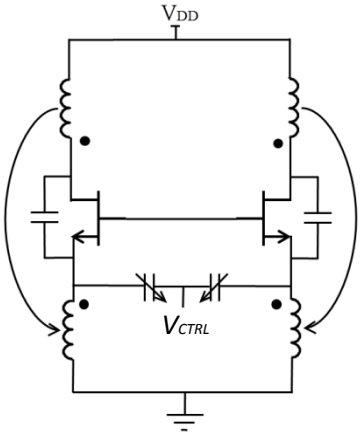

Figure 2.9. A simplified circuit schematic of a transformer-coupled Colpitts oscillator, republished with permission from IEEE, [23].

Figure 2.9's structure benefits from the Colpitts oscillator's good ISF noise-shaping performance. The modified structure enables a high *Q* inductor and a larger voltage swing across the tank circuit. Figure 2.10 shows another alternative, with a cascode amplifier using capacitive feedback from the tank circuit. The oscillator in Figure 2.10 has an output power of -21.12 dBm, a FoM of -183 dBc/Hz, and a phase noise of -108 dBc/Hz at an offset frequency of 1 MHz, and it yields a tuning range of 9% and consumes 10.8 mW while occupying 0.46 mm^2. Figure 2.11 shows a schematic of a current-reuse oscillator.

The feedback structure benefits from the Colpitts oscillator's cyclostationary noise properties and therefore lends itself to the design of low phase noise oscillators.

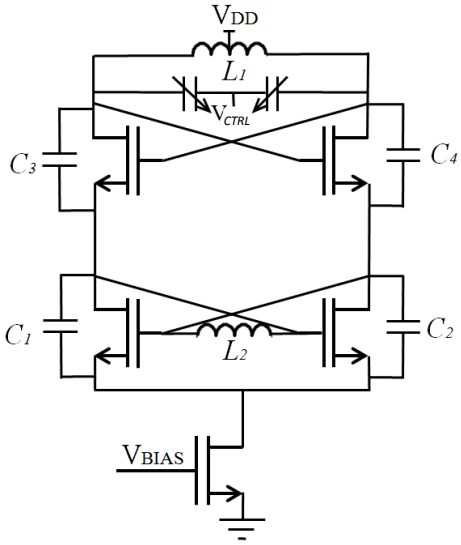

Figure 2.10. A simplified circuit schematic of a cascode differential oscillator, republished with permission from IEEE, [24].

The current-reuse oscillator, shown in Figure 2.11, is inherently immune to the phase noise degradation caused by the second harmonic term and the common-source node [11].

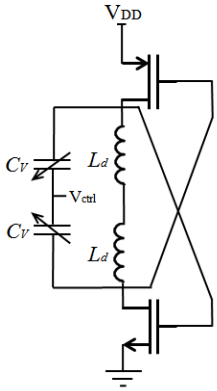

Figure 2.11. A simplified circuit schematic of a current-reuse oscillator, republished with permission from IEEE, [11].

Figure 2.11 shows how further enhancement of the structure, through the introduction of transformer coupling leading to additional benefits associated with transformer-coupled oscillators, is obtained. The oscillator is extended by mirroring the simplified circuit in Figure 2.11. This allows for improved phase noise performance due to even harmonic component cancelation, as well as larger oscillation voltage, at the penalty of increased current consumption.

2.2.3.2 Standing wave oscillator

An oscillator based on standing waves is shown in Figure 2.12. The distributed nature of the transmission lines allows for the oscillation frequency to be set near the f_T of the active devices.

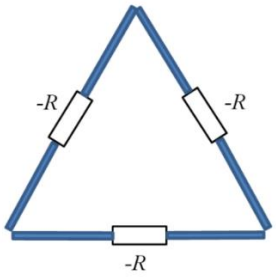

Figure 2.12. A simplified example of a standing wave oscillator, republished with permission from IEEE, [22].

The current is injected at each of the -*R* nodes in Figure 2.12, when the voltage at that node of the transmission line is at a maximum. The output frequency can be adjusted by adding a varactor into the transmission line loop [25]. Standing wave oscillators yield good phase noise performance and good FoMs. The oscillator's output power tends to be low, and the oscillation frequency will be strongly affected by any loading effects caused by a buffer being added to the circuit. Some other examples of standing wave oscillators are shown in Figure 2.13.

Figure 2.13 demonstrates how the travelling waves form standing waves over a fixed transmission line.

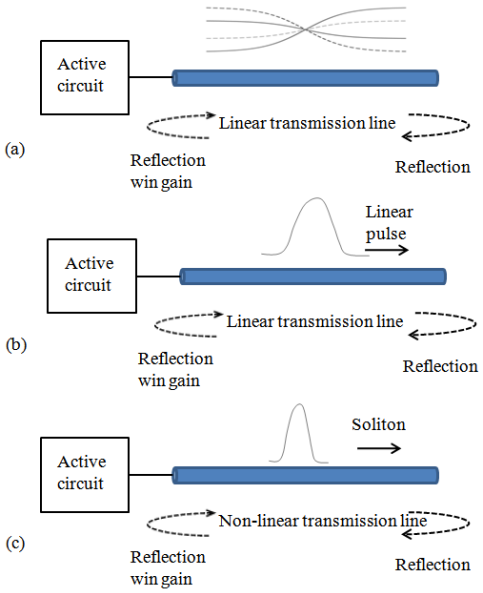

Figure 2.13. A simplified example of standing wave oscillator variations, (a) λ/2 sinusoidal standing wave, (b) linear pulse oscillator, (c) soliton pulse oscillator, republished with permission from IEEE, [26].

2.2.3.3 Single-transistor oscillator

Single-transistor oscillators can be realised with good phase noise performance. A common base oscillator is shown in Figure 2.14.

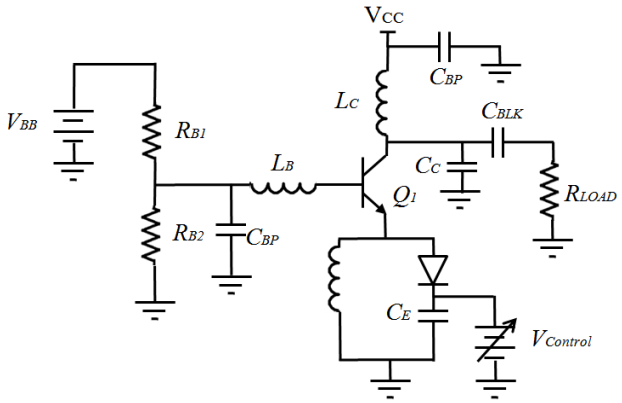

Figure 2.14. A common base wideband oscillator, republished with permission from IEEE, [22].

Through careful feedback design, the tuning range of Figure 2.14 is extended to the bandwidth of the tank circuit. The phase noise performance is good relative to the aforementioned structures. The structure however requires large DC to ensure that the start-up condition is maintained. This leads to larger power dissipations. The single transistor design does not suffer from large parasitic capacitances and this allows the wide tuning range to be realised. It is quite common for the VCO to drive succeeding frequency multipliers and mixers, which would require an output power of at least 0 dBm in this case, [22].

2.2.3.4 Voltage feedback oscillators

The Colpitts structure is the final single-phase oscillator to be investigated. A simplified Colpitts oscillator is shown in Figure 2.15.

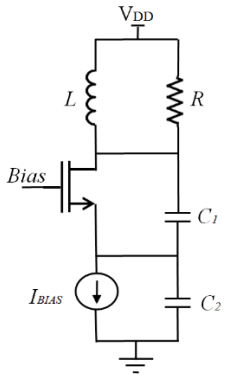

Figure 2.15. A simplified circuit schematic of a Colpitts oscillator, republished with permission from IEEE, [28].

The Colpitts oscillator in Figure 2.15 has superior cyclostationary properties, and may thus potentially achieve lower phase noise performance than other oscillator structures. The Colpitts structure is not widely used in oscillator designs, as its single-ended nature tends to make the oscillator more sensitive to process and supply voltage variations. Substrate noise will also couple more significantly into the single-ended design. Furthermore, the start-up condition of the Colpitts oscillator is more stringent than the cross-coupled oscillator, and this tends to increase the power consumption of the architecture, and results in the less frequent use of the structure, as opposed to a cross-coupled pair. Many systems require quadrature oscillators, and this means that the single-phase Colpitts oscillator proves unsuitable. A comparison of the cyclostationary properties of cross-coupled oscillators, including single and dual cross-coupling, and the Colpitts oscillator is shown in Figure 2.16. Figure 2.17 shows that the ISF weighted by the noise modulation function (NMF) is the smallest for the Colpitts structured oscillator [28]. The NMF is the weighted noise contribution over the oscillator's period. If the Colpitts oscillator's large start-up conditions can be overcome, then a low phase noise, low power dissipation oscillator can be realised.

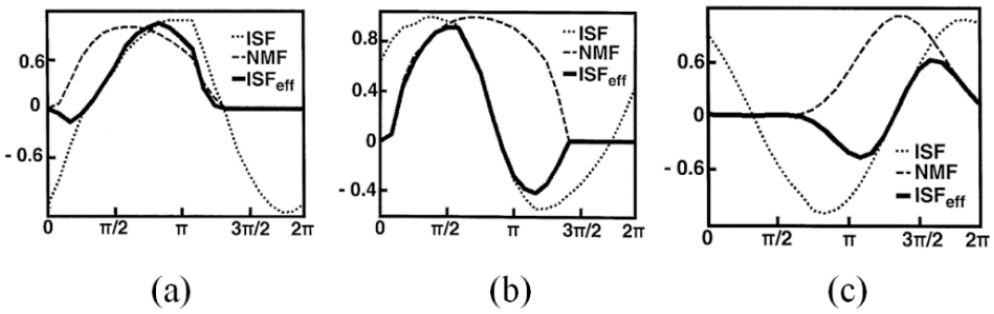

Figure 2.18. The ISF and noise modulation function for three different oscillator configurations: (a) cross-coupled oscillator as in Figure 2.6; (b) NMOS and PMOS cross-coupled oscillators as in Figure 2.7; and (c) Colpitts oscillator as in Figure 2.15, republished with permission from IEEE, [28].

2.2.3.5 Oscillator comparison

A comparison of CMOS oscillators is presented in Table 2.2. The oscillators are defined in terms of the oscillator architecture and the process technology node. All the listed oscillators are differential in nature and serve only to produce single-phase oscillations.

Table 2.2. Comparison of CMOS single and differential oscillator performance.

Reference	Coupling Topology	CMOS Process	Freq. (GHz)	FTR (%)	PN @ 1 MHz (dBc/Hz)	V_{DD} (V)	P_{DC} (mW)	P_{RF} (dBm)	Chip Size (mm^2)	FoM (2.29)	FoM_T (2.30)	FoM_A (2.31)
[20]	Transformer-Feedback	0.18 µm	21.9	5	-109.8	0.6	3.5	-8.6	0.47	-191.17	-185.15	-194.45
[30]	Cross-Coupled	0.18 µm	18.95	3.58	-110.82	1.35	3.3	-20	0.24	-191.19	-182.26	-197.38
[24]	Cascode with Capacitive Feedback	0.18 µm	20.7	8.7	-108.67	1.8	10.8	-21.1	0.46	-184.66	-183.45	-188.03
[31]	Standing wave	0.18 µm	40	20	-100	1.5	27	-13.6	0.32	-177.73	-183.75	-182.68
[12]	Colpitts	0.18 µm	23.4	2.1	-115.2	1.5	27	-8.5	0.35	-188.27	-174.72	-192.83
[29]	Colpitts with Cross-Coupled Boosting	0.18 µm	30	1.34	-104.1	1	2.3	-15	0.24	-190.03	-172.57	-196.22
[11]	Current-reuse	90 nm	20.8	4.8	-116	1.2	3	-23	0.47	-198	-197.60	-203.98
[30]	Colpitts	0.13 µm	4.9	2.5	-132.6 @ 3 MHz	0.475	2.7	-23	-	-192.55	-180.51	-
[21]	Transformer-Feedback	0.13 µm	29.66	3.71	-98.7	1.2	2.32	-	0.5	-174.95	-166.33	-177.96
[32]	Current-reuse	0.13 µm	22.8	7	-115	1.2	1.4	-23	0.5	-201	-199	-204

2.2.4 Multiphase oscillators

Most modern communication systems require LOs that are in quadrature. The quadrature oscillator allows for improved image rejection as well as higher order modulation schemes [11]. The quadrature oscillator is required to drive a PSHM. A PSHM is necessary to overcome some of the problems associated with a zero-IF receiver. The LOs operate at half of the centre carrier frequency [3]. To create the quadrature oscillator, different tank circuits are coupled together, and current injection is used to force the different oscillators' tank circuits into quadrature. The coupling currents pull the oscillation frequency away from its centre value, and tend to reduce the oscillator's phase noise performance. The coupling currents between the different tank circuits will define the phase and amplitude errors between the different oscillator phases [35]. The oscillator architectures defined in the previous section may be extended to enable the generation of the four quadrature phases. Ring oscillators are capable of generating multiple-phase oscillators with the correct phases. These tend to have poor phase noise performance, and poor trade-off between increased power consumption versus improved phase noise performance [36].

2.2.4.1 Parallel-coupled quadrature oscillators

The quadrature oscillator is realised by cross-coupling currents between two differential oscillators. The structure of the oscillator can be of any of the forms discussed in section 2.2.2.1, The oscillator will inherit the characteristics specific to the chosen architecture with an increase in phase noise [37]. The generalised phase noise of the quadrature oscillator is given in (2.56), [37].

$$\mathcal{L}(\Delta\omega) = \frac{kT}{C} \cdot \frac{\omega_{res}}{Q} \cdot \frac{D^2}{N} \cdot \frac{1}{(\Delta\omega)^2} \cdot \frac{1+F_N}{A^2}, \tag{2.56}$$

where N is the number of coupled tank circuits, D^2 is the phase noise degradation due to the detuning of the oscillators' tank circuit, F_N is the noise coefficient F defined [13]weighted with $\frac{1+m}{1+m.\cos(\phi)}$, and ϕ is the phase shift introduced by each of the tank circuits. In another

approach, the noise coefficient F is weighted by $\sqrt{1+m^2}$. This is only valid when the coupling coefficient is less than 10 [36]. The variable m denotes the ratio of cross-coupled or injected current against the bias current of the oscillator's tank circuit. The increase in phase noise is associated with the LTI model that defines phase noise. It should be noted that the current injection of the coupled tank leads to noise being injected into the tank current when the ISF is at a maximum and most susceptible to phase noise contributions. Thus, the phase noise performance of the quadrature oscillator is expected to be poorer than its single or differential counterpart.

To analyse the quadrature parallel-coupled oscillator, consider the equivalent oscillator model in Figure 2.19.

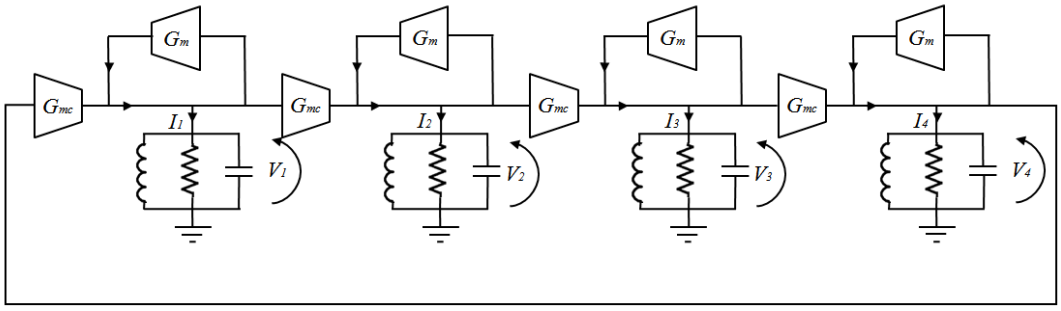

Figure 2.19. An equivalent model of a parallel-coupled oscillator, republished with permission from IEEE, [37].

G_m represents the transconductance associated with the tank voltage, and G_{mc} is the transconductance associated with the cross-coupled current in Figure 2.19. In Figure 2.20, the currents and voltage for a single-tank circuit are considered. The currents and voltage are represented in phasor form. G_mV_n is the current induced by the n^{th} tank voltage and the transconductance G_m. $G_{mc}V_k$ is the current induced by V_k, where k is the tank preceding the n^{th} tank, and G_{mc} is the transconductance. The current injected into the n^{th} tank is therefore G_mV_n + $G_{mc}V_k$. $\phi(t)$ is the instantaneous phase difference between the total current injected into the n^{th} tank and $G_{mc}V_k$. $\psi(t)$ is the instantaneous phase difference G_mV_n and the total injected current. The result of the current injection into the tank circuit is that the oscillation frequency shifts away from the tank resonant frequency, as shown in Figure 2.20. The new oscillation frequency is given by equation (2.57), [35].

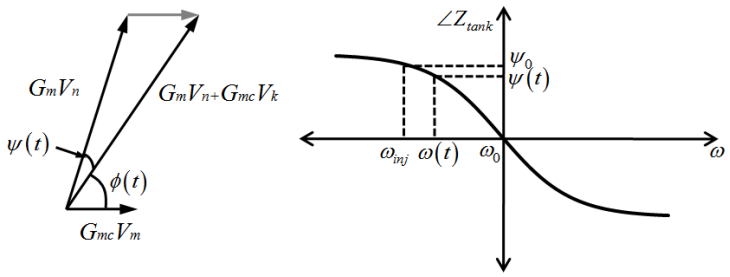

Figure 2.20: Phasor diagram representing currents injected into tank circuit and the relative tank impedance, republished with permission from IEEE, [35].

The oscillation frequency predictions are only accurate if the injected current is small relative to the oscillation current.

$$\omega_{QVCO} = \omega_0 \pm \left(\frac{\omega_0}{2Q}\right)\frac{G_{mc}V_k}{G_mV_n}, \tag{2.57}$$

where ω_0 is the tank resonant frequency, and Q is the tank circuit's quality factor.

Another method to predict the oscillation frequency is provided in (2.58), and the amplitude of oscillation by (2.59). The oscillation frequency is only valid deep in the voltage limiting regime, and this estimate is only useful in this region.

$$\omega_{QVCO} = \sqrt{\omega_0^2 + \left(\left(\frac{\omega_0}{2Q}\right)\frac{\frac{G_{mc}}{G_m}\sin\left(\pi/N\right)}{1+\frac{G_{mc}}{G_m}\cos\left(\pi/N\right)}\right)^2} + \left(\frac{\omega_0}{2Q}\right).\frac{\frac{G_{mc}}{G_m}\sin\left(\pi/N\right)}{1+\frac{G_{mc}}{G_m}\cos\left(\pi/N\right)} \tag{2.58}$$

$$A = \frac{2}{\pi} I_{BIAS}.R\left(1+m\cos\left(\frac{\pi}{N}\right)\right), \tag{2.59}$$

where I_{BIAS} is the bias current of the tank circuit, and R is the tank impedance at the oscillation frequency. The process variations cause the value of the tank circuit's inductance and capacitance to vary. The variation between the tank circuits of the in-phase and quadrature oscillations will lead to both amplitude and phase mismatches [36]. The amplitude and phase

mismatches are analysed in terms of mismatches in the tank inductance and capacitance. If the mismatch in resonant frequency is considered due to the variations in the capacitance and inductance, then the phase mismatch can be predicted by (2.60).

$$\psi_e = \frac{\sigma_\omega}{\omega_0} 2Q \sqrt{\frac{N-1}{N}} \frac{\left(1+m\cos\left(\phi\right)\right)^2}{m\left(m+\cos\left(\phi\right)\right)}, \tag{2.60}$$

where σ_ω is the standard deviation of the frequency shift due to tank mismatches [37]. If the mismatches are given as relative mismatches, ΔL and ΔC, then the phase mismatches can be calculated by (2.61), [36]:

$$\psi_e = \frac{Q}{2}\left(\frac{\Delta L}{L}+\frac{\Delta C}{C}\right)\left(1-m\right)^2. \tag{2.61}$$

In a different approach to solving the phase mismatches, a different estimate for the phase error is given by (2.62),[38]:

$$\psi_e = \frac{Q}{2m^2}\left(\frac{\Delta L}{L}+\frac{\Delta C}{C}\right). \tag{2.62}$$

The amplitude mismatches are provided in (2.63) and (2.64), where the amplitude mismatches are calculated using two different approaches

$$\varepsilon_e = \frac{Q}{2}\left(\frac{\Delta L}{L}+\frac{\Delta C}{C}\right)\left(1-m\right), \tag{2.63}$$

$$\varepsilon_e = \frac{Q}{m}\left(\frac{\Delta L}{L}+\frac{\Delta C}{C}\right). \tag{2.64}$$

Equations (2.62), (2.63), and (2.64) are plotted in Figure 2.21. The values used are for a 5% mismatch in the tank circuits, and a tank quality factor of 10, as shown in Figure 2.21.

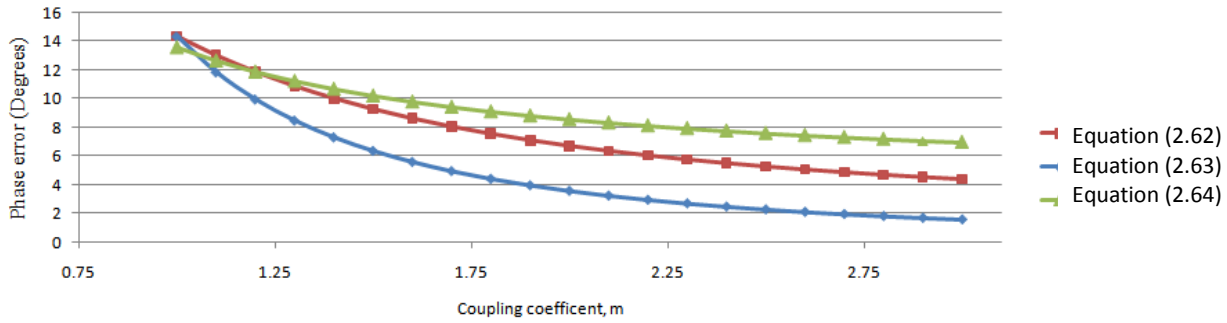

Figure 2.21. A comparison of the phase error values given by (2.62), (2.63), and (2.64), republished with permission of IEEE, from [37].

It is noted that although the multiphase oscillator, shown in Figure 2.21, has several different oscillation modes, the mode that will prevail regardless of the initial conditions is centred at ω_{QVCO}, and the four phases will be separated by $\frac{\pi}{N}$ [37].

2.2.4.2 Quadrature oscillator structures

To make a reasonable comparison of the achievable FoMs for quadrature oscillators to their single-ended and differential counterparts, the structures that were used to generate the single and differential phase oscillations are compared to the same structures for quadrature oscillation generation. All the properties associated with an oscillator structure that were relevant in section 2.2.3.1 apply directly, with a slight degradation in phase noise performance, as discussed in section 2.2.4.1.

2.2.4.2.1 Cross-coupled quadrature oscillator

The cross-coupled quadrature oscillator benefits from a large start-up condition, and oscillations will begin under different processes and temperature variations. The structure is also able to generate oscillations with large amplitudes limited only by the supplies, and this decreases the phase noise. Figure 2.22 shows the oscillator. The unit cell is repeated in Figure 2.22 and the tank circuits are coupled as shown [3].

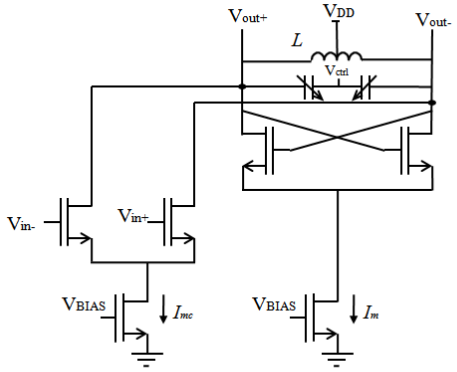

Figure 2.22. A simplified example of a cross-coupled quadrature oscillator, republished with permission from IEEE, [3].

2.2.4.2.2 Transformer-coupled quadrature oscillator

Figure 2.23 shows a simplified example of a transformer-coupled quadrature oscillator.

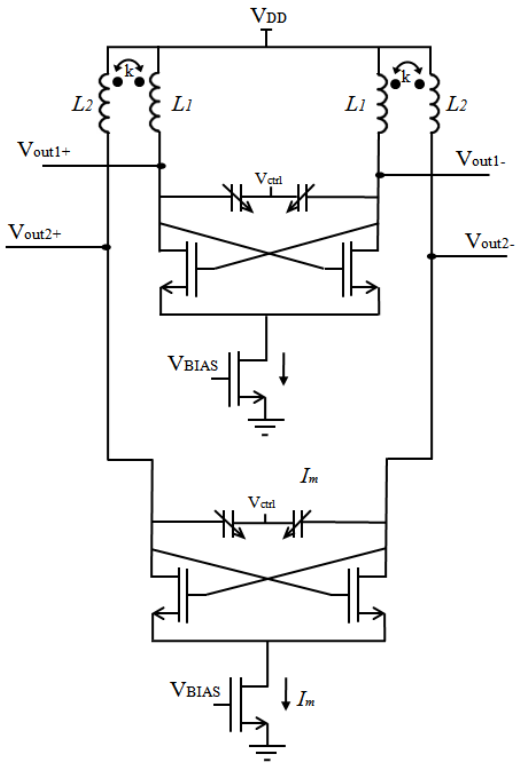

Figure 2.23. A simplified example of a transformer-coupled quadrature oscillator, republished with permission from IEEE, [39].

The transformer coupling in Figure 2.23 removes the supply limitation on the oscillation amplitude, and directly improves an oscillator's phase noise performance.

2.2.4.2.3 Current-reuse oscillator

A current-reuse oscillator that has transformer feedback included in a modified structure is shown in Figure 2.22.

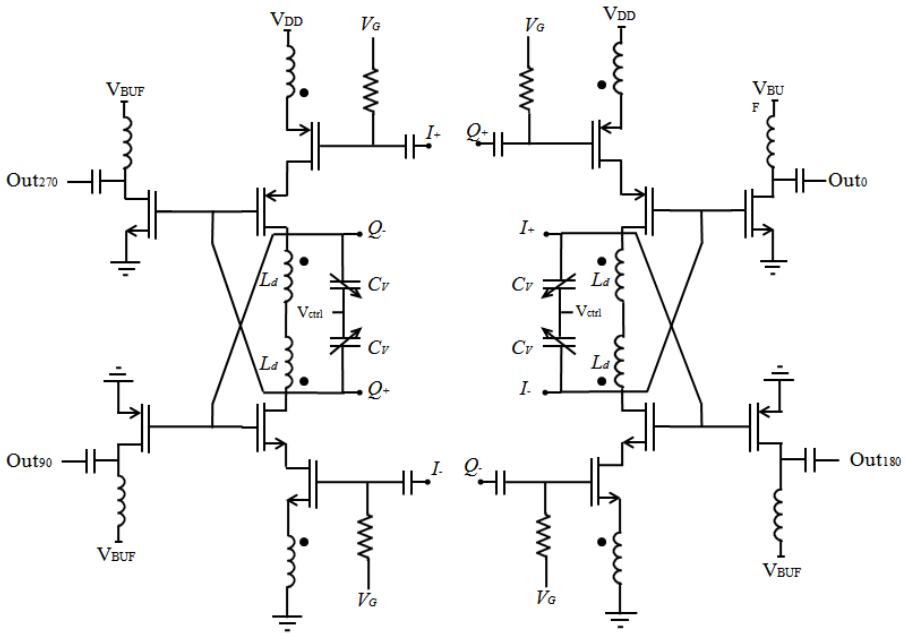

Figure 2.24. A QVCO with current-reuse and transformer feedback techniques, republished with permission from IEEE, [11].

The start-up conditions and power consumption of the oscillator, shown in Figure 2.22, are reduced with the current reuse architecture. This leads to increases in the performance metrics of the oscillator.

2.2.4.2.4 Quadrature standing wave oscillator

A simplified quadrature standing wave oscillator is shown in Figure 2.25. Phase delays in the transmission lines in Figure 2.25 act as inductors causing the oscillation of the circuit. These structures are good for high-frequency oscillators; they do not yield particularly good phase noise metrics.

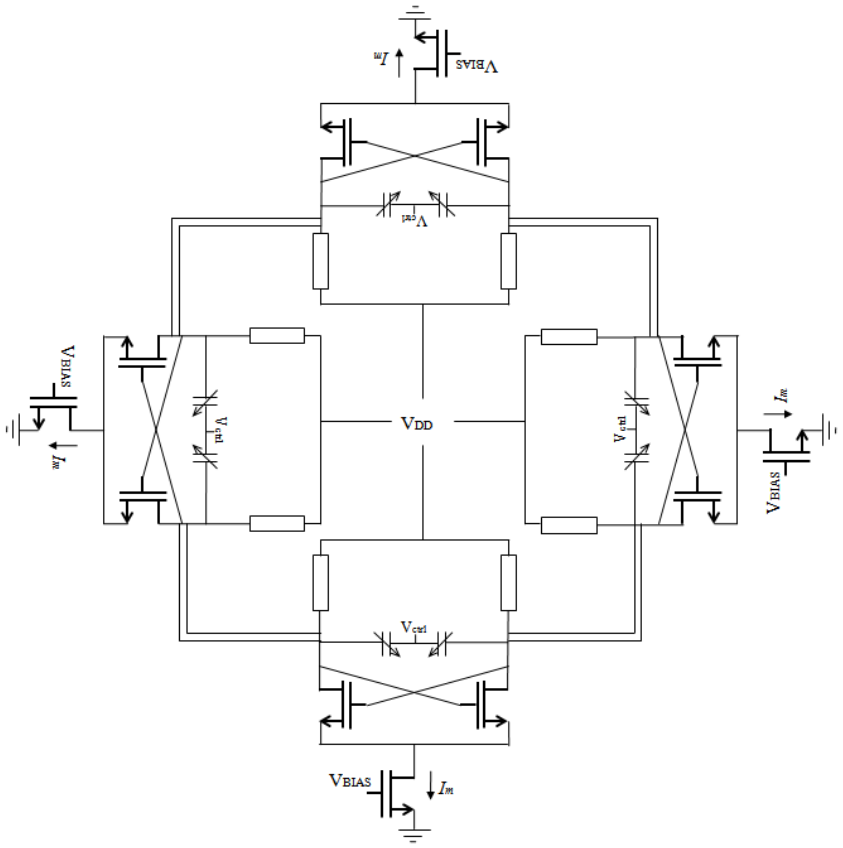

Figure 2.25. A millimetre-wave rotary wave oscillator with four standing wave oscillator stages distributed around a transmission line coupling network, republished with permission from IEEE, [4].

2.2.4.2.5 Superharmonic-coupled oscillator

Two differential oscillators can oscillate in quadrature by letting a coupling network enforce an anti-phase relationship between the second-order harmonics. In Figure 2.26 V_S is the source-coupled voltage of the cross-coupled transistors. The source voltage causes the oscillator to clamp at high bias currents, and causes the oscillator to enter the voltage-limited regime. The drain voltage of the transistors cannot be lower than the source voltage and prevents the oscillation voltage from dropping below the source voltage. The oscillations that occur at V_S are not optimally aligned with the output voltage, and the dynamic impedance tends to increase mismatch in alignment (see Figure 2.27).

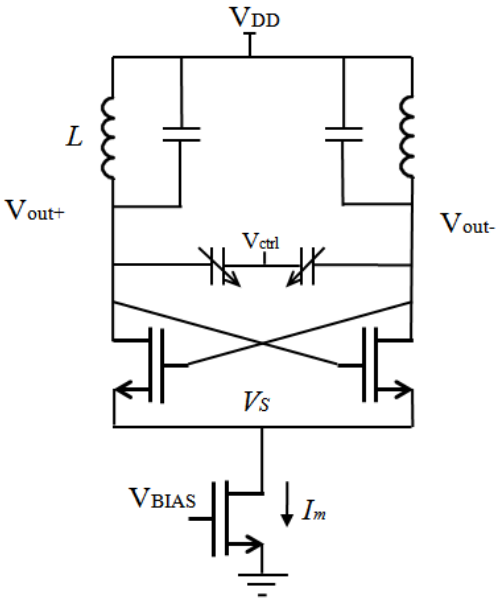

Figure 2.26. Single differential cross-coupled oscillator, republished with permission from IEEE, [40].

The single differential cross-coupled oscillator shown in Figure 2.26 can form the base unit of a multiphase oscillator. The voltages at the different circuit nodes are also shown in Figure 2.27.

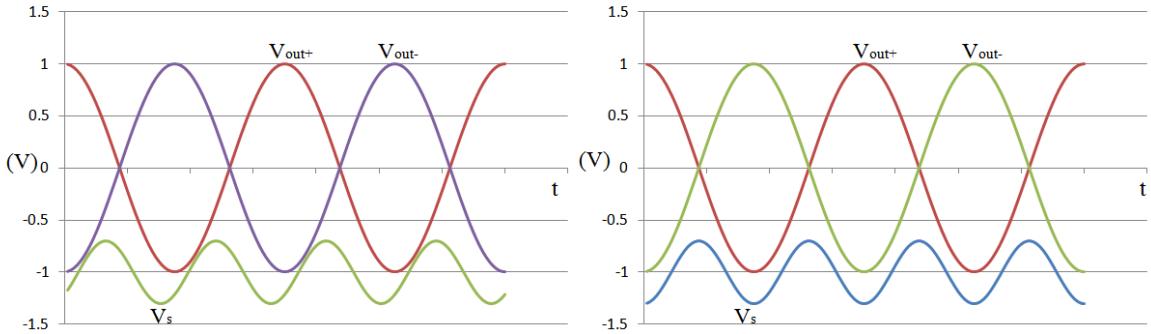

Figure 2.27. Output voltage associated with Figure 2.26, republished with permission from IEEE, from [40].

The circuit shown in Figure 2.27 has two modes of oscillation, namely in-phase and quadrature oscillation. The mode that is selected by the circuit–irrespective of the initial conditions–is the mode with the largest oscillation amplitude. The oscillation frequency is lower than the tank circuit's resonant frequency [40]. The superharmonic-coupled oscillator in Figure 2.28 has increased voltage swing across the tank, which reduces the oscillator's phase noise.

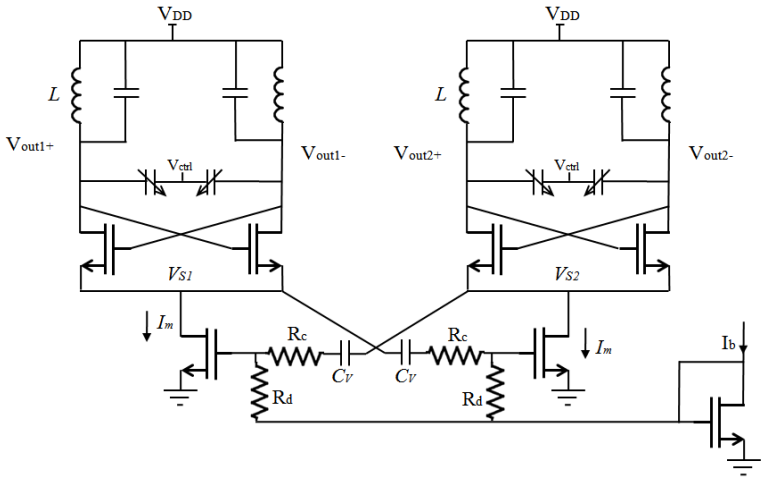

Figure 2.28. A superharmonic-coupled oscillator, republished with permission from IEEE, [41].

The oscillation frequency in Figure 2.28 is calculated to be:

$$\omega_Q = \omega_0\left(1-\frac{3}{2}\frac{1-m\theta_x^*}{3+mQ}-\frac{m}{Q(3+m)}\sin\left(\arctan\left(\frac{\alpha\sin\varphi-\sin\gamma}{1+\alpha\sin\varphi\sin\gamma}\right)\right)\right), \tag{2.65}$$

where $\theta_x^* = \frac{3}{40Q}\frac{5-9m}{3+m}$, $\alpha = \frac{|Z(2\omega_0)|}{2}\frac{g_{mc}R_D}{R_c+R_d}$, $\varphi = \angle Z(2\omega_0)$, and $\gamma\frac{6}{5}\theta_x^*$.

2.2.4.2.6 Quadrature Colpitts oscillator

Figure 2.29 shows a quadrature Colpitts oscillator. The injected current effects the ISF, as the noise is injected into the tank circuit of the oscillator by the cross-coupled current that ensures the realisation of quadrature oscillation. The increase in the magnitude of the combination of the NMF and ISF explains the reduction in the oscillator's phase noise performance. The oscillation frequency is also shifted from the tank circuit's resonance frequency, and this tends to further reduce the oscillator's phase noise performance. The nodes that are connected are denoted by V_1, V_2, V_3, and V_4, respectively. Figure 2.29 is the connection of differential Colpitts oscillators to form a multiphase oscillator. The Colpitts oscillator has properties that make it an ideal candidate for a low-phase oscillator.

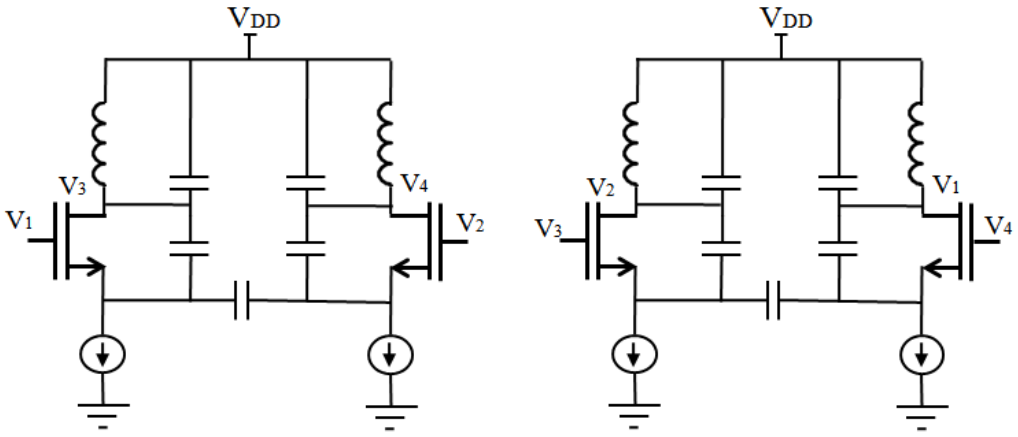

Figure 2.29. A quadrature Colpitts oscillator, republished with permission from IEEE, [37].

2.2.4.3 Oscillator comparison

Table 2.3 presents a comparison of CMOS oscillators. The oscillators are defined in terms of the oscillator architecture and the process technology node. All the listed oscillators are QVCOs.

2.2.1 Conclusion

After analysing the different oscillator structures and comparing these oscillators to their quadrature equivalents, it is noted that currents through the tank circuits are injection-locked for the quadrature oscillator. Even if the magnitude of the current injected into the tank circuits of the oscillator remains the same, the phase noise performance tends to be reduced. It is also shown that injection-locking an oscillator yields an improvement in phase noise performance. It was expected that this trend in the improvement of phase noise performance would increase logarithmically as the number of injection-locked oscillators is increased. However, this improvement is not seen in quadrature oscillators, and the literature review proposes several explanations. If the ISF weighted by the NMF of a Colpitts oscillator is considered, and the noise injection of a single Colpitts oscillator is compared to a quadrature Colpitts oscillator, it is apparent that the root mean squared value (RMSV) is increased by the injection current that is no longer injected at the minimum point of oscillation. This minimum point where the current of a single Colpitts oscillator is injected, is the point in the ISF where the phase noise conversion mechanisms are least significant. Optimum current injection into the tank circuit is not maintained in the quadrature oscillator. This further explains the degradation in the phase noise performance.

Table 2.3. Table comparing CMOS single and differential oscillator performance.

Reference	Coupling Topology	CMOS Process	Freq. (GHz)	FTR (%)	PN @ 1 MHz (dBc/Hz)	V_{DD} (V)	P_{DC} (mW)	P_{RF} (dBm)	Chip Size (mm2)	FoM (2.29)	FoM_T (2.30)	FoM_A (2.31)
[2]	Cross-coupled	65 nm	14	26.3	-110	0.65	15	-5	0.45	-181.16	-189.56	-184.63
[39]	Transformer-coupled quadrature oscillator	0.13 µm	10.4	38.5	-119 @ 3MHz	1.2	19.2	-25	0.84	-176.97	-188.67	-177.72
[43]	Transformer-coupled quadrature oscillator	65 nm	58.2	4.35	-95	1	22	-	0.075	-167.33	-160.10	-178.58
[10]	Current-reuse oscillator	90 nm	20.9	3.1	-117.2	1.7	6.3	-15	0.77	-195.61	-185.43	-196.74
[3]	Standing-wave	0.12 µm	45	6.5	-91	1.2	13.8	-21.6	0.25	-172.67	-168.92	-178.68
[40]	Superharmonic-coupled	0.25 µm	4.9	12.2	-125	2.5	22	-3	-	-185.38	-187.10	-
[38]	Colpitts	0.18 µm	2.2	11.8	-130.4 @ 3MHz	1.2	14.4	-40	-	-176.12	-177.56	-

Chapter 2 examined the different factors that directly influence phase noise performance and the FoM associated with the oscillator. The study shows that by increasing the tank circuit's *Q* factor, phase noise performance is improved. Similar phase noise improvements can be achieved by improving the loaded *Q* factor. There is a compromise between phase noise and phase and amplitude mismatches in the quadrature oscillator and the *Q* factor. It is shown that by decreasing the feedback value, the phase noise contribution from the collector current is reduced. If the transconductance gain of the small signal is increased, the phase noise performance will also improve. By changing the base resistance of the transistors in the oscillator, improved phase noise performance can be achieved. The analysis allows the design of a unique oscillator that can benefit from the prior art. The aspects that are useful to low phase noise are emulated and improved upon to achieve a unique multiphase oscillator with improved phase noise performance. This is done by reducing current consumption and altering the feedback structure to achieve an improved ISF for the multiphase oscillator, ultimately leading to an improved FoM.

CHAPTER 3 RESEARCH METHODOLOGY

3.1 CHAPTER OVERVIEW

The research identified the mechanisms through which a circuit's noise components are transformed into phase noise. The previous chapter presented a qualitative review of oscillator structures (section 2.2.3). Chapter 3 analyses the aforementioned factors in terms of circuit structure. The research aimed to introduce modifications that will optimise several of the larger causes of phase noise in an oscillator.

To verify the magnitude of the effects of the proposed modifications, a standard Colpitts oscillator was compared to a modified Colpitts oscillator. The VCO was simulated to verify that the phase noise performance could be improved using methods identified during the literature study. The oscillators were then prototyped in a 0.13 µm bipolar complementary metal oxide semiconductor (BiCMOS), SiGe process. The goal was to enable measurements of the oscillator's phase noise performance, and the measurements were then compared to both the theoretical and simulated values.

3.1.1 Research methodology

The research methodology employed in this study allowed for hypothesis formulation by identifying deficiencies in the current body of knowledge. This study challenges assumptions regarding the first harmonic transfer function of a transistor, in order to yield improved oscillator performance. These assumptions were tested via experimentation, including simulation and measurement, in order to verify the hypothesis, as presented in Chapter 1.

The research flow process was not linear, but rather an iterative and adaptive process. Figure 3.1 is an illustrating diagram of the research methodology.

The hypothesis was tested iteratively using the research methodology in Figure 3.1. The process began with a review of the existing literature, as presented in Chapter 2. Thus, fundamental

theories, and new and established concepts were studied in relation to the challenges regarding the hypothesis proposed in this work.

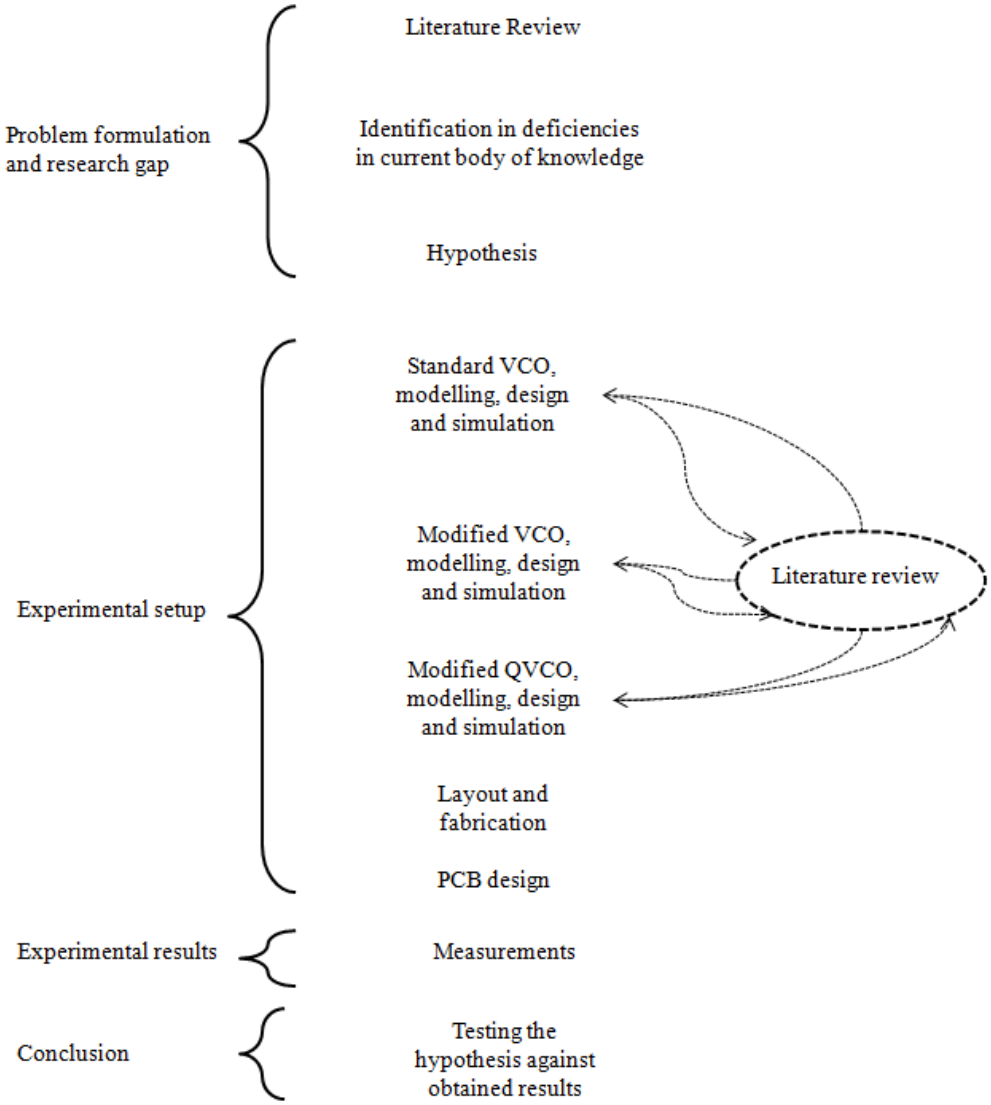

Figure 3.1. A diagrammatic overview of the research methodology.

3.1.2 Approach to reducing phase noise

The key performance attribute of a VCO is the phase noise measurement at a 1 MHz offset. The VCO's performance can be defined by the FoMs identified in 2.2.1.5. The oscillator structure has a large influence on the achievable phase noise performance. The following list defines some of the key methods by which the VCO and the QVCO were approached in order to improve their respective FoMs:

1. a theoretical background of the VCO was compiled to determine which factors could be modified to improve the VCO's FoM;
2. the Colpitts structure was identified as having the potential to yield low phase noise oscillations with several known limitations;
3. the identified VCO structure was modified, and the modifications altered the parameters known to influence phase noise, with the aim of improving the VCO's FoM, as well as overcoming some of the drawbacks associated with the VCO's structure; and
4. the VCO was extended to enable the generation of quadrature oscillations; the parameters that were altered to improve the VCO's FoM were included, and other improvements were also introduced to the QVCO.

The VCO and QVCO were simulated using the Cadence Virtuoso package from Cadence Design Systems, an electronic design automation (EDA) tool. The simulation tools were used to verify whether or not the proposed circuit modifications improved the VCO and QVCO FoMs.

3.1.3 Technical software packages

Various technical packages were chosen to enable the verification of the hypothesis and to complete the study Table 3.1 presents the various packages that were used to characterise the oscillatory system fully, and to predict phase noise in a single and multiphase oscillator. The software packages presented in Table 3.2 are listed with version numbers to ensure compatibility. Cadence Virtuoso was updated to version IC6.1.3.500.13, while the PDK version 1.2.1.0HP was used to complete DRC and LVS tests. The 64-bit MATLAB R2010b was used for mathematical modelling of frequency, amplitude, and phase noise in an oscillatory system.

Enabling a comparison between the standard VCO and QVCO structures to the modified structures required that the two circuits be manufactured, tested, measured, and then compared to theoretical and simulation results. The circuits were manufactured in a 0.13 µm SiGe BiCMOS process. The basic circuit performance was modelled using low-level transistor models. While parasitics were not initially considered, they were subsequently introduced into the oscillator analysis in order to achieve a more accurate representation of physical circuit performance.

Table 3.3. Software packages used to formulate and verify the research hypothesis.

Software	Version	Functionality
MATLAB	R2010b version 7.11.0.584 (64-bit)	Mathematical computing
Cadence Virtuoso Schematic Editor	IC6.1.3.500.13	Schematic composer
Cadence Virtuoso Analog Design Environment	IC6.1.3.500.13	SPICE-based simulator
Cadence Virtuoso Layout Editor	IC6.1.3.500.13	IC layout composer
IBM 8HP Process Development Kit	1.2.1.0HP	DRC, LVS, and layer density checks

The oscillators were set to the desired frequency. Component selection was dominated by both active and passive device performance. The maximum oscillation amplitude allowed by the supply voltage specific to the process was selected. Research indicates that this is the optimal point for circuit performance in terms of the defined FoM. The Colpitts oscillator selected for the purpose of the demonstration of improvements possible through circuit modifications was determined through circuit-level analysis. The phase noise models introduced in the literature review were applied to the oscillator. The study presents an attempt to manipulate the FoM through circuit structure modifications. The effects of the modification were modelled, and the FoM improvement were predicted.

Circuit performance was simulated using a Virtuoso analogue design environment (ADE) from Cadence, one of the industry's leading EDA tools. Transient analysis was undertaken to verify that both VCO and QVCO start-up conditions were sufficient. The transient analysis also enabled the prediction of the DC power consumption of the circuit. The ADE environment was used to perform a harmonic balance simulation.

The harmonic balance simulation predicted the oscillation frequency and amplitude of both the VCO and QVCO. The phase and amplitude mismatches present due to tank mismatches in the QVCO were also modelled using the harmonic balance analysis. The harmonic balance analysis

is a non-linear, frequency-domain, steady-state simulation. The simulations of the oscillator's performance were made after the oscillators reached steady-state equilibrium.

The analysis was based on the fact that voltage and current sources result in discrete spectrum components. The harmonic balance simulation analysed system behaviour in the time-domain, and then transformed the results into the frequency domain where linear circuit interactions were performed.

The shooting method was also employed, and results were compared to the results achieved by the harmonic balance analysis. The shooting method is designed to solve boundary problems, using iterative techniques. The shooting-based methods provided accurate simulations when the circuit being analysed was highly non-linear and the number of harmonic components generated were significant. Both methods provided numerical solutions and provided an accurate projection of what circuit performance could be expected. A steady-state analysis of the oscillator was then performed to determine the oscillator's phase noise performance. The results of the simulations were compared to the values predicted during the circuit-level system analysis.

The circuit layout was completed using the Virtuoso layout editor. The layout integrity was verified through Assura LVS and DRC.

3.1.4 Mathematical modelling

Mathematical models predicting the oscillator response and phase noise performance were created in MATLAB. This study employed MATLAB extensively to estimate the phase noise performance, and also the oscillator amplitude and frequency response. The MATLAB models were used to calculate the circuit's impedance in the small- and large-signal modes of operation. These scripts were used to get initial component values for equivalent circuits, and improvements to the accuracy of these results could then commence in the Simulation Programme with Integrated Circuit Emphasis- (SPICE) based simulation software. The various models used for completing the oscillator designs were compiled in MATLAB (see Addendum A). These were then compared to the SPICE results. These results were used to determine the optimum circuit component values and structures for the best possible phase noise performance numerically.

3.1.5 Qualification test protocol

The aim of the study was to identify circuit-specific characteristics that influence phase noise. This was initially achieved via a thorough literature review. Upon completion of the review, the study built on several different conclusions regarding oscillators and phase noise performance. This chapter presents a detailed mathematical model describing phase noise performance.

A control study was required in order to allow the hypothesis to be tested in a logical way. Different processes yield oscillators with different key performance parameters. Therefore, a single-phase oscillator without any specific modifications was set as the control study. The circuit modifications that yielded improved phase noise performance added additional overhead to the oscillator. The increased power consumption did not justify the implementation of a single-phase oscillator. The second control study involved the differential Colpitts oscillator. The modifications were tested on the differential oscillator.

The main goal was to improve phase noise performance in a multiphase oscillator. The circuit-level improvements translated best to the multiphase oscillator where the additional circuit overhead was traded off for improved phase noise performance. The improvements were qualified via comparisons to the control study, the single and differential Colpitts oscillators. The different metrics used to validate the improvements included the power consumption of each oscillator.

The power consumption was normalised to the number of oscillating tank circuits within an oscillator. The fact that phase noise performance and voltage developed across the tank circuit are directly proportional, means that the power consumption of a given oscillator is important in the comparison between different oscillators. The phase noise measurement at 1 MHz above the centre of oscillation became the qualifying metric. Figure 3.2 shows the measurement outcomes projected to characterise the oscillator performance in a comparable manner.

The different blocks in Figure 3.2 demonstrate a characterisation of each oscillator. The power consumption of each oscillator combined with the relative phase noise performance were key metrics in specifying whether or not an oscillator was improved by specific circuit-level alterations. The power consumption of the differential and multiphase oscillators is expected to

be higher than that of a single-phase oscillator. This had to be taken into account when comparing the oscillators' relative FoMs.

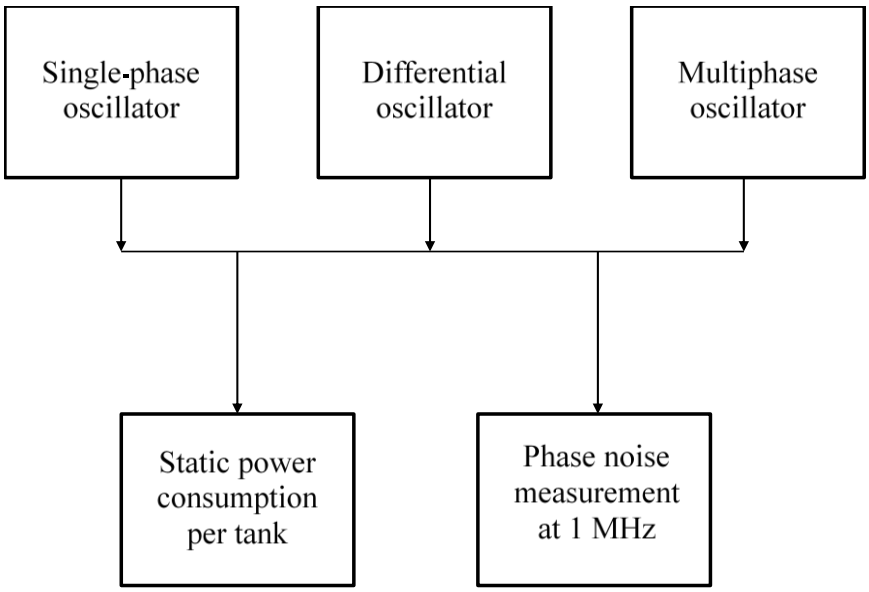

Figure 3.2. A diagrammatic overview of the measurement approach.

The improved multiphase oscillator formed part of a direct down-conversion receiver in the mm-wave range, where the mixing stage was performed with a PSHM. The PSHM required a large differential voltage with low phase noise to yield a satisfactory error vector magnitude, which was required for high data throughput and maximum use of available bandwidth. This study identified the factors that contribute to phase noise in an autonomous oscillator. Following the identification of the largest contribution to the phase noise in an autonomous oscillator, a method to yield improved phase noise may be proposed. Therefore, this study investigated the various implementation options, along with the associated strength of each given oscillator structure, in order to propose a method to predict phase noise accurately.

There are specific parameters, which are process-dependent, limiting the inherent best achievable phase noise. The context of the phase noise conversion process, allows for the proposal of specific circuit-level modifications, in order to further improve an oscillator's FoM.

The outcomes were first demonstrated on a single-phase oscillator and then extended to the multiphase oscillator. The final measurement setup was unable to demonstrate conclusively that

the proposed circuit-level improvements to both the single-phase and differential oscillator led to improved FoM. A significant pad was missing in the layout. The error occurred during the combination of the layouts into the global layout for manufacturing in the MPW. This prevented the correct biasing of the multiphase oscillator and prevented oscillations from occurring. However, the mathematical work demonstrates that the proposed methods to improve phase noise performance are not only plausible; given that the increased difficulty in circuit layout can be overcome, it is possible to yield oscillators with improved FoMs. The feedback structure of the multiphase oscillator requires four additional inductors occupying a large die area, and thus requires transmission lines to couple the signals between the various tank circuits, resulting in a complicated physical layout.

Thus, it is concluded that many oscillators would benefit from structural improvements targeting methods identified in this work, and although ultimately, technology node limitations will place an upper bound on achievable performance, in most cases, the best achievable threshold has not yet been achieved.

3.1.6 Conclusion

The characterisation of an oscillatory system requires a full mathematical model describing the transfer function of the system. The research identified a stochastic relationship between the noise components inherent in any physical system and the deterministic transfer function of the autonomous oscillator.

The body of research identifies various oscillator structures that inherently have better phase noise performance and yield oscillators with better FoMs. These improvements are used and enhanced upon to yield a refined multi-phase oscillator. This work isolated the mechanism through which phase noise is generated by the oscillator's underlying circuit structure, and then proposed circuit-level modifications that yield better FoMs for the oscillators. The mechanisms identified for single-phase oscillators are thus extended to differential and quadrature oscillators.

The hypothesis was tested through the modelling, layout, and manufacture of an integrated circuit (IC). Unfortunately the measurement section of the circuit could not be completed because of a missing pad that occurred during the joining of the projects into the MPW. The key focus was the improvement of the multiphase oscillator incorporating the circuit-level

modifications, which yielded better phase noise performance. The circuits were modelled using various tools available and all were in agreement with the expected improvement in phase noise performance of the multiphase oscillator. The measurement results, if in agreement with the simulation results, would confirm the theory that phase noise performance can be manipulated by altering the oscillator's feedback structure. This however could not be completed owing to technical difficulties in the graphic data system (GDS) file for the MPW. The mathematical model however demonstrates clear improvements with the modified feedback structure.

CHAPTER 4 MATHEMATICAL MODELLING AND SIMULATIONS

4.1 CHAPTER OVERVIEW

The *LC* oscillator was investigated in three different forms. A single-phase oscillator was studied and compared to a differential and multiphase oscillator. The final selected structure for the oscillator was based on the Colpitts oscillator. To clarify the improvements of the new oscillator, it was compared to the cross-coupled pair.

4.1.1 Single-phase Colpitts oscillator

The analysis of the multiphase oscillator is presented first, using a single-phase Colpitts oscillator. The analysis is extended to a differential oscillator. The final multiphase oscillator is presented in Figure 4.1, in the form of a standard single-phase Colpitts oscillator.

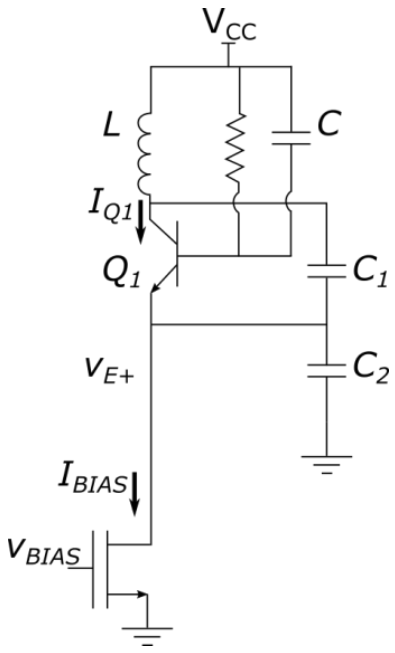

Figure 4.1. A standard single-phase Colpitts oscillator, republished with permission from IEEE, [44].

A standard single-phase Colpitts oscillator is shown in Figure 4.1.

$$i_{Q1+} + \frac{\int_{-\infty}^{t}\left(v_{1+}(\tau) - V_{CC}\right)\partial\tau}{L} + C_{tot}\frac{\partial v_{1+}}{\partial t} = 0\,. \tag{4.1}$$

Differentiating with respect to *t*, equation (4.1) can be rewritten as:

$$\frac{\partial^2 v_+}{\partial t^2} + \frac{\partial i_+}{C_{tot}\partial t} + \frac{v_+(\tau)}{C_{tot}L} = 0\,. \tag{4.2}$$

The collector current can be obtained by making use of the Ebers-Moll equations, large-signal model for bipolar junction transistors. Equation (4.2) can then be rewritten as:

$$\frac{\partial^2 v_+}{\partial t^2} + \frac{\partial\left(I_s\left(\exp\left(\frac{V_{BE}}{V_T}\right) - \frac{1}{\alpha_R}\exp\left(\frac{V_{BC}}{V_T}\right)\right)\right)}{C_{tot}\partial t} + \frac{v_+(\tau)}{C_{tot}L} = 0\,. \tag{4.3}$$

This equation then resembles the Van der Pol equation, which has been extensively studied. Equation (4.3) does not have an explicit closed form solution. It should be noted that the rate of change of phase is frequency. Therefore, the equations were used to generate phase plots, which enabled phase noise calculations to be done, before applying the harmonic balance method, with $v = A\cos(\omega t)$, $\frac{\partial v}{\partial t} = -A\omega\sin(\omega t)$, and $\frac{\partial^2 v}{\partial t^2} = -A\omega^2\cos(\omega t)$. Substituting into (4.3) yields:

$$-A\omega^2\cos(\omega t) + A\left(C_1 \Big/ V_T(C_1 + C_2)\right)\omega\sin(\omega t)\times$$

$$\frac{\left(I_s\exp\left(\frac{V_B}{V_T}\right)\left(\exp\left(\frac{-\left(C_1/(C_1+C_2)\right)A\cos(\omega t)}{V_T}\right)\right)\right)}{C_{tot}} + \frac{A\cos(\omega t)}{C_{tot}L} = 0 \tag{4.4}$$

The Taylor expansion of the exponential function is $\exp(x) = 1 + x + \frac{x^2}{2!} + \frac{x^3}{3!} + \cdots$

$$-A\omega^2\cos(\omega t)+\frac{I_s\exp\left(\frac{V_B}{V_T}\right)A\left(C_1/V_T(C_1+C_2)\right)\omega}{C_{tot}}\sin(\omega t)\times \sum_{n=0}^{\infty}\left(C_1/V_T(C_1+C_2)\frac{-A\cos(\omega t)}{n!}\right)^n+\frac{A\cos(\omega t)}{C_{tot}L}=0. \quad (4.5)$$

The formula for the expansion of the odd and even power cosine is given by (4.9):

$$\cos^{2n+1}(\omega\tau)=\frac{1}{2^{2n}}\sum_{k=0}^{n}\binom{n}{k}\cos\left((2n+1-2k)\theta\right), \quad (4.6)$$

$$\cos^{2n}(\omega\tau)=\frac{1}{2^{2n}}\binom{2n}{n}+\frac{2}{2^{2n}}\sum_{k=0}^{n-1}\binom{2n}{k}\cos\left((2n-2k)\theta\right),. \quad (4.7)$$

Substituting (4.6) and (4.7) into (4.5) yields:

$$-A\omega^2\cos(\omega t)+\frac{I_s\exp\left(\frac{V_B}{V_T}\right)A\left(C_1/V_T(C_1+C_2)\right)\omega}{C_{tot}}\sin(\omega t)\times \sum_{n=0}^{\infty}\left(C_1/V_T(C_1+C_2)\frac{-A\cos(\omega t)}{n!}\right)^n+\frac{A\cos(\omega t)}{C_{tot}L}=0 \quad (4.8)$$

$$\cos^{2n+1}(\omega\tau)=\frac{1}{2^{2n}}\left(\begin{array}{l}\binom{2n+1}{n}\cos(\omega\tau)+\binom{2n+1}{n-1}\cos(3\omega\tau)+\ldots\\ \binom{2n+1}{0}\cos\left((2n+1)\omega\tau\right)\end{array}\right)+, \quad (4.9)$$

$$\cos^{2n}(\omega\tau)=\frac{1}{2^{2n}}\left(\begin{array}{l}\binom{2n}{n}+\\ (2)\left(\binom{2n}{n-1}\cos(2\omega\tau)+\binom{2n}{n-3}\cos(4\omega\tau)+\ldots\binom{2n}{0}\cos\left((2n)\omega\tau\right)\right)\end{array}\right) \quad (4.10)$$

The first harmonic is then equated to zero. The terms $\sin(\omega t)$ and $\cos^{2n+1}(\omega t)$ are both odd terms, with $\cos^{2n}(\omega\tau)$ being an even term. The multiplication of two odd terms results in an even term, and odd terms multiplied by even terms are odd. The first harmonic is under

consideration and therefore the terms containing even and odd terms are considered, in order to simplify the equations.

$$-A\omega^2\cos(\omega t)+\frac{I_s\exp\left(\frac{V_B}{V_T}\right)A\left(C_1\middle/V_T\left(C_1+C_2\right)\right)\omega}{C_{tot}}\sin\left(\omega t\right)\times$$
$$\sum_{n=0}^{\infty}\left(\left(C_1\middle/V_T\left(C_1+C_2\right)\frac{A}{(2n)!}\right)^{2n}\left(\cos\left(\omega t\right)\right)^{2n}\right)+\frac{A\cos\left(\omega t\right)}{C_{tot}L}=0\,. \tag{4.11}$$

Equation (4.11) is effectively an odd function with all even terms being dropped. Substituting equation (4.10) into (4.11) yields:

$$-A\omega^2\cos(\omega t)+\frac{I_s\exp\left(\frac{V_B}{V_T}\right)A\left(C_1\middle/V_T\left(C_1+C_2\right)\right)\omega}{C_{tot}}\sin\left(\omega t\right)\times$$
$$\sum_{n=0}^{\infty}\left(\left(C_1\middle/V_T\left(C_1+C_2\right)\frac{A}{(2n)!}\right)^{2n}\left(\frac{1}{2^{2n}}\left(\binom{2n}{n}+(2)\left(\binom{2n}{n-1}\cos\left(2\omega\tau\right)+\binom{2n}{n-3}\cos\left(4\omega\tau\right)+\ldots\binom{2n}{0}\cos\left((2n)\omega\tau\right)\right)\right)\right)+\frac{A\cos\left(\omega t\right)}{C_{tot}L}=0 \tag{4.12}$$

then

$$-A\omega^2\cos(\omega t)+\frac{I_s\exp\left(\frac{V_B}{V_T}\right)A\left(C_1\middle/V_T\left(C_1+C_2\right)\right)\omega}{C_{tot}}\times$$
$$\sum_{n=0}^{\infty}\left(\left(C_1\middle/V_T\left(C_1+C_2\right)\frac{A}{(2n)!}\right)^{2n}\left(\begin{array}{l}\frac{1}{2^{2n}}\binom{2n}{n}\sin\left(\omega t\right)+\\ \frac{1}{2^{2n-1}}\left(\begin{array}{l}\binom{2n}{n-1}\left(\frac{\sin\left(\omega t-2\omega t\right)+\sin\left(\omega t+2\omega t\right)}{2}\right)+\\ \binom{2n}{n-3}\left(\frac{\sin\left(\omega t-4\omega t\right)+\sin\left(\omega t+4\omega t\right)}{2}\right)+\ldots\\ \binom{2n}{0}\left(\frac{\sin\left(\omega t-(2n)\omega t\right)+\sin\left(\omega t+(2n)\omega\tau\right)}{2}\right)\end{array}\right)\end{array}\right)\right)+\frac{A\cos\left(\omega t\right)}{C_{tot}L}=0 \tag{4.13}$$

The first harmonic of (4.13) can be rewritten as:

$$A\left(\frac{1}{C_{tot}L}-\omega^2\right)\cos(\omega t)+\frac{I_s\exp\left(\frac{V_B}{V_T}\right)\omega}{C_{tot}}\times$$
$$\sum_{n=0}^{\infty}\left(\left(C_1\Big/V_T\left(C_1+C_2\right)\frac{A}{(2n)!}\right)^{2n+1}\left(\frac{1}{2^{2n}}\left(\binom{2n}{n}\sin(\omega t)-\binom{2n}{n-1}\sin(\omega t)\right)\right)\right)=0. \quad (4.14)$$

Then:

$$A\left(\frac{1}{C_{tot}L}-\omega^2\right)\cos(\omega t)+\frac{I_s\exp\left(\frac{V_B}{V_T}\right)\omega}{C_{tot}}\times$$
$$\sum_{n=0}^{\infty}\left(\left(C_1\Big/V_T\left(C_1+C_2\right)\frac{A}{(2n)!}\right)^{2n+1}\left(\frac{1}{2^{2n}}\left(\binom{2n}{n}\frac{1}{(n+1)}\right)\right)\right)\sin(\omega t)=0 \quad (4.15)$$

and finally:

$$A^2\left(\frac{1}{C_{tot}L}-\omega^2\right)^2-\left(\frac{I_s\exp\left(\frac{V_B}{V_T}\right)\omega}{C_{tot}}\right)^2\times$$
$$\left(\sum_{n=0}^{\infty}\left(\left(C_1\Big/V_T\left(C_1+C_2\right)A\right)^{2n+1}\left(\frac{1}{2^{2n}}\frac{1}{\left((2n)!\right)^{2n}(n+1)!n!}\right)\right)\right)^2=0. \quad (4.16)$$

The solution to (4.16) is then further simplified to:

$$-\omega^2\cos(\omega t)+$$
$$\frac{I_s\exp\left(\frac{V_B}{V_T}\right)\omega}{C_{tot}}\times\left(\frac{-1}{I_s\exp\left(\frac{V_B}{V_T}\right)R_P}\sin(\omega t)+\sum_{n=0}^{\infty}\left(K_1\left(K_1\frac{A}{(2n)!}\right)^{2n}\times\left(\frac{1}{2^{2n}}\left(\binom{2n}{n}\sin(\omega t)+\left(K_3+K_4+\ldots K_5\right)\right)\right)\right)\right)$$
$$+\cos(\omega t)\left(\frac{1}{C_{tot}L}\right)=0 \quad (4.17)$$

where $K_3 = \binom{2n}{n-1}\left(\sin(\omega t - 2\omega t) + \sin(\omega t + 2\omega t)\right)$, $K_4 = \binom{2n}{n-3}\left(\sin(\omega t - 4\omega t) + \sin(\omega t + 4\omega t)\right)$, $K_5 = \binom{2n}{0}\left(\sin(\omega t - (2n)\omega t) + \sin(\omega t + (2n)\omega \tau)\right)$, which yields a slight overestimate, assuming V_B is below the bandgap voltage of the process [44].

This is the bias voltage and sets the bias current of the active transistor. For large bias currents, the non-linearity becomes very large and frequency pulling becomes obvious. For V_B greater than the bandgap voltage, the oscillation frequency is predicted to be 1.8% more than the resonant frequency of the tank circuit, which is the oscillation frequency anticipated for an oscillator that is in the voltage-limited region. This point has been demonstrated to yield optimal conditions for phase noise performance in an oscillator. The transistor model is simplified and the base-to-collector current is ignored. This is a valid assumption if the transistor is in the region of being current-limited or in the early voltage-limited area. Under the assumption that the optimal point is selected:

$$\omega \approx \sqrt{\frac{1}{C_{tot} L}} \tag{4.18}$$

The aforementioned being the generally accepted solution. This study diverges from the more general assumptions applied to oscillators, defining the generally accepted procedural methods that led to the design of a low phase noise oscillator. It now demonstrates the key difference between the final modified oscillator and its comparative unmodified counterpart. The impedance and oscillation amplitude can be estimated using section A.1.

The limitation to (4.3) is the assumption that the combination of C_1 and C_2 does not load the tank circuit. This assumption allows the base-emitter voltage to be expressed as a fraction, defined by *n*, of the tank voltage. Therefore, the assumptions are valid for large values of *n*, as well as for small bias currents, where the impedance into the emitter is larger than the tank impedance. The factors that influence phase noise and the assumption that the tank is not significantly loaded by the feedback circuit, led to the incorrect assumption that the oscillation amplitude and bias currents cannot be separated.

The theory states that if the bias current is reduced, the oscillation amplitude must decrease. This result can be verified with most feedback oscillators. The two are in fact not necessarily interdependent, and they can be decoupled if an external current is injected into the emitter of the active transistor. The remaining limitation is that the active device in the oscillator goes into the reverse active region if the oscillation amplitude grows large enough.

Firstly, it will be demonstrated that the assumption that the first harmonic is limited by bias current is not necessarily true. Starting with the circuit in Figure 4.1 and Figure 4.2, another state variable is included in the form of v_E, the emitter voltage. It is assumed that the transistor β is large, and the transistor emitter and collector currents can be interchanged. This is only true if the transistor is in saturation, which could be violated and should be verified not to be so in each specific case. Equation (4.2) can be modified to become:

$$i_{Q1+} + \frac{\int_{-\infty}^{t}\left(v_+(\tau)-V_{CC}\right)\partial\tau}{L} + C_1\frac{\partial\left(v_{1+}-v_E\right)}{\partial t} + \frac{\left(v_+(\tau)-V_{CC}\right)}{R_P} = 0 \tag{4.19}$$

and the additional node added to obtain the following sets of equations:

$$i_E - I_{CONST} - \frac{C_2\partial v_E}{\partial t} - \frac{C_1\partial\left(v_E - v_+\right)}{\partial t} = 0 \tag{4.20}$$

$$2i_{Q1+} + \frac{\int_{-\infty}^{t}\left(v_+(\tau)-V_{CC}\right)\partial\tau}{L} - I_{CONST} - \frac{C_2\partial v_E}{\partial t} + \frac{\left(v_+(\tau)-V_{CC}\right)}{R_P} = 0 \tag{4.21}$$

$$\left(\frac{2I_S\left(-\frac{\partial v_E}{\partial t}\right)}{V_T}\exp\left(\frac{K-v_E}{V_T}\right)\right) - \frac{C_2\partial {v_E}^2}{\left(\partial t\right)^2} + v_+\left(\frac{1}{L}+\frac{1}{R_P}\right) = 0 \tag{4.22}$$

$$v_+ = \left(L \parallel R_P\right)\left(\frac{C_2\partial^2 v_E}{\left(\partial t\right)^2} + \frac{2I_s\left(\frac{\partial v_E}{\partial t}\right)}{V_T}\exp\left(\frac{K-v_E}{V_T}\right)\right) \tag{4.23}$$

$$\frac{\partial v_E}{\partial t}\left(C_1+C_2\right) = C_1\frac{\partial v_1}{\partial t} + I_S\exp\left(\frac{V_B - v_E}{V_T}\right) - I_{CONST} \tag{4.24}$$

.

To solve for the new variables, (4.22) and (4.23) are solved. The solution to (4.22) was approached in a similar fashion as before. The solution of (4.23) is assumed to have the form:

$v_E = A_1\cos(\omega t) + A_2\cos(2\omega t)$ and $v_1 = A\cos(\omega t)$, and I_{CONST} is set by the bias conditions. Substituting these values into (4.24) and (4.32) and then solving simultaneously for the variables A_1, A_2, ω, and A lead to the following set of equations:

$$\begin{aligned}
&\left(-A_1\omega\sin(\omega t) - A_2 2\omega\sin(2\omega t)\right)\left(C_1 + C_2\right) = \\
&-C_1 A\omega\sin(\omega) - I_{CONST} + \\
&I_s\exp\left(\frac{V_B}{V_T}\right)\left(1 + \frac{A_1^2}{4V_T^2} + \frac{A_2^2}{4V_T^2} - \frac{A_1^2 A_2}{8V_T^3}\right) + \\
&I_s\exp\left(\frac{V_B}{V_T}\right)\left(\frac{A_1^2 A_2^2}{8V_T^4} + \frac{A_1 A_2}{2V_T^2} - \frac{A_1}{V_T} - \frac{A_1 A_2^2}{4V_T^3}\right)\cos(\omega t) + \\
&I_s\exp\left(\frac{V_B}{V_T}\right)\left(\frac{A_1^2 A_2^2}{8V_T^4} + \frac{A_1^2}{4V_T^2} + - \frac{A_2}{V_T} - \frac{A_1^2 A_2}{4V_T^3}\right)\cos(2\omega t)
\end{aligned} \tag{4.25}$$

which lead to three separate equations:

$$I_s\exp\left(\frac{V_B}{V_T}\right)\left(1 + \frac{A_1^2}{4V_T} + \frac{A_2^2}{4V_T} - \frac{A_1^2 A_2}{8V_T^2}\right) - I_{CONST} = 0 \tag{4.26}$$

$$\left(C_1 A\omega - \left(C_1 + C_2\right)A_1\omega\right) = \left(I_s\exp\left(\frac{V_B}{V_T}\right)\left(\frac{A_1^2 A_2^2}{8V_T^4} + \frac{A_1 A_2}{2V_T^2} - \frac{A_1}{V_T} - \frac{A_1 A_2^2}{4V_T^3}\right)\right) \tag{4.27}$$

$$i_{Q1+} + \frac{\int_{-\infty}^{t}\left(v_+(\tau) - V_{CC}\right)\partial\tau}{L} + C_1\frac{\partial\left(v_{1+} - v_E\right)}{\partial t} + \frac{\left(v_+(\tau) - V_{CC}\right)}{R_P} = 0 \tag{4.28}$$

$$I_s\exp\left(\frac{V_B}{V_T}\right)\left(\frac{A_1^2 A_2^2}{8V_T^4} + \frac{A_1^2}{4V_T^2} + - \frac{A_2}{V_T} - \frac{A_1^2 A_2}{4V_T^3}\right)\cos(2\omega t) = -A_2 2\omega\sin(2\omega t)\left(C_1 + C_2\right). \tag{4.29}$$

Equations (4.26) to (4.29) are only valid for small values of A_1 and A_2. The error in the truncated exponential function also results in large errors when using (4.28) and (4.29) to estimate the oscillation frequency. However, the equations do provide a basis for the estimation of the ratio of A_1/A_2. The result from (4.30) shows that the average current into the emitter is a function of the emitter voltage, not just the bias current. Increasing the feedback voltage will increase the average current and the associated shot noise. The first harmonic of the collector current is not limited by the bias current, and will continue to increase as the emitter feedback voltage is

increased. To investigate the oscillation frequency more accurately, (4.29) is considered. The equation can be expanded using (4.30). The exponential term is separated into even and odd components as before. The result is given by (4.31).

$$\left(\frac{A}{L \parallel R_P} + C_2 A_1 \omega^2\right)\cos(\omega t) =$$
$$P\omega\left(\left(A_1(T_1T_2)\right) + \left(A_2T_2T_3\right) - A_2T_4T_1 - A_2T_5T_1 - \left(\frac{A_1}{4}\right)T_6T_4 + \left(\frac{A_1}{4}\right)T_6T_5\right)\sin(\omega t) + \tag{4.30}$$
$$P\omega\left(\frac{A_2}{2}T_6T_4 + \frac{A_2}{2}T_6T_5 - A_2 2T_2^2 + \left(\frac{A_1}{2}T_1T_3\right) - \frac{A_1}{2}T_4T_2 - \frac{A_1}{2}T_5T_2\right)\sin(2\omega t)$$

with the coefficients defined by:

$$T_1 = \sum\left(\frac{{A_1}^{2n}}{2^{2n}\left((2n)!V_T\right)^{2n}}\binom{2n}{n}\left(\frac{1}{n+1}\right)\right),\ T_2 = \sum\frac{{A_1}^{2n}}{2^{2n}\left((2n)!V_T\right)^{2n}}\binom{2n}{n},\ T_{3=}\sum\frac{{A_1}^{2n}}{2^{2n}\left((2n)!V_T\right)^{2n}}\left(\binom{2n+1}{n}\right),$$

$$T_4 = \sum_{n=0}^{\infty}\left(\left(A_1/(2n+1)!V_T\right)^{2n+1}\frac{1}{2^{2n}}\left(\binom{2n+1}{n}\right)\right),\ T_5 = \sum_{n=0}^{\infty}\left(\left(A_1/(2n+1)!V_T\right)^{2n+1}\frac{1}{2^{2n}}\binom{2n+1}{n-1}\right), \text{ and}$$

$$T_6 = \sum_{n=0}^{\infty}\left(\left(A_1/(2n+1)!V_T\right)^{2n+1}\frac{1}{2^{2n}}\left(\binom{2n}{n}\left(\frac{4n+2}{(n+1)(n+2)}\right)\right)\right)$$

The result of the analysis is that the amplitude of A_1 relative to A, the oscillation amplitude, is not equal to $A\left(\frac{C_2}{C_2+C_1}\right)$.

$$\left(\frac{A}{L \parallel R_P} + C_2 A_1 \omega^2\right)\cos(\omega t) =$$
$$P\omega\left(\left(A_1(T_1T_2)\right) + \left(A_2T_2T_3\right) - A_2T_4T_1 - A_2T_5T_1 - \left(\frac{A_1}{4}\right)T_6T_4 + \left(\frac{A_1}{4}\right)T_6T_5\right)\sin(\omega t) + \tag{4.31}$$
$$P\omega\left(\frac{A_2}{2}T_6T_4 + \frac{A_2}{2}T_6T_5 - A_2 2T_2^2 + \left(\frac{A_1}{2}T_1T_3\right) - \frac{A_1}{2}T_4T_2 - \frac{A_1}{2}T_5T_2\right)\sin(2\omega t)$$

Equation (4.31) may be used to predict the oscillation frequency as well as the values of A_1 and A_2, the amplitude of the first and second harmonic component of the oscillator. Increasing the ratio $\left(\frac{C_2}{C_2+C_1}\right)$ will increase the amplitude of the first harmonic of the collector current, if the

tank circuit is not significantly loaded, which is not true for the general oscillator. The structure must be modified to allow the tank loading to be decoupled from the feedback ratio.

The results show that if a small loop gain can be set to ensure the initialisation of the oscillation, the average collector current can be reduced after oscillation begins, or if the closed loop gain is increased, the bias current can be reduced by almost the same factor. Equation (4.31) shows that for large quality factors, the oscillation frequency will decrease rapidly as the number of harmonics in the feedback voltage is increased. The number of harmonics in the feedback voltage is not related to the number of harmonics present in the tank, but rather the amplitude of the feedback voltage. A shooting balance method is used to check the accuracy of the numerical estimations presented in this work, in Addendum A (section A.2).

4.1.2 Differential Colpitts oscillator

The single-phase Colpitts oscillator was modified. Two tank circuits were coupled and forced to oscillate out of phase. The modification is shown in Figure 4.2.

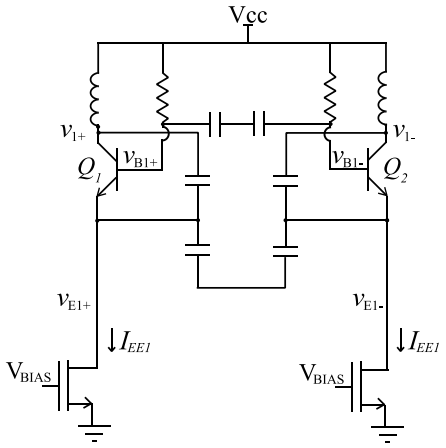

Figure 4.2. Differential Colpitts oscillator, republished with permission from IEEE, [44].

The two coupled single-phase Colpitts oscillators in Figure 4.2 are identical. Nodal analysis leads to (4.32) and (4.33):

$$v_{E1+} + v_{B1+} - v_{B1-} + v_{E1-} = 0\,, \tag{4.32}$$

$$v_{B1+} - v_{E1+} = V_T \ln\left(\frac{i_{C1+}}{I_{S1}}\right), \tag{4.33}$$

where i_{C1+} is the collector current of Q_1. I_{S1} is the saturation current. V_T is the thermal voltage, v_{B1+} and v_{B1-} are the base voltages of Q_1 and Q_2 respectively. Then applying the same steps as before, it can be shown that:

$$\left(i_{C1+} - i_{C1-}\right) + \frac{\int_{-\infty}^{t}\left(v_{1+}(\tau) - v_{1-}(\tau)\right)\partial\tau}{L} + C_{tot}\frac{\partial\left(v_{1+} - v_{1-}\right)}{\partial t} + \left(i_{2+} - i_{2-}\right) = 0 \tag{4.34}$$

The collector current is set by the base emitter voltage of the particular transistor. The currents can be further expanded and the result is shown in (4.35):

$$\frac{\partial\left(-I_s \exp\left(\frac{V_{B+}}{V_t}\right)\left(\sinh\left(\frac{-\left(\frac{C_2}{C_1+C_2}v_{1D}\right)}{2V_t}\right)\right)\right)}{\partial t} + \frac{v_{1D}}{L} + C_{tot}\frac{\partial^2 v_{1D}}{\partial t^2} = 0 \tag{4.35}$$

where v_{1D} is the differential voltage across both tank circuits. Then, applying the partial derivative, it can be shown that:

$$\frac{\partial^2 v_{1D}}{\partial t^2} + \frac{\left(-I_s \exp\left(\frac{V_{B+}}{V_t}\right)\left(\cosh\left(\frac{-\left(\frac{C_2}{C_1+C_2}v_{1D}\right)}{2V_t}\right)\right)\right)}{\partial t C_{tot}} \times \left(\frac{-\left(\frac{C_2}{C_1+C_2}\right)}{2V_t}\right)\left(\frac{\partial v_{1D}}{\partial t}\right) + \frac{v_{1D}}{C_{tot}L} = 0 \tag{4.36}$$

The system is expanded as a set of first-order differential equations:

$$\frac{\partial v_{1D}}{\partial t} = x_1 \tag{4.37}$$

$$\frac{\partial x_1}{\partial t} = Q.K\left(\cosh\left(K v_{1D\angle G}\right)\right) \times \left(x_{1\angle G}\right) - \frac{v_{1D}}{C_{tot}L} \tag{4.38}$$

where $Q = \frac{-I_s \exp\left(\frac{V_{B+}}{V_t}\right)}{C_{tot}}$, $K = \left(\frac{-\left(\frac{C_2}{C_1 + C_2}\right)}{2V_t} \right)$; by using these equations a numerical solution for the differential equation can be derived. The equation can also be used directly to generate phase plots for the system. An approximate closed form solution defining the oscillation frequency and amplitude can be derived, using the same harmonic balance technique given in the previous section.

4.1.3 Multiphase Colpitts oscillator

The results of the previous section were expanded to the final circuit form for the generation of a low-noise multiphase oscillator. There was only a subtle difference between the circuit that was presented with the modification and the unmodified multiphase Colpitts oscillator. This circuit structure was the conceptual expansion of the standard Colpitts oscillator to a form capable of generating quadrature oscillations. The second difference in the structure of a conventional Colpitts oscillator and differential Colpitts oscillator was the separation of the tail current branches specific to each tank circuit within the oscillator system. The currents of two differential Colpitts oscillators were cross-coupled in order to enable the generation of a quadrature oscillator. When the two differential tank circuits were coupled, the result was a 90° shift in the differential voltages and four oscillations that were separated by equal phases were generated. The modified Colpitts oscillator is shown in Figure 4.3. An additional gain stage was introduced into the feedback loop. This enabled the alteration of the start-up conditions associated with the Colpitts oscillator.

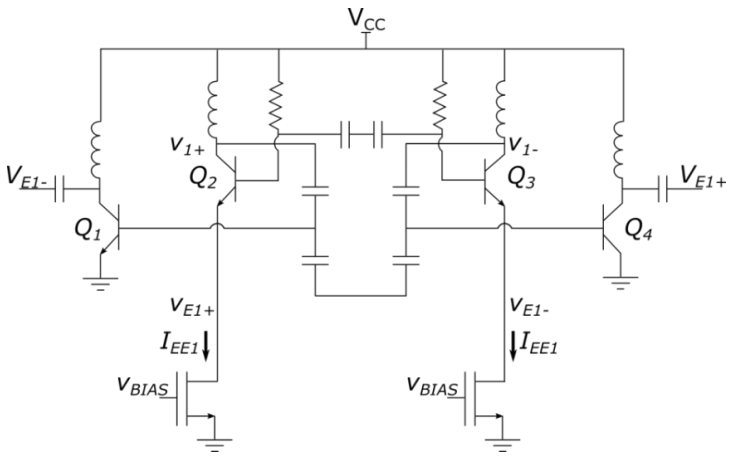

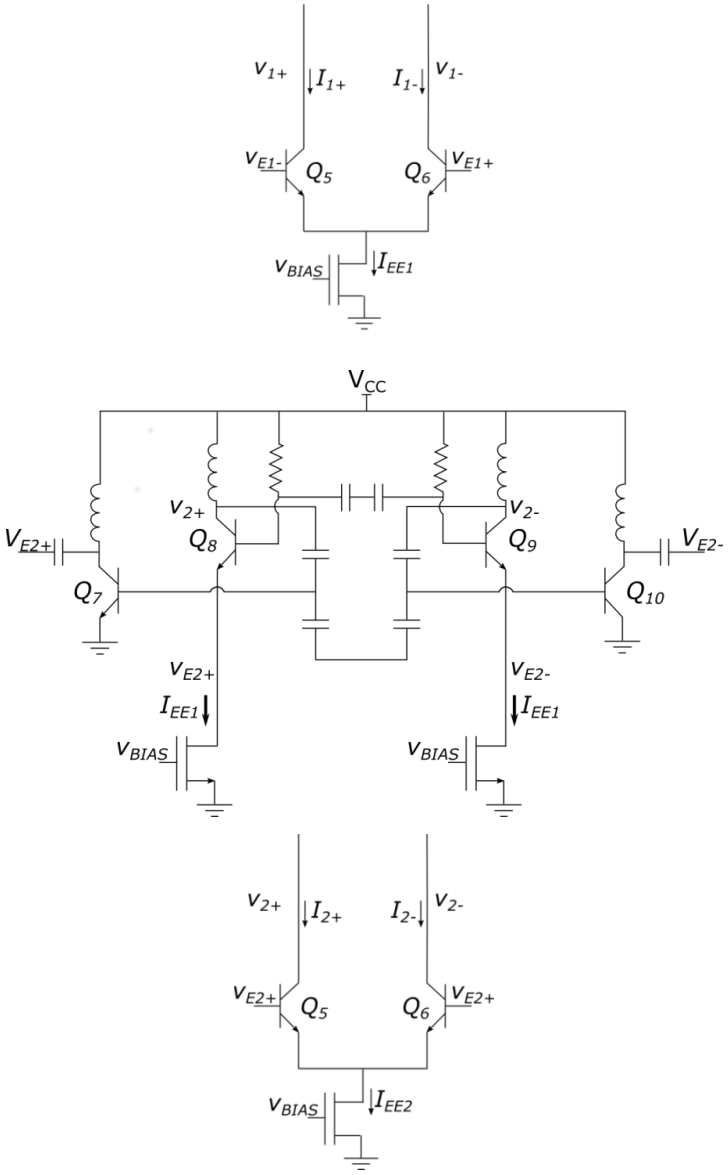

Figure 4.3. Modified multiphase Colpitts oscillator, republished with permission from IEEE, [44].

$$-v_{E1+} + v_{B1+} - v_{B2-} + v_{E2-} = 0, \tag{4.39}$$

$$v_{B1+} - v_{E1+} = V_t \ln\left(\frac{i_{C1+}}{I_{S1}}\right), \tag{4.40}$$

$$v_{B1-} - v_{E1-} = V_t \ln\left(\frac{i_{C1-}}{I_{S1}}\right), \tag{4.41}$$

$$\frac{\partial\left(v_{E+}-v_{E-}\right)}{\partial t}=\frac{\partial\left(2v_{E+}\right)}{\partial t}, \tag{4.42}$$

then:

$$i_{C1+}-i_{C1-}=-I_s\exp\left(\frac{V_{B+}}{V_t}\right)\left(\sinh\left(f\left(2v_{E+}\right)\right)\right), \tag{4.43}$$

where $v_{DE1}=v_{E1+}-v_{E1-}$, and $\left(f\left(\bullet\right)\right)$ is the transfer function of the gain stage in the feedback loop of Figure 4.3. It is (4.39) that guarantees the phase shift between the two complementary tank circuits.

If Kirchhoff's Current Law is applied to the four tank circuits, the following equations can be derived:

$$i_{C1+}+\frac{\int_{-\infty}^{t}\left(v_{1+}\left(\tau\right)-V_{CC}\right)\partial\tau}{L}+C_{tot}\frac{\partial v_{1+}}{\partial t}+i_{2+}=0, \tag{4.44}$$

$$i_{C1-}+\frac{\int_{-\infty}^{t}\left(v_{1-}\left(\tau\right)-V_{CC}\right)\partial\tau}{L}+C_{tot}\frac{\partial v_{1-}}{\partial t}+i_{2-}=0, \tag{4.45}$$

$$i_{C2+}+\frac{\int_{-\infty}^{t}\left(v_{2+}\left(\tau\right)-V_{CC}\right)\partial\tau}{L}+C_{tot}\frac{\partial v_{2+}}{\partial t}+i_{1-}=0, \tag{4.46}$$

$$i_{C2-}+\frac{\int_{-\infty}^{t}\left(v_{2-}\left(\tau\right)-V_{CC}\right)\partial\tau}{L}+C_{tot}\frac{\partial v_{2-}}{\partial t}+i_{1+}=0. \tag{4.47}$$

Taking note of the difference between equation (4.44) and (4.45), the following equation is defined:

$$\left(i_{C1+}-i_{C1-}\right)+\frac{\int_{-\infty}^{t}\left(v_{1+}\left(\tau\right)-v_{1-}\left(\tau\right)\right)\partial\tau}{L}+C_{tot}\frac{\partial\left(v_{1+}-v_{1-}\right)}{\partial t}+\left(i_{2+}-i_{2-}\right)=0. \tag{4.48}$$

Taking note of the difference between equation (4.46) and (4.47), the following equation is derived:

$$\left(i_{C2+}-i_{C2-}\right)+\frac{\int_{-\infty}^{t}\left(v_{2+}\left(\tau\right)-v_{2-}\left(\tau\right)\right)\partial\tau}{L}+C_{tot}\frac{\partial\left(v_{2+}-v_{2-}\right)}{\partial t}+\left(i_{1-}-i_{1+}\right)=0 \qquad (4.49)$$

It is clear that the collector currents are a function of the base and emitter voltages of the respective transistors. The circuit was designed to enable the feedback voltages at the base of transistors Q_2, Q_3, Q_8, and Q_9 to be smaller than 50 mV, which enabled small-signal linear analysis of the gain to be applied. The modification improved the phase noise performance by exploiting several different facts. The bias currents required to ensure the start-up of the oscillators were reduced, and a very low power oscillator was realised. The ratio of the capacitors C_1 and C_2 may be increased by approximately the same factor as the gain added to the feedback loop. The loaded quality factor of the tank circuit was improved. The cross-coupled voltages remained equivalent to the unmodified system, leaving the harmonic content of the tank circuit unaffected. The current injections into the tank circuit were optimum in terms of the ½π shift between the current and voltage. The noise contribution to the tank circuit was reduced by careful selection of the gain block parameters. The remaining noise components were set by the specific process and the quality of the passive components.

Therefore, the objective of the proposed modifications was to improve every aspect identified to have an influence on the oscillators' phase noise performance, except for device and component level optimisations. The gain of the transistors Q_1, Q_4, Q_7, and Q_{10} was set to 18 dB. The following equations then define the emitter voltages:

$$v_{E1+}=-8.5\left(\frac{C_2}{C_2+C_1}\right)v_{1-}\angle G, \qquad (4.50)$$

$$v_{E1-}=-8.5\left(\frac{C_2}{C_2+C_1}\right)v_{1+}\angle G, \qquad (4.51)$$

$$v_{E2+}=-8.5\left(\frac{C_2}{C_2+C_1}\right)v_{2-}\angle G, \qquad (4.52)$$

$$v_{E2-}=-8.5\left(\frac{C_2}{C_2+C_1}\right)v_{2+}\angle G, \qquad (4.53)$$

where $\angle G$ is the phase shift associated with the gain stage. If equations (4.48) and (4.49) are differentiated with respect to *t*, then the following equations are derived:

$$\frac{\partial i_{CD1}}{\partial t}+\frac{v_{1D}}{L}+C_{tot}\frac{\partial^2 v_{1D}}{\partial t^2}+\frac{\partial i_{2D}}{\partial t}=0 \tag{4.54}$$

$$\frac{\partial i_{CD2}}{\partial t}+\frac{v_{2D}}{L}+C_{tot}\frac{\partial^2 v_{2D}}{\partial t^2}-\frac{\partial i_{1D}}{\partial t}=0 \tag{4.55}$$

where $i_{CD1}=i_{C1+}-i_{C1-}$, $i_{CD2}=i_{C2+}-i_{C2-}$, $v_{1D}=v_{1+}-v_{1-}$, $v_{2D}=v_{2+}-v_{2-}$, $i_{1D}=i_{1+}-i_{1-}$, and $i_{2D}=i_{2+}-i_{2-}$. Then substituting (4.43) into (4.55), results in (4.56) as:

$$\frac{\partial\left(-I_s\exp\left(\frac{V_{B+}}{V_t}\right)\left(\sinh\left(\frac{-\left(\frac{8.5C_2}{C_1+C_2}\angle G v_{1D}\right)}{2V_t}\right)\right)\right)}{\partial t}+\frac{v_{1D}}{L}+C_{tot}\frac{\partial^2 v_{1D}}{\partial t^2}+\frac{\partial i_{2D}}{\partial t}=0, \tag{4.56}$$

$$\frac{\partial\left(-I_s\exp\left(\frac{V_{B+}}{V_t}\right)\left(\sinh\left(\frac{-\left(\frac{8.5C_2}{C_1+C_2}\angle G v_{2D}\right)}{2V_t}\right)\right)\right)}{\partial t}+\frac{v_{2D}}{L}+C_{tot}\frac{\partial^2 v_{2D}}{\partial t^2}-\frac{\partial i_{1D}}{\partial t}=0 \tag{4.57}$$

By comparing the currents $i_{1+}-i_{1-}$ and $i_{2+}-i_{2-}$, it is evident that differential currents can be defined by the following equations:

$$i_{1+}-i_{1-}=\alpha_F I_{EE2}\tanh\left(\frac{-\left(v_{E1+}-v_{E1-}\right)}{2V_t}\right), \tag{4.58}$$

$$i_{2+}-i_{2-}=\alpha_F I_{EE2}\tanh\left(\frac{-\left(v_{E2+}-v_{E2-}\right)}{2V_t}\right). \tag{4.59}$$

Finally, (4.60) and (4.61) were derived from the previous equations:

$$\frac{\partial\left(-I_s\exp\left(\frac{V_{B+}}{V_t}\right)\left(\sinh\left(\frac{-\left(\frac{8.5C_2}{C_1+C_2}\angle Gv_{1D}\right)}{2V_t}\right)\right)\right)}{\partial t}+\frac{v_{1D}}{L}+C_{tot}\frac{\partial^2 v_{1D}}{\partial t^2}$$
$$+\frac{\partial\left(\alpha_F I_{EE1}\tanh\left(\frac{-\left(\frac{8.5C_2}{C_1+C_2}\angle Gv_{2D}\right)}{2V_t}\right)\right)}{\partial t}=0, \quad (4.60)$$

$$\frac{\partial\left(-I_s\exp\left(\frac{V_{B+}}{V_t}\right)\left(\sinh\left(\frac{-\left(\frac{8.5C_2}{C_1+C_2}\angle Gv_{2D}\right)}{2V_t}\right)\right)\right)}{\partial t}+\frac{v_{2D}}{L}+C_{tot}\frac{\partial^2 v_{2D}}{\partial t^2}$$
$$-\frac{\partial\left(\alpha_F I_{EE1}\tanh\left(\frac{-\left(-\frac{8.5C_2}{C_1+C_2}\angle Gv_{2D}\right)}{2V_t}\right)\right)}{\partial t}=0. \quad (4.61)$$

Equations (4.60) and (4.61) were restructured to give the following equations:

$$\frac{\partial^2 v_{1D}}{\partial t^2}+\frac{\partial\left(-I_s\exp\left(\frac{V_{B+}}{V_t}\right)\left(\sinh\left(\frac{-\left(\frac{8.5C_2}{C_1+C_2}\angle Gv_{1D}\right)}{2V_t}\right)\right)\right)}{\partial t C_{tot}}+\frac{v_{1D}}{C_{tot}L}$$
$$+\frac{\partial\left(\alpha_F I_{EE1}\tanh\left(\frac{-\left(\frac{8.5C_2}{C_1+C_2}\angle Gv_{2D}\right)}{2V_t}\right)\right)}{\partial t\times C_{tot}}=0, \quad (4.62)$$

$$\frac{\partial^2 v_{2D}}{\partial t^2}+\frac{\partial\left(-I_s\exp\left(\frac{V_{B+}}{V_t}\right)\left(\sinh\left(\frac{-\left(\frac{8.5C_2}{C_1+C_2}\angle Gv_{2D}\right)}{2V_t}\right)\right)\right)}{\partial tC_{tot}}+\frac{v_{2D}}{C_{tot}L}$$
$$-\frac{\partial\left(\alpha_F I_{EE1}\tanh\left(\frac{-\left(-\frac{8.5C_2}{C_1+C_2}\angle Gv_{1D}\right)}{2V_t}\right)\right)}{\partial tC_{tot}}=0 \quad (4.63)$$

.

Then, applying the chain rule to the second term in both equations (4.62) and (4.63), the following equations were defined:

$$\frac{\partial^2 v_{1D}}{\partial t^2}+\frac{\left(-I_s\exp\left(\frac{V_{B+}}{V_t}\right)\left(\cosh\left(\frac{-\left(\frac{8.5C_2}{C_1+C_2}\angle Gv_{1D}\right)}{2V_t}\right)\right)\right)}{\partial tC_{tot}}\times\left(\frac{-\left(\frac{8.5C_2}{C_1+C_2}\angle G\right)}{2V_t}\right)\left(\frac{\partial v_{1D}}{\partial t}\right)$$
$$+\frac{\alpha_F I_{EE1}}{C_{tot}}\left(1-\tanh^2\left(\frac{-\left(\frac{8.5C_2}{C_1+C_2}\angle Gv_{2D}\right)}{2V_t}\right)\right)\left(\left(-\frac{8.5C_2}{C_1+C_2}\angle G\right)\times\left(\frac{\partial v_{2D}}{\partial t}\right)+\frac{v_{1D}}{C_{tot}L}=0\right) \quad (4.64)$$

$$\frac{\partial^2 v_{2D}}{\partial t^2}+\frac{\left(-I_s\exp\left(\frac{V_{B+}}{V_t}\right)\left(\cosh\left(\frac{-\left(\frac{8.5C_2}{C_1+C_2}\angle Gv_{2D}\right)}{2V_t}\right)\right)\right)}{\partial tC_{tot}}\left(\frac{-\left(\frac{8.5C_2}{C_1+C_2}\angle G\right)}{2V_t}\right)\times\left(\frac{\partial v_{2D}}{\partial t}\right)$$

$$+\left(\frac{\alpha_F I_{EE1}}{C_{tot}}\right)\left(\tanh^2\left(\frac{-\left(-\frac{8.5C_2}{C_1+C_2}\angle Gv_{1D}\right)}{2V_t}\right)-1\right)\times\left(\frac{-\left(-\frac{8.5C_2}{C_1+C_2}\angle G\right)}{2V_t}\right)\times\left(\frac{\partial v_{1D}}{\partial t}\right) \tag{4.65}$$

$$+\frac{v_{2D}}{C_{tot}L}=0$$

defining $K=\frac{8.5C_2}{2V_t\left(C_1+C_2\right)}$, $A=\frac{2\alpha_F I_{EE2}}{C_{tot}}, B\Rightarrow\frac{\alpha_F I_{EE1}}{C_{tot}}=P.A$, $x_1=\frac{\partial v_{1D}}{\partial t}, x_2=\frac{\partial v_{2D}}{\partial t}$, $Q=-I_s\exp\left(\frac{V_{B+}}{V_t}\right)$:

$$\frac{\partial v_{1D}}{\partial t}=x_1 \tag{4.66}$$

$$\frac{\partial v_{2D}}{\partial t}=x_2 \tag{4.67}$$

$$\frac{\partial x_1}{\partial t}=Q.K\left(\cosh\left(Kv_{1D\angle G}\right)\right)\times\left(x_{1\angle G}\right)+ \tag{4.68}$$

$$P.A.K\left(1-\tanh^2\left(Kv_{2D\angle G}\right)\right)\times\left(x_{2\angle G}\right)-\frac{v_{1D}}{C_{tot}L},$$

$$\frac{\partial x_2}{\partial t}=Q.K\left(\cosh\left(Kv_{2D\angle G}\right)\right)\times\left(x_{2\angle G}\right)+ \tag{4.69}$$

$$P.A.K\left(\tanh^2\left(Kv_{1D\angle G}\right)-1\right)\times\left(x_{1\angle G}\right)-\frac{v_{2D}}{C_{tot}L}.$$

The function v_{2D} was defined as a forcing function. The solution of v_{2D} was of the form: $v_{2D}=A_1\cos\left(\varpi t+\theta_1\right)$. Higher order terms were omitted to allow for the solution to remain tractable, but may be included if greater accuracy is required. The amplitude of higher order harmonics was limited by the tank impedance, and larger Q inductors will be accurately

represented. $v_{2D\angle G}$ was then given as: $v_{2D\angle G} = A_1 \cos(\varpi t + \theta_1 + \angle G)$. The period of oscillation remains unknown, and $x_2 = -A_1 \omega \sin(\omega t + \theta_1 + \angle G)$.

$$\frac{\partial^2 v_{1D}}{\partial t^2} + Q.K\left(\cosh\left(Kv_{1D\angle G}\right)\right)\times\left(x_{1\angle G}\right)\times\left(\frac{\partial v_{1D}}{\partial t}\right) + \frac{v_{1D}}{C_{tot}L} = P.A.K\left(1-\tanh^2\left(Kv_{2D\angle G}\right)\right)\times\left(x_{2\angle G}\right), \tag{4.70}$$

The Taylor expansion for $\tanh(x)$ is $x - \frac{x^3}{3} + \frac{2x^5}{15} + \ldots$. It was apparent that the phase shift introduced by the gain component in the feedback loop can be included as:

$$V_{2D\angle G} = A_1 \cos(\angle G)\cos(\varpi t + \theta_1) - A_1 \sin(\angle G)\sin(\varpi t + \theta_1). \tag{4.71}$$

If the phase shift caused by the gain component is assumed to be small, then the above equation can be simplified to $v_{2D\angle G} \approx v_{2D}$. The function $\tanh(Kv_{2D\angle G})$ can be expressed as: $Kv_{2D} - \frac{Kv_{2D}{}^3}{3} + \frac{2Kv_{2D}{}^5}{15} + \ldots$. The function can then be approximated using only the first term Kv_{2D}. Applying this to the above equations, it is given that:

$$\frac{\partial^2 v_{1D}}{\partial t^2} + Q.K\left(1 + \frac{Kv_{1D}{}^2}{2}\right)\times\left(\frac{\partial v_{1D}}{\partial t}\right) + \frac{v_{1D}}{C_{tot}L} = P.A.K\left(1 - Kv_{2D}\right)\times\left(\frac{\partial v_{2D}}{\partial t}\right), \tag{4.72}$$

$$\frac{\partial^2 v_{2D}}{\partial t^2} + Q.K\left(1 + \frac{Kv_{2D}{}^2}{2}\right)\times\left(\frac{\partial v_{2D}}{\partial t}\right) + \frac{v_{2D}}{C_{tot}L} = P.A.K\left(Kv_{1D} - 1\right)\times\left(\frac{\partial v_{1D}}{\partial t}\right). \tag{4.73}$$

The system can then be described by the following equations:

$$\frac{\partial v_{1D}}{\partial t} = x_1 \tag{4.74}$$

$$\frac{\partial v_{2D}}{\partial t} = x_2 \tag{4.75}$$

$$\frac{\partial x_1}{\partial t} = Q.K\left(1 + \frac{Kv_{1D}{}^2}{2}\right)\times\left(x_1\right) - \frac{v_{1D}}{C_{tot}L} + P.A.K\left(1 - Kv_{2D}\right)\times\left(x_2\right), \tag{4.76}$$

$$\frac{\partial x_2}{\partial t} = Q.K\left(1+\frac{Kv_{2D}{}^2}{2}\right)\times(x_2) - \frac{v_{2D}}{C_{tot}L} + P.A.K\left(Kv_{1D}-1\right)\times(x_1). \tag{4.77}$$

The above equations can be rewritten as follows:

$$\frac{\partial x_1}{\partial t} = Q.K\left(1+\frac{Kv_{1D}{}^2}{2}\right)\times(x_1) - \frac{v_{1D}}{C_{tot}L} + \tag{4.78}$$

$$P.A.K\left(1-K\left(A_1\cos(\varpi t+\theta_1)+A_3\cos(3\omega t+\theta_3)\right)\right)\times$$

$$\left(-A_1\omega\sin(\omega t+\theta_1)-A_3 3\omega\sin(3\omega t+\theta_3)\right).$$

Then the solution to the above equation is given as:

$v_{1D} = A_1\cos(\varpi t+\theta_1+\theta_x)+A_3\cos(3\omega t+\theta_3+\theta_x)$,

$x_1 = -A_1\omega\sin(\omega t+\theta_1+\theta_x)-A_3\omega\sin(3\omega t+\theta_3+\theta_x)$, and

$$\frac{\partial x_1}{\partial t} = -A_1\omega^2\cos(\omega t+\theta_1+\theta_x)-A_3 9\omega^2\cos(3\omega t+\theta_3+\theta_x).$$

$$-A_1\omega^2\cos(\omega t+\theta_1+\theta_x)-A_3 9\omega^2\cos(3\omega t+\theta_3+\theta_x) \tag{4.79}$$

$$+A.K\left(1-K\left(A_1\cos(\varpi t+\theta_1+\theta_x)+A_3\cos(3\omega t+\theta_3+\theta_x)\right)\right)\times$$

$$\left(-A_1\omega\sin(\omega t+\theta_1+\theta_x)-A_3\omega\sin(3\omega t+\theta_3+\theta_x)\right)=$$

$$+\frac{A_1\cos(\varpi t+\theta_1+\theta_x)+A_3\cos(3\omega t+\theta_3+\theta_x)}{c_{tot}L}=$$

$$P.A.K\left(1-K\left(A_1\cos(\varpi t+\theta_1)+A_3\cos(3\omega t+\theta_3)\right)\right)$$

$$\times\left(-A_1\omega\sin(\omega t+\theta_1)-A_3 3\omega\sin(3\omega t+\theta_3)\right)$$

The analysis presented up to this point enabled the calculation of the phase portraits for each specific case. To compare the proposed circuit modifications, it was necessary to perform a comparison against a more standard configuration, using ideal component models. The oscillation frequency was roughly set as the maximum tank circuits' impedance. The bias currents and voltages were set to ensure oscillation started up and that the oscillator was biased on the verge of being voltage-limited. A set of difference equations were then defined using the approach in (4.44) to (4.47). Any number of numerical algorithms may be used to solve for the

time evolution of the systems' state variables at discrete time steps. The algorithm presented in the previous section was applied to calculate the system's phase noise estimates.

The presentation here is based on a reduced state space. The system was reduced to ensure that it was invertible and expressed in a standard form that enabled the application of standard numerical techniques. The noise sources were translated to the circuit nodes of interest, by applying the specific translation to the required circuit node. The transient analysis was performed using a Runge-Kutta estimation of the differential equation. The system was also solved using a shooting balance technique. This method solved for the Hessian of the system directly and allowed the additional step of calculating the first Floquet multipliers' eigenvector to be skipped in the algorithm presented. Further harmonic balance methods were not presented in this work, although the truncated analytical approach that was used above was based on this premise. The noise modification function over the period of the oscillators' stable limit cycle was then calculated. Figure 4.4 shows the transient analysis of the modified multiphase Colpitts oscillator presented in Figure 4.3.

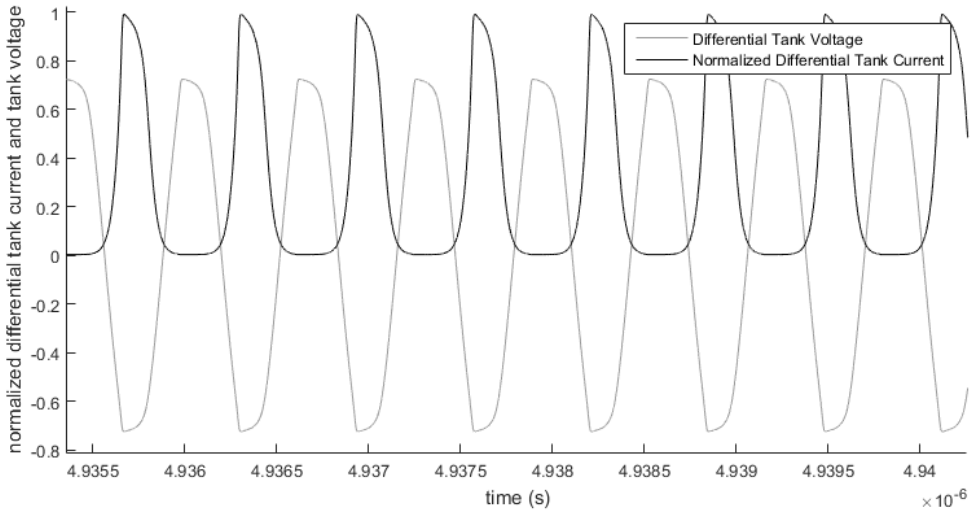

Figure 4.4. Differential tank voltage and normalised differential tank current, section A.4

A Monte-Carlo simulation of the transient circuit is presented in Figure 4.4 for both the proposed circuit modifications and the unmodified multiphase oscillator. Noise was generated using a wideband noise source, then modified to have the correct spectral density. The noise was then added in at the representative circuit node with the circuit parameters performing the natural filtering. Figure 4.5 shows the spectrum of the oscillator's output. The relative change in the

noise spread is apparent in the figure. It is interesting to note that the power at the harmonic remained unaltered, but the noise floor of the system was raised by an average of 4 dB.

The way in which the noise influenced the phase response of the system was demonstrated in the system's phase portrait. The differential tank circuit was used as the observation point. The tank voltage and the first derivative, the tank current, were then plotted in Figure 4.6. The interesting point to observe is the change in sensitivity of the phase portrait as the oscillator rotates through the limit cycle. The phase portrait deviated most from the stable limit cycle at the point when the tank voltage had a zero crossing, and was least sensitive when the tank voltage passed through its peak.

The noise modulation function then changed the influence of the noise sources over the period of the oscillator. The shot noise of the injection current from the transistor dominated the noise sources, and was controlled to be at points where the system was least sensitive to the noise to phase noise conversion process. The spectra of both the modified and unmodified oscillators are shown in Figure 4.5.

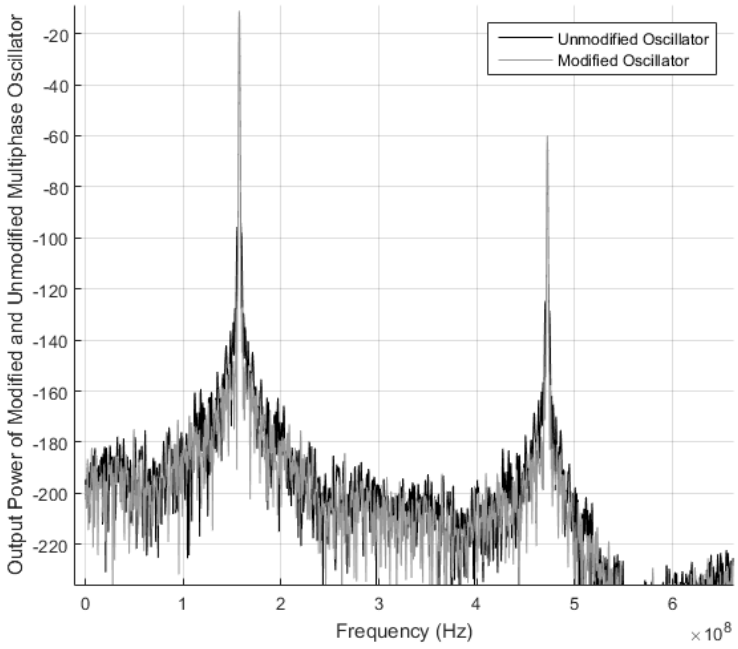

Figure 4.5. Modified and unmodified multiphase oscillator power spectral density, section A.4.

Figure 4.5 shows how the phase noise of the modified oscillator is improved. Once the stable noiseless limit cycle had been estimated, as shown in Figure 4.6, Euler's Method was used to calculate the noise to phase noise conversion function. The implicit Euler's Method was numerically stable and yielded accurate results.

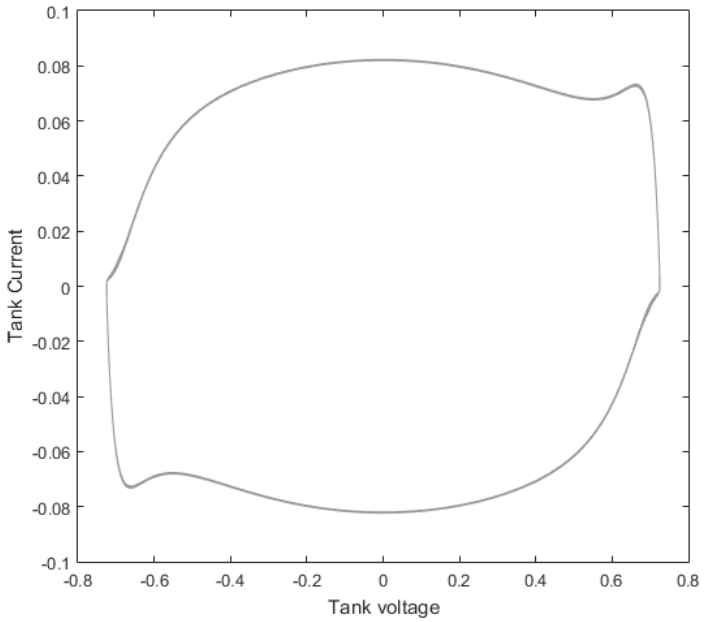

Figure 4.6. Modified and unmodified multiphase oscillator stable limit cycle, section A.4.

The fact that the system had a single Floquet multiplier that must be 1 to ensure a single stable limit cycle also meant that forward techniques would tend to explode and yield results that had no physical meaning. Given the system of equations (4.63) to (4.69), the Jacobian of the system relative to the state variables x_1, x_2, x_3, and x_4 was calculated, where the variables x_3 and x_4 were the partial derivatives of x_1 and x_2 with respect to time.

$$A(t)=\begin{pmatrix} 1 & 0 & 0 & 0 \\ Q.K^2\sinh(Kv_{1D})x_2-\dfrac{1}{C_{tot}L} & Q.K(\cosh(Kv_{1D})) & -2P.A.K^2\tanh(Kv_{2D})(1-\tan^2(Kv_{2D})) & P.A.K(1-\tanh^2(Kv_{2D})) \\ 0 & 0 & 1 & 0 \\ Q.K^2\sinh(Kv_{1D})x_2-\dfrac{1}{C_{tot}L} & Q.K(\cosh(Kv_{1D})) & 2P.A.K^2\tanh(Kv_{2D})(1-\tan^2(Kv_{2D})) & P.A.K(\tanh^2(Kv_{2D})-1) \end{pmatrix} \quad (4.80)$$

The time domain solution for the multiphase oscillator produced the solution to state transition matrix and the solution to the first derivative of the system in respect of time. The Jacobian of

the system was calculated *a priori*. The next step in calculating the oscillator's phase noise was to solve the adjoint system. Then, with scaling defined by the algorithm in section 2.2.1.5, the noise modulating function for the oscillator over a period of oscillation was calculated and is shown in Figure 4.7.

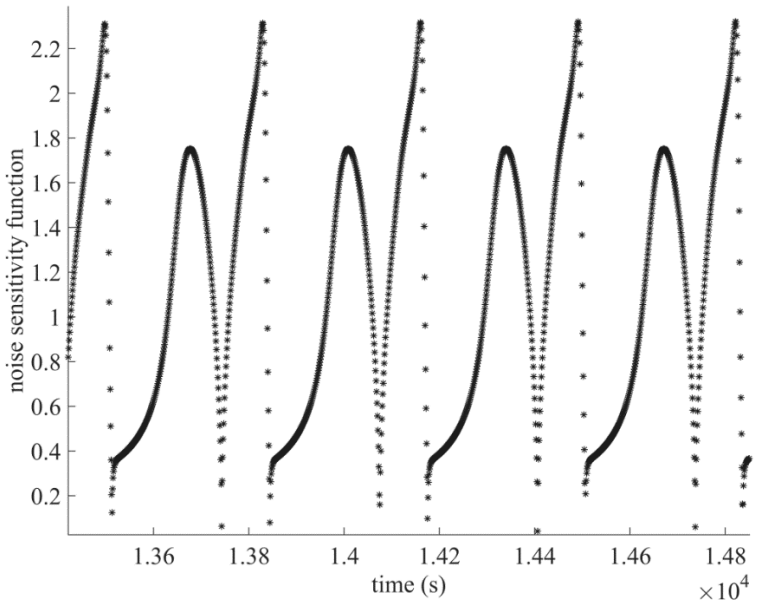

Figure 4.7. Modified sensitivity function for the oscillator, section A.5.

Figure 4.7 demonstrates how noise components injected into the tank circuit were translated into phase noise. The current noise components had to be mapped to the output node of the circuit. The tank voltages and currents were given as the difference between the two tank circuits in a single output of a phase oscillating structure. The current injection into the tank circuit occurred at the points where the function tended to zero, and therefore minimised the oscillator's phase noise. The forcing currents from the quadrature oscillator were forced in at the second zero point of the ISF through the period of the oscillation. Figure 4.8 shows the noise to phase noise translation with the current injection into the tank circuit overlaid. Figure 4.8 shows that the current injection into the tank circuit was optimised in terms of the noise to phase noise conversion time in the stable limit cycle. The base spreading resistance was approximately 300 Ω. The total contributions of the main noise components are provided in Table 4.1.

It is demonstrated that the phase noise performance of a Colpitts oscillator can be significantly improved by making the proposed changes to the oscillator. Therefore, the oscillator's FoM was improved even further. If it is considered that in most cases the collector current will account

for at least 70% of the phase noise, it is clear that the methods proposed in this study will improve phase noise performance, for example, from a given level of -106 dBc/Hz to -113 dBc/Hz.

Figure 4.8. The normalised modified and unmodified multiphase oscillator, section A.5.

Table 4.1. Table comparing CMOS single and differential oscillator performance.

Noise source	Relative contribution
Collector current	72%
Cross-coupled current	8%
Base spreading resistance	11%
Other	9%

This improvement is less than what would actually be achieved, as improvements in the overall limit cycle were not factored into the previous example. The FoM would be improved further

by another 9 dB by the change in the power consumption relating to an average increase in performance of 16 dB.

4.1.4 Conclusion

The characteristics that define an oscillator, place an inherent limit on the achievable phase noise performance in a given technology node. The quality factor of the tank circuit, both loaded and unloaded, is the most significant factor in an oscillator's phase noise performance, given that the oscillator is set at the optimum point. The literature review presents factors that show that there is an optimum point in terms of phase noise performance of the oscillator. This point occurs when the oscillator is on the verge of the voltage-limited regime. This point scales moderately well into the complementary and multiphase oscillators. This study identifies the main limitations to improving phase noise performance. The goal of the study was to target these limitations in an attempt to decouple several compromises associated with the oscillator design.

This chapter identified the noise modulating function of an oscillator, and presented a procedure to calculate it. This lead to the conclusion that if the current injected into the tank circuit can be controlled over an oscillation cycle, then the phase noise performance can be improved. The starting structure of the multiphase oscillator was based on the Colpitts oscillator, which naturally has a structure that minimises the noise-modulating function of the oscillator. One of the more limiting factors for this given oscillator structure is that the start-up current required to begin oscillation is larger than the optimum current for minimum phase noise performance. The oscillator is biased further into the voltage-limiting regime than what optimum phase noise performance dictates.

The modification to the oscillator structure removed the start-up current limitation with the open loop gain of the oscillator improved by a significant margin. Decoupling the start-up current and the tank injection current resulted in a reduction of the bias current by a factor of almost 10. This metric was used in the FoM of the oscillator and therefore significantly improved this measure for the oscillator. The second result of the modification was that the shape of the oscillator's noise modulating function was improved, resulting in a lower noise to phase noise conversion characteristic. The complementary currents were injected out of phase to each other and were both at the optimum point in terms of the noise-modulating function with respect to

the tank circuits. The cross-coupled currents that forced the oscillator into quadrature oscillation were not injected into the tank circuit at the optimal point. The requirement for quadrature oscillation limited the point in the oscillation period when the current was injected into the particular tank circuit.

The magnitude of the injected current is the only degree of freedom that is available, but changing this parameter will limit the phase accuracy of the quadrature oscillators. The tail current of the cross-coupling coupled pair will then define the noise characteristic of the cross-coupled currents. The noise modulating function is naturally at a minimum for the cross-coupling currents and does not significantly increase the phase noise performance in a significant way. The quadrature oscillator would reduce the loaded tank quality; however, this dependency is eliminated in the modified oscillator structure. The base spreading resistance of the voltage-controlled transistor will dominate the noise profile of the oscillator, and is constant throughout the oscillation period, only modulated by the noise transfer function. This process-dependent parameter must be controlled in order to achieve optimal phase noise performance from a given oscillator; thus, transistor sizing is an important factor

CHAPTER 5 MEASUREMENT RESULTS

5.1 CHAPTER OVERVIEW

This chapter discusses the relevant aspects specific to each oscillator in considering the frequency domain transfer function of a bipolar junction transistor, as well as the results yielded in this study. Furthermore, this chapter presents the characteristic assumptions regarding the typical optimal performance of a single-phase oscillator. The results are extrapolated to the multiphase oscillator version. Finally, the specific separation between the classical approach and the improvements presented in this work are discussed.

5.1.1 Characterising the single-phase Colpitts oscillator

The analysis began with a standard Colpitts oscillator, shown in Figure 5.1.

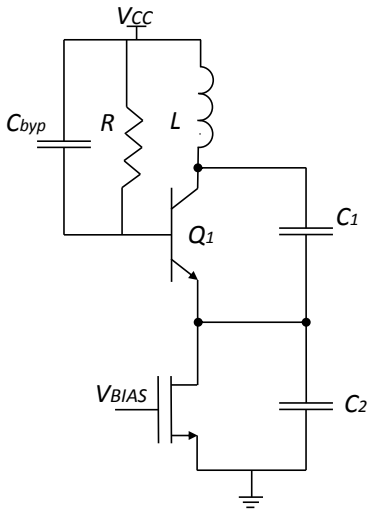

Figure 5.1. Simplified Colpitts oscillator.

Figure 5.1 shows the basic Colpitts oscillator, excluding the bias circuitry. The input impedance looking into the emitter of Q_1 was characterised. The feedback loop was broken, as shown in Figure 5.2. The *h*-parameters of the common base transistor were derived. The *h*-parameters were then:

$$h \simeq \begin{vmatrix} \dfrac{z_\pi r_0}{g_m z_\pi r_0 + r_0 + z_\pi} & \dfrac{z_\pi}{r_0 + z_\pi + g_m z_\pi r_0} \\ \dfrac{g_m z_\pi + \dfrac{1}{r_0}}{g_m z_\pi + 1 + \dfrac{z_\pi}{r_0}} & \left(\dfrac{1}{r_0} + \dfrac{1}{z_\mu}\right)^{-1} \end{vmatrix}. \quad (5.1)$$

From (5.1), using the circuit layout shown in Figure 5.2, the system was converted to Z-parameters and the input impedance into the network was calculated.

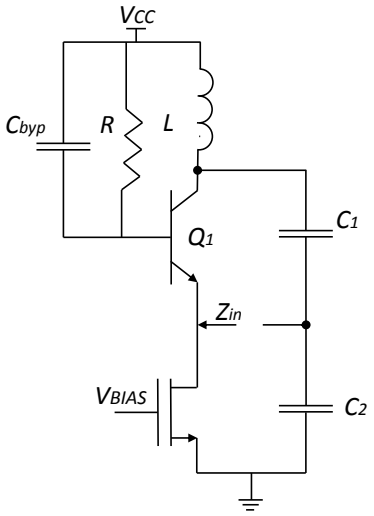

Figure 5.2. Model to calculate impedance seen by the tank circuit.

Figure 5.2 shows the circuit-level representation of how the impedance Z_{in} was calculated. The small-signal analysis was performed on Figure 5.3:

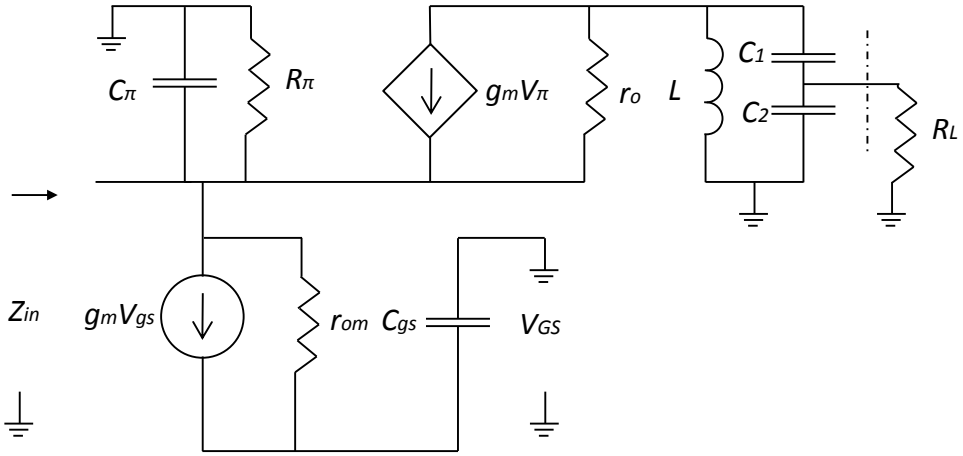

Figure 5.3. Small-signal model for an oscillator.

Figure 5.3 then formed the basis for the relative impedance calculations used to determine the relative *h*-parameters. Then to determine the input and output impedance, Figure 5.4 was considered:

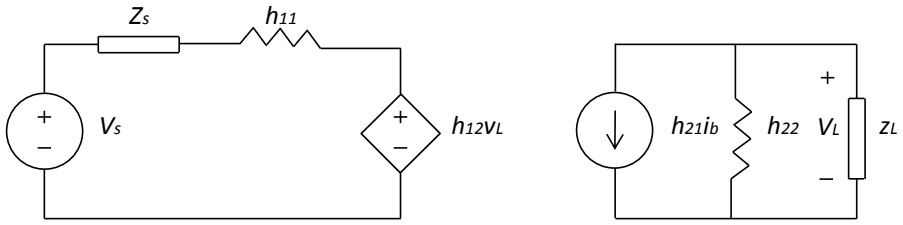

Figure 5.4. *h*-parameter network with relative parameters given in (5.1).

The output impedance of the current source in Figure 5.4 was excluded, as it would not significantly change the values derived next.

$$\frac{V_L}{V_S} = -\frac{Z_L h_{21} h_{22}}{h_{22} + Z_L - h_{22} h_{21} h_{12} Z_L}. \tag{5.2}$$

From (5.2), if h_{12} is very small, then the voltage gain is approximately:

$$\frac{V_L}{V_S} \simeq -h_{21}\left(Z_L \,//\, h_{22}\right). \tag{5.3}$$

Including all the terms of (5.2) resulted in the input impedance having the potential to become inductive at very high frequencies, but for selected transistor geometries this was not the case for the oscillators that were considered. From the input impedance of Figure 5.4, the following was defined:

$$\frac{V_L}{V_S} \simeq -h_{21}\left(\frac{h_{11}}{h_{11} + Z_S}\right)\left(Z_L \,//\, h_{22}\right). \tag{5.4}$$

Although the equations described previously define the start-up gain required to begin and sustain oscillations, the limiting behaviour of the oscillator would cause the current gain to decrease, as the feedback voltage becomes larger than the typical small-signal assumption. It

therefore became necessary to consider the feedback ratio and bias currents that would ensure oscillation. Small-signal analysis was used to determine the following equation:

$$I_C \geq \frac{V_T n^2}{Z_T (1-n)}, \tag{5.5}$$

where I_C was the minimum bias current required to ensure oscillation would begin. The equation was then parameterised to find an acceptable region for n, given the quality factor of the used tank circuit. The following equation was defined:

$$0.026n^2 + 0.4575n - 0.4575 > 0. \tag{5.6}$$

This set a value for n of greater than 18. The feedback ratio was naturally interdependent on the selected bias current. This natural amplitude limiting caused the oscillation amplitude to stabilise at a certain level. A more thorough determination of the impedance of the transistors used in this work is given in Addendum A.1. Addendum A.2 provides a more analytical approach to determining the oscillation amplitude.

The single-phase oscillator was modelled using two separate methods. The first was the shooting balance method. This predicted the oscillation amplitude and frequency. A MATLAB script that solved the single-phase oscillator is given in Addendum A.1. The sensitivity of the oscillation frequency and amplitude to circuit parameters was investigated by varying speic parameters within the system in section A.2. Typically, at this point, to estimate the amplitude of oscillation, it was necessary to assume that the feedback network did not significantly load the tank circuit and describe functions were used to predict the large signal current gain. The single-phase oscillator realised in a 0.13 µm BiCMOS process is shown in Figure 5.5.

The bias currents were set by an external feedback resistor and mirrored to the active device within the oscillator in Figure 5.5. The bias currents were set to 1 mA and the output of the oscillator was measured. This study does not present measurements of oscillations above -28 dBm. The suspected reason for the failure to gather data successfully in the case of these oscillations was a poor output matching network, due to incorrect bonding on the output. The

original intention of the study was to use a G-S-G probe with a 50 Ω input characteristic impedance to measure the output of the oscillator. This was later altered, and a PCB was made

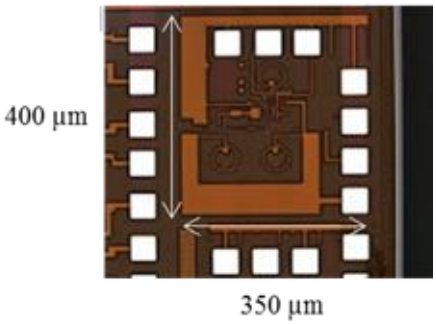

Figure 5.5. Photograph of the single-phase Colpitts oscillator.

to deliver power to an output port. An additional inductance of approximately 1 nH was added in series with the pad. This impedance required an external matching network. There was an error in the layout and an output signal pad went missing; this was probably the cause of no measurable output power.

5.1.1.1 Characterising the multiphase oscillator

The limiting nature of the oscillator defines the maximum oscillation amplitude; the amplitude is either voltage-limited or current-limited. In the previous section, the minimum start-up requirements were defined for the specific tank quality circuit that was selected in the implementation of the oscillator. The transistor will exit the forward-active region and inject current into the collector from the base. The oscillator must be biased at the point where the oscillation amplitude is limited by the large signal current gain in the active transistor. Therefore, there is a fundamental limitation in the achievable performance of the given oscillator independent of the bias current, dependent only on the feedback ratio and the unloaded quality factor of the tank circuit.

The independence from the bias current is only partially true, and the oscillations will potentially not begin if the bias current is not sufficiently large. The feedback ratio thus plays two important roles, setting the start-up gain for the circuit as well as defining the maximum achievable current limited voltage generated across the tank circuit. The proposed modification to improve the oscillator's phase noise performance was not considered. The multiphase oscillator was

modelled using the script shown in Addendum A.4. The maximum bias voltage was set by the technology process node and was not a targetable parameter for the increase in phase noise performance for the multiphase oscillator. The maximum target voltage for the system was set to 1.2 V peak to peak. This then also defined the maximum achievable tank circuit power and indirectly the maximum achievable phase noise performance.

An additional common emitter stage was introduced to the oscillator in an attempt to increase impedance, as seen by the tank circuit. The output impedance of the amplifier is considered:

$$Z_O = \frac{Z_{in}\left(Z_\mu + Z_\pi\right) + Z_\mu Z_\pi}{\left(\beta + 1\right) Z_{in} + Z_\pi}. \tag{5.7}$$

The input impedance in this case is the output impedance of the unloaded tank circuit in combination with the active device. The load of the circuit is then the input impedance into the emitter of the active device driving the tank circuit, as shown in Figure 5.3. There is partial isolation between the output and input impedance of the common-base amplifier. However, the collector-emitter capacitance is insufficiently small at the frequency of interest, and the output impedance will decrease. The second point of interest is the loaded input impedance into the common base amplifier. This is defined as:

$$Z_{in} = \frac{Z_\pi Z_\mu}{Z_\pi + Z_\mu} - \frac{\left(\left(g_m + 1/Z_\mu\right)\left(Z_\mu + Z_E\right)\right)}{Z_\mu^2 Z_E}, \tag{5.8}$$

where Z_E refers to the input impedance of the common-base amplifier active device. This shows that at frequencies much smaller than the active device's transition frequency, the input impedance reduces to the typical value of Z_π. This is larger than the impedance into the emitter of the active device. A simultaneous conjugate match between the additional gain stage and the feedback to the oscillator becomes possible. The input impedance is increased trivially by an order of magnitude at the frequency of interest. The small-signal gain of the modified circuit is then given approximately as:

$$A_v \approx \frac{1}{n}\left(g_{m2} Z_T \,//\, n^2 Z_\pi\right). \tag{5.9}$$

This suggests that the gain achieved was only through the ratio of the bias current in the second active gain stage compared to that of the active device in the oscillator. Even if the current had been maintained, the gain increased by a factor of nearly two just from the impedance transformation. The current can nevertheless be altered through the active device and still achieve acceptable start-up gain, keeping the total current consumption within the system in the same order of magnitude.

The common-base transistor's bias current was reduced by a factor of 8.5 while keeping the common-emitter transistor biased at 1 mA. Then, referring to section 4.1.3, the rest of the circuits' characteristics are evident. The multiphase oscillator was implemented in a 0.13 µm process. Figure 5.6 shows a photo of the core of the multiphase oscillator:

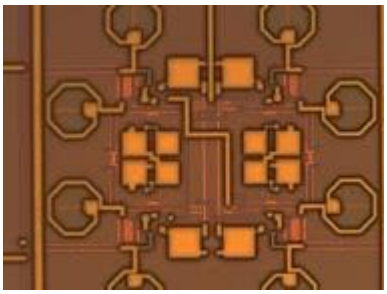

Figure 5.6. Photograph of the core of the multiphase oscillator.

Figure 5.6 demonstrates the interconnection of the additional buffering and cross-coupling tank circuits. The oscillator was buffered to the output ports and the intention was to measure the output using a G-S-G probe, as shown in Figure 5.7.

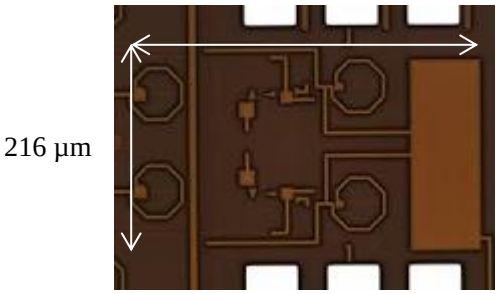

Figure 5.7. Photograph of the buffer circuitry and biasing pads for the multiphase oscillator.

Figure 5.7 demonstrates the buffer circuitry for the improved multiphase oscillator. The second portion of the oscillator buffer circuitry is shown in Figure 5.8.

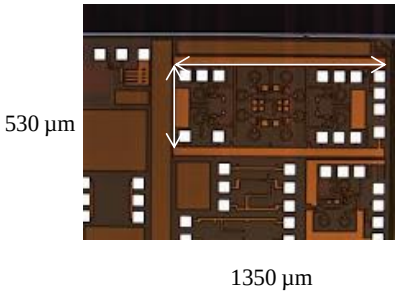

Figure 5.8. Photograph of the buffer circuitry; a missing source pad is clearly visible on the left towards the centre of the photograph

Figure 5.8 shows how the multiphase oscillator was significantly more difficult to lay out and measure than the single-phase oscillator. There was a severe problem with the final submitted layout for the multiphase oscillator. The S pin of the G-S-G pin of the output network a`s missing from one of the multiphase oscillator outputs. The pad went missing in the flattening of the layout into the final layout for submission. The original intention for the oscillator was to measure the performance using a four-port G-S-G probe, which was not practical.

In order to measure the oscillator, the output of two of the buffers was bonded onto a PCB. The bias circuitry was set on a chip with an external resistor used to control current biasing within the oscillator. The bias voltages were measured using a standard multimeter, and were within the design tolerances. The oscillation of the multiphase oscillator was not measurable. The problem was not specifically isolated. The most probable cause of the failure was either the asymmetrical loading effects of the measurement circuitry, or poor output matching of the system.

Figure 5.9 is the floor plan for the IC. The IC is part of a MPW, with the specific oscillator circuits being placed in the top right-hand corner of the IC. The IC was completed as part of the requirements for the determination of the hypothesis. The IC required external connections to enable the measurement of the various devices that were tested; these connections are shown in Figure 5.11. Figure 5.12 shows the IC with only relevant circuitry drawn. The IC was placed on an alumina substrate with a dielectric constant of 9.8. The completed PCB is shown in Figure 5.12, with the complete metal enclosure and external power connections shown in Figure 5.13. The transmission lines on the PCB were characterised, and are shown in Figure 5.14.

Although the measurements were not able to characterise the phase noise improvements from the proposed circuit-level modifications, a significant amount of work was completed in order to quantify phase noise accurately and in the best possible way. All the work presented confirms the initial heuristic selection of the oscillator structure as the starting point of the multiphase oscillator. It is through circuit-level modifications that the optimal structure for a multiphase oscillator that yields the lowest possible phase noise measurement for a given supply voltage is realised.

It is unfortunate that the measurements were unable to validate the hypothesis conclusively. The IC was manufactured as part of an MPW. The prototyping is costly, and runs at US $6 300.00 per mm-squared with a minimum fabrication cost of $5 040. For a single die of the multiphase oscillator it would cost $12 600.00. The project was shared with three other students and a single design file was submitted to the manufacturer for the group. By way of the MOSIS Educational Programme (MEP), a once-off sponsorship was received. The file is a GDSII file, which is a flattened grouping of each of the students' layout. It is likely that during the joining of the groups' GDSII file an error occurred and pads went missing from the multiphase oscillator. Some metallisation also went missing in the global file submitted to the manufacturer. The project yielded 20 raw die, which were shared between three students. Five raw die were available for measuring the multiphase oscillator. A wafer probing station was to be used to bias and measure the multiphase oscillator. Unfortunately the required setup was not achievable with the equipment that was available. Given challenges with measurement equipment, alternative measurement arrangements were made. The available measurement equipment required a cable assembly and the respective port connections to the circuit. The off-chip measurements required additional matching networks to account for unintended bond wires. The IC took four months to manufacture. The possibility of repeating the prototyping was thus not possible in view of the prohibitive cost, once-off MEP sponsorship and complexity of the manufacturing. The raw die was bonded directly to an aluminium substrate PCB. This PCB was manufactured by a third party and took several months to complete. The manufacturing was also sponsored through SAAB Electronic Defence Systems. The wire-bonding requires special facilities, and was an expensive and time-consuming exercise as well. Because of budget constraints only a single PCB and casing were manufactured. The measurement equipment was only available for a few hours at the CSIR. Because of limited access to the measurement equipment, no meaningful oscillations were observed. The bias current was at the correct level. The MPW projects are

scheduled three times a year; however, only one of the manufacturing runs had all the metal layers the process offers available for use. This resulted in only one process run per year being available to manufacture the IC. In a typical high-speed circuit two or three prototype runs are not unusual and given the typical time delays involved throughout the entire project, this can easily run over three or more years. The sound mathematical work that is presented unequivocally proves the validity of the theory. Furthermore, the IC prototyping occurs in the United States, with new restrictions imposed on exportability, as the devices may be considered for usage in the military.

Figure 5.9 shows the floor plan of the joint IC.

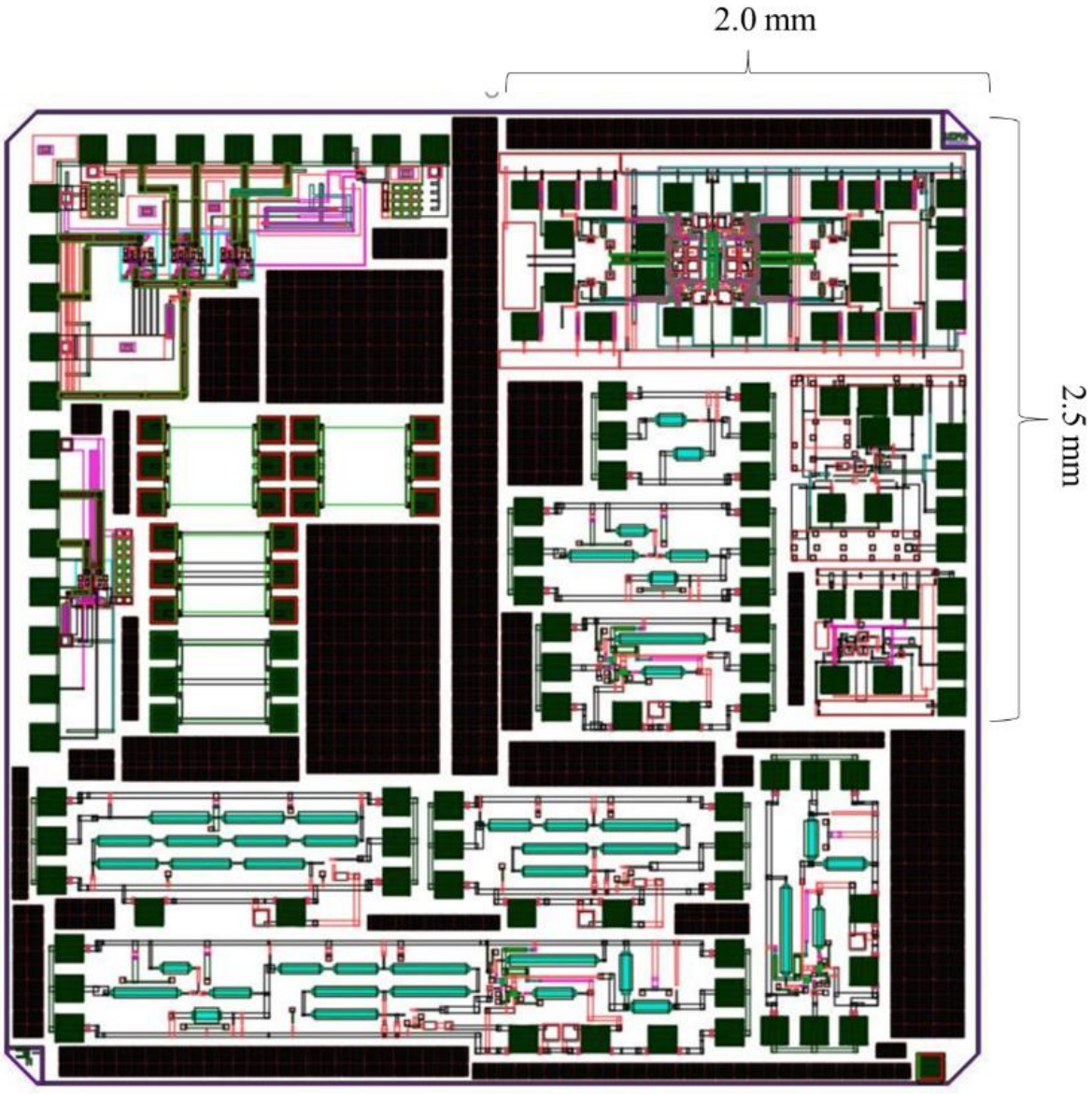

Figure 5.9. Floor planning of the shared MPW run IC (4 mm × 4 mm).

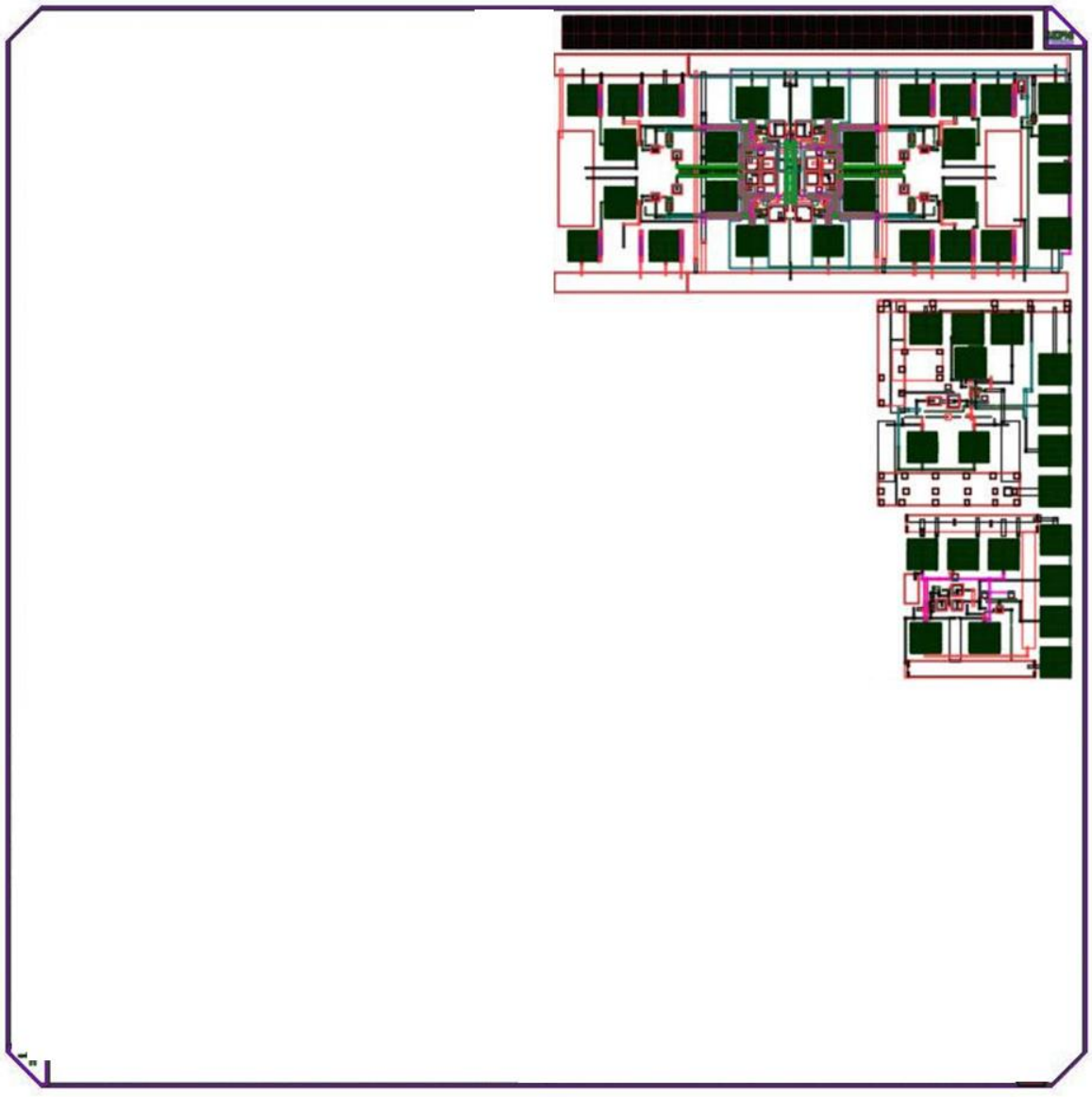

Figure 5.10. Floor planning of only relevant section of the IC (4 mm × 4 mm).

Figure 5.10 shows the relevant sections of the multiphase oscillator.

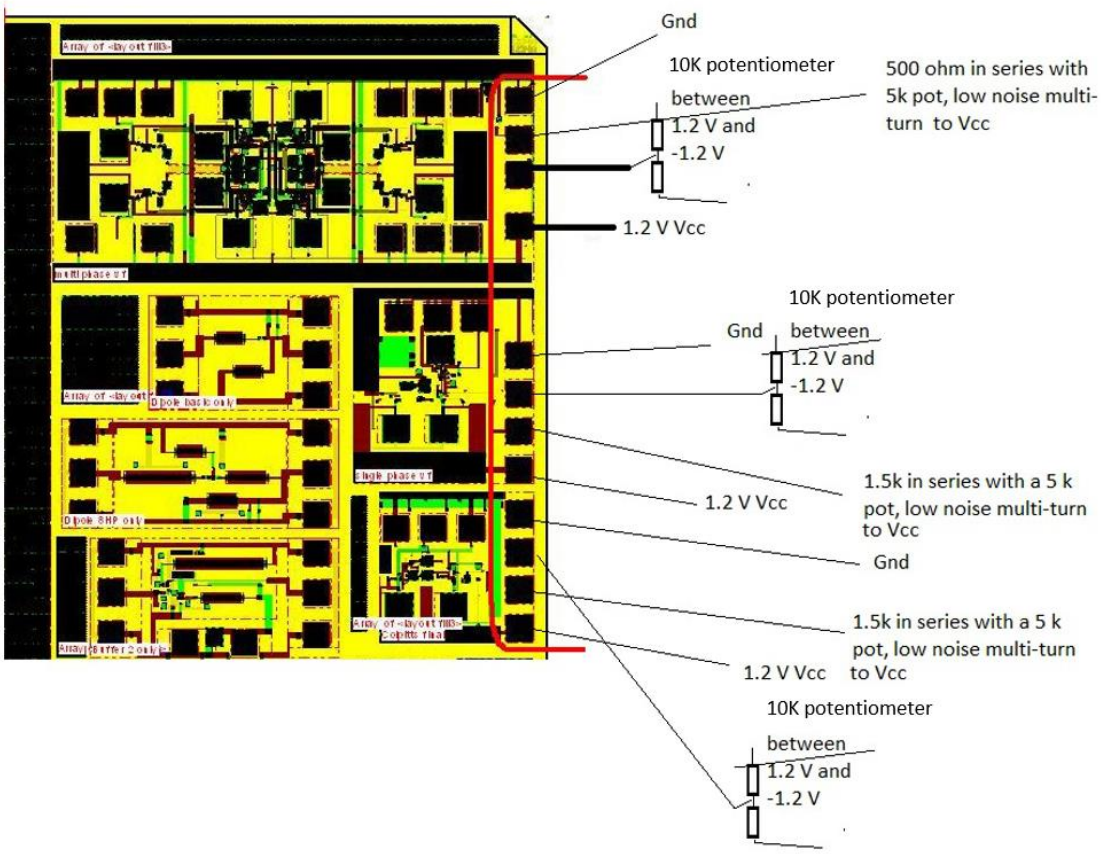

Figure 5.11. Image of the physical connections of the device under test (DUT) to the PCB.

Figure 5.11 shows how the different circuit components were connected for measurement.

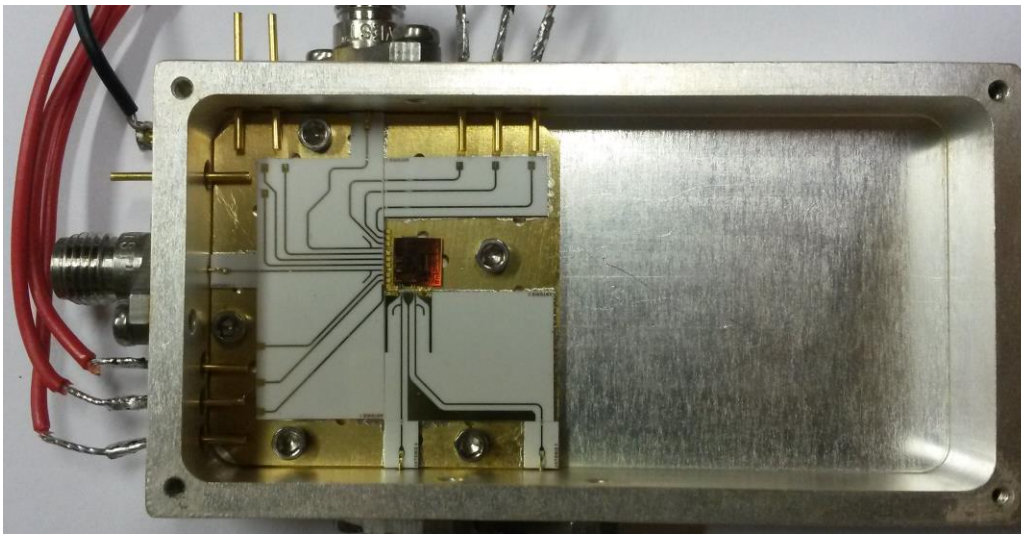

Figure 5.12. Printed circuit board with the DUT placed at the centre.

Figure 5.12 shows a photograph of the physical realisation of Figure 5.11.

Figure 5.13. Printed circuit board enclosed in the metal casing.

Figure 5.13 shows a photograph of the closed measurement device.

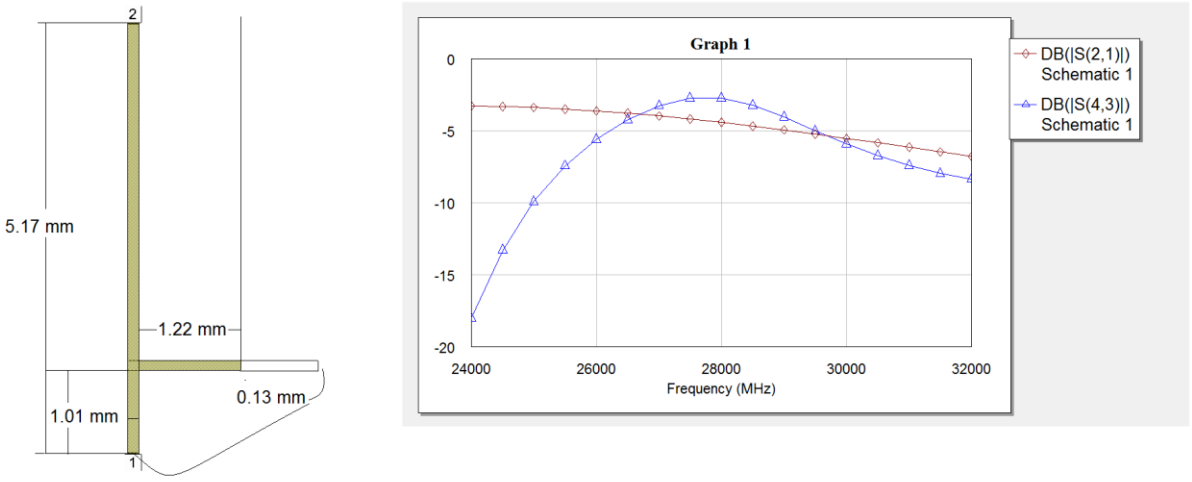

Figure 5.14. Analysis of PCB transmission lines.

Figure 5.14 shows the simulation results of the matched transmission line for the measurement of the output of the oscillator.

5.1.2 Conclusion

The degree of difficulty in the measurement setup of the multiphase oscillator proved to be significantly high. The oscillator is a four-port device and direct probing was not possible, as asymmetrical loading was a problem. The phase measurement can be made on any of the four ports, given that each port is properly terminated. The signal pad for one of the four phase outputs of the oscillator was not in the GDS file for IC manufacturing. This resulted in the multiphase oscillator not being measurable. The current consumption of the oscillator was at the expected level, but no oscillations were observable. The different loading and bonding effects, combined with problems such the missing bond pad, resulted in measurements from the device not being usable to draw direct conclusions regarding the hypothesis: oscillation did not begin and phase noise measurements were not possible.

The oscillator's DC biasing conditions were measured to be correct; however, no oscillations were measured from the device, due to the mentioned problems. Although the transmission lines and additional bond wires were considered when designing the output matching networks and measuring ports, the original output goal for the work was to conduct measurements using an on-wafer probe.

The additional expected losses on the output power are reflected in Figure 5.14. The additional power loss, combined with the measurement of a single output port, placed the expected measured power at the oscillation frequency in the region of -20 dBm, which would have made low phase noise measurements very difficult. However, it would still have been possible to characterise the phase noise of the multiphase oscillator with the correct equipment and four-port probing station, which were not available. Because of financial constraints, only a single die was placed on a PCB and measured, extending the uncertainty of the actual cause of failure, which was most likely due to asymmetrical loading of the oscillator buffer circuits caused by the missing signal pad. However, given the simulation results and the mathematical models presented, the work is sound, and given a sufficiently completed layout, with all design components in the manufactured IC, combined with the correct measurement setup, the simulation would yield results very close to those that were predicted.

CHAPTER 6 CONCLUSION

6.1 INTRODUCTION

This chapter summarises the research findings based on the literature, simulations, and experimental work completed in this dissertation. The work is critically evaluated through reflection, and future improvements are discussed.

6.1.1 Critical hypothesis evaluation

The main goal of this body of work was to improve the phase noise performance of a multiphase oscillator. The study investigated the cause of phase noise in an oscillator system. A specific definition has been provided. This study shows significant effort in terms of isolating the factors that may be manipulated to alter an oscillator's phase noise performance. The work makes certain assumptions within these identified factors. The study does not investigate the impact on phase noise performance that component-level improvements would have. This dissertation provides results using an on-chip inductor available in the technology process node. An improvement in the quality factor of the tank circuits' inductor would reduce phase noise proportionally.

There are three main schools of thought regarding phase noise, which are discussed in 2.2.1.5. The current body of work is of general consensus that the approach selected in this work is the most accurate method to predict phase noise performance in an oscillatory system. When calculating phase noise, a non-trivial transfer function regarding noise is derived. This work targeted parameters that would allow these factors to be improved. The approach was mathematically sound and phase noise improvements were demonstrated using an accurate model for the given circuit. By changing certain parameters within the circuit, phase noise was improved. The factors identified are easily verifiable in terms of the improvement of phase noise by altering specific parameters within the model.

The changes, from traditional design methods for oscillators, are heuristically predicted to have certain effects on phase noise performance. The model is able to predict oscillation frequency

as well as amplitude when compared to known oscillators in literature. Although the measurements were unable to verify the model, no measurable oscillations were achieved; the proposed modifications were demonstrated with a rigorous mathematical model to improve the phase noise performance of the oscillator. The proposed modifications offer significant improvements in the FoM of both the quadrature and multiphase oscillators. Therefore, the original hypothesis is successfully verified.

6.1.2 Challenges and limitations

The most significant challenge regarding this work was the fact that the multiphase oscillator could not be measured. The financial, time, and technical constraints encountered were large. Measurement equipment was only available for a limited amount of time. The layout of the circuit was not completed with sufficient rigour, in part because of time constraints. The project was part of an MWP, which resulted in significant time delays. IC manufacturing was limited to a single run a year. This caused each iteration to add a year of delay to the project. Because of the structure of the feedback network in the modified multiphase oscillator, the circuit structure size became as large as the electrical length of the oscillation output. This resulted in a layout that was particularly complicated and required the assistance of an experienced engineer. The specific layout challenges were beyond the scope of the research and not part of the goal of the study, but were prohibitively difficult to overcome. There were also problems with the GDSII file that was submitted, which made measurements nearly impossible. The work also suffered from lack of a control oscillator against which phase noise could have been compared. The transmission line effects between the various parts of the multiphase oscillator were not taken into consideration, and proved to severely affect the operation of the oscillator. The measurement requirement and setup were challenging and advanced measurement equipment was required. The oscillator's phase noise was targeted for improvement. By changing the quality factor of the inductor, the phase noise performance of the multiphase oscillator would be directly improved by the relative improvement factor. A full characterisation targeting all factors would yield a more optimal multiphase oscillator.

6.1.3 Suggested future work

The multiphase oscillator and its performance are a complex system to design and measure. To characterise the multiphase oscillator more accurately, it would have be more instructive and

would lead to more accurate conclusions to enable the of use the multiphase oscillator in a modulation system where the error vector magnitude could be measured on a higher order constellation and phase noise could be calculated from these measurements. This would allow a more balanced circuit layout and reduce the measurement complexity.

Further improvements should be achieved with passive level component optimisation. The additional parameters and aspects identified, including transformer coupling and tail current shaping, to further improve the slow manifold of the oscillator, should be investigated. Research could be dedicated to improving the specific inductors to achieve even greater phase noise performance.

The work presented here is optimised to the quality factor of the on-chip inductor, and given a larger *Q* inductor, currents could be changed. A transformer-coupled inductor would also allow the output voltage to be increased beyond the supplies of the oscillator, leading to further phase noise improvement.

Finally, tail current shaping to modify the slow manifold of the oscillator would lead to further improvements in the phase noise performance. More specific improvements on this study would be to extend the degree of freedom to which the solution was applied, allowing for optimal phase noise achievable for any specific oscillator configuration.

REFERENCES

[1] D.G. Crnkovic, "Theory of science," Mälardalen Real-Time Research Centre, Mälardalen University, Technical Report (ISRN) MDH-MRTC-64/2001-1-SE, September 2001.

[2] D. Ma, F.F. Dai, R.C. Jaeger, J.D. Irwin, "An X- and Ku- band wideband recursive receiver MMIC with gain-reuse," *IEEE Journal of Solid-State Circuits*, vol. 46, no. 3, pp. 562-571, March 2011.

[3] A. Mazzanti, M. Sosio, M. Repossi, F. Svelto, "A 24 GHz subharmonic direct conversion receiver in 65 nm CMOS", *IEEE Transactions Circuits and Systems - I*, vol. 58, no. 1, pp. 88-97, January 2011.

[4] N. Nouir, J.F. Buckwalter, "A 45-GHz rotary-wave voltage-controlled oscillator," *IEEE Transactions on Microwave Theory and Techniques*, vol. 99, no. 2, pp. 383-392, February 2011.

[5] P.R. Gray, P.J. Hurst, S.H. Lewis, R.G. Meyer, "Noise in integrated circuits," in *Analysis and Design of Analog Integrated Circuits* 4th edition, vol. 1. New York: John Wiley & Sons, 2009, pp. 748-756.

[6] A. Hajimiri, T.H. Lee, "A general theory of phase noise in electrical oscillators," *IEEE Journal of Solid-State Circuits*, vol. 33, no. 2, pp. 179-194, February 1998.

[7] D. George, S. Sinha, "Phase noise analysis for a mm-wave VCO configuration," *Microwave and Optical Technology Letters*, vol. 55, no. 2, pp. 290-295, February 2013.

[8] A. Tasić, W.A. Serdijn, J.R. Long, "Spectral analysis of phase noise in bipolar LC-oscillators – theory, verification, and design", *IEEE Transactions on Circuits and Systems I: Regular Papers*, vol. 57, no. 4, pp. 737-751, April 2010.

[9] K.K. Clarke, D.T. Hess, "Nonlinear controlled sources," in *Communication Circuits: Analysis and Design* 2nd edition, vol. 1, London: Krieger Publishing Company, pp. 114-120, January 1994.

[10] Z. Deng, A.M. Niknejad, "A 4-port inductor-based VCO coupling method for phase noise reduction," *IEEE Journal of Solid-State Circuits*, vol. 46, no. 8, pp. 1772-1781, August 2011.

[11] H-Y. Chang, Y-T. Chiu, "K-band CMOS differential and quadrature voltage-controlled oscillators for low phase-noise and low-power applications," *IEEE Transactions on Microwave Theory and Techniques*, vol. 60, no. 1, pp. 46-59, January 2012.

[12] A. Demir, A. Mehrotra, J. Roychowdhury, "Phase noise in oscillators: a unifying theory and numerical methods for characterisation," *IEEE Transactions on Circuits and Systems I: Fundamental Theory and Applications*, vol. 49, no. 5, pp. 655-674, May 2000.

[13] D.B. Leeson, "A simple model of feedback oscillators noise spectrum," *Proceedings of the IEEE*, vol. 52, no. 2, pp. 329-330, January 1966.

[14] A. Demir, A. Sangiovanni-Vincentelli, "Analysis and simulation of noise in nonlinear electronic circuits and systems," *Springer*, vol. 425, pp. 163-213, January 1998.

[15] A. Mehrotra, "Simulation and modelling techniques for noise in radio frequency integrated circuits." Ph.D. dissertation, Dept. Elect. Eng. Univ. California, Berkeley, 1999.

[16] C.W. Gardiner. *Handbook of Stochastic Methods for Physics, Chemistry, and the Natural Sciences* 2nd edition, volume 13 of Springer series in synergetics. Berlin: Springer-Verlag, 1983, 4.1, 4.1, 4.1.2, 4.1.2.

[17] J.W. Lambrechts, S. Sinha, "Phase noise analysis of a tail-current shaping technique employed on a BiCMOS voltage controlled oscillator," CAS 2010 Proceedings (International Semiconductor Conference), vol. 2, pp 509-512, October 2010.

[18] H. Risken, *The Fokker-Planck Equation: Methods of Solution and Applications* 2nd edition, volume 18 of Springer series in synergetics. Berlin: Springer-Verlag, Berlin; New York, 1996, 4.1

[19] S.S. Broussev, N.T. Tchamov, "Quality factor analysis for cross-coupled *LC* oscillators using a time-varying root locus," *IEEE Transactions on Circuits and Systems —II: Express Briefs*, vol. 99, no. 99, pp. 1-5, January 2011.

[20] K. Kwok, H.C. Luong, "Ultra-low-voltage high performance CMOS VCOs using transformer feedback," *IEEE Journal of Solid-State Circuits*, vol. 40, no. 3, pp. 652-660, March 2005.

[21] H.C. Chang, "Phase noise in self-injection-locked oscillators – theory and experiment," *IEEE Transactions on Microwave Theory and Techniques*, vol. 51, pp. 1994-1999, September 2003.

[22] S-L. Liu, K-H. Chen, T. Chang, A. Chin, "A low-power K-band CMOS with four-coil transformer feedback," IEEE *Microwave and Wireless Components*, vol. 20, no. 8, pp. 459-461, August 2010.

[23] C-K. Hsieh, K-Y. Kao, J.R. Tseng, K.-Y. Lin, "A *K*-band CMOS low power modified Colpitts VCO using transformer feedback," in *2008 IEEE MTT-S International Microwave Symposium Digest – MTT 2008*, pp. 1293-1296, June 2009.

[24] C.M. Yang, H.L. Kao, Y.C. Chang, M.T. Chen, H.M. Chang, C.H. Wu, "A low phase noise 20 GHz voltage control oscillator using 0.18-μm CMTOS technology," in

Design and Diagnostic of Electronic Circuits and Systems (DDECS), 2010 IEEE 13th International Symposium on, pp. 185-188, April 2010.

[25] T-Y. Lu, W-Z. Chen, "A 38/114 GHz switched-mode and synchronous lock standing wave oscillator," *IEEE Microwave and Wireless Components Letters*, vol. 21, no. 1, pp. 40-42, January 2011.

[26] X. Li, O.O. Yildirim, W. Zhu, D. Ham, "Phase noise of distributed oscillators," *IEEE Transactions of Microwave Theory and Techniques*, vol. 58, no. 8, pp. 2105-2117, August 2010.

[27] J-J. Kuo, Z-M. Tsai, P-C. Huang, C-C. Chiong, K-Y. Lin, H. Wang, "A wide tuning range voltage controlled oscillator using common-base configuration and inductive feedback," *IEEE Microwave and Wireless Components Letters*, vol. 19, no. 10, pp. 653-655, October 2009.

[28] R. Aparicio, A. Hajimiri, "A noise-shifting differential Colpitts VCO," *IEEE Journal of Solid-State Circuits*, vol. 37, no. 12, pp. 1728-1736, December 2002.

[29] T-P. Wang, "A CMOS Colpitts VCO using negative-conductance boosted technology," *IEEE Transactions on Circuits and Systems —1: Regular Papers*, vol. 58, no. 11, pp. 2623-2635, November 2011.

[30] T-P. Wang, "A K-band low-power Colpitts VCO with voltage-to-current positive-feedback network in 0.18 µm CMOS," *IEEE Microwave and Wireless Components Letters*, vol. 21, no. 4, pp. 218-220, April 2011.

[31] J-C. Chien, L-H. Lu, "Design of wide-tuning-range millimetre-wave CMOS VCO with a standing-wave architecture," *IEEE Journal of Solid-State Circuits*, vol. 42, no. 9, pp. 1942-1952, September 2007.

[32] Z-D. Huang, C-Y. Wu, "The design of double-positive-feedback voltage-controlled oscillator," *IEEE Microwave and Wireless Component Letters*, vol. 21, no. 7, pp. 386-388, July 2011.

[33] T.W. Brown, F. Farhabakhshian, A.G. Roy, T.S. Fiez, K. Mayaram, "A 475 mV, 4.9 GHz enhanced swing differential Colpitts VCO with phase noise of -136 dBc/Hz at a 3 MHz offset frequency," *IEEE Journal of Solid-State Circuits*, vol. 46, no. 8, pp. 1782-1795, August 2011.

[34] F-R. Liao, S-S. Lu, "30 GHz transformer-coupled and reused injection-locked VCO/divider in 0.13 µm CMOS process," *IET Electronics Letters*, vol. 44, no. 10, pp. 625-626, January 2006.

[35] N.R. Lanka, S.A. Patnaik, R.A. Harjani, "Frequency-hopped quadrature frequency synthesizer in 0.13-µm technology", *IEEE Journal of Solid-State Circuit*, vol. 46, no. 9, pp. 2021-2032, September 2011.

[36] H. Ghonoodi, H.M. Naimi, "A phase and amplitude tuneable quadrature *LC* oscillator: analysis and design," IEEE *Transactions on Circuits and Systems – 1: Regular Papers*, vol. 58, no. 4, pp. 677-689, April 2011.

[37] L. Romanò, S. Levantino, C. Samori, A.L. Lacaita, "Multiphase *LC* oscillators," *IEEE Transactions on Circuits and Systems 1: Regular Papers*, vol. 53, pp. 1579-1588, July 2006.

[38] A. Mazzanti, F. Svelto, P. Andreani, "On the amplitude and phase errors of quadrature LC-tank CMOS oscillators," *IEEE Journal of Solid-State Circuits*, vol. 41, no. 6, pp. 1305-1313, June 2006.

[39] S. Rong, H.C. Luong, "Analysis and design of transformer-based dual-band VCO for software-defined radios," *IEEE Transactions on Circuits and Systems – 1: Regular Papers*, vol. 59, no. 3, pp. 1-15, March 2012.

[40] S.I.J. Gierkink, S. Levantino, R.C. Frye, C. Samori, V. Boccuzzi, "A low-phase-noise 5-GHz CMOS quadrature VCO using superharmonic coupling," *IEEE Journal of Solid-State Circuits*, vol. 38, no. 7, pp 1148-1154, July 2003.

[41] A. Buonomo, M.P. Kennedy, A.L. Schiavo, "On the synchronization condition for superharmonic coupled QVCOs," *IEEE Transactions on Circuits and Systems – 1: Regular Papers*, vol. 58, no. 7, pp. 1637-1646, July 2011.

[42] U. Yodprasit, C.C. Enz, "Realization of a low-voltage and low-power Colpitts quadrature oscillator," in *Circuits and Systems, 2006. ISCAS 2006. Proceedings. 2006 IEEE International Symposium*, pp. 4289-4292, December 2006.

[43] U. Decanis, A. Ghilioni, E. Monaco, A. Mazzanti, F. Svelto, "A low-noise quadrature VCO based on magnetically coupled resonators and a wideband frequency divider at millimeter waves," *IEEE Journal of Solid-State Circuits*, vol. 46, no. 12, pp. 2943-2955, December 2011.

[44] A.C. Alberts, S. Sinha, "An optimized multiphase oscillator with harmonic balance analysis for frequency amplitude prediction," *Radioelektronika (RADIOELEKTRONIKA)*, April 16-17, 2013, IEEE.

ADDENDUM A: MATLAB CODE FOR DIPOLE MODELLING

A.1 OSCILLATOR IMPEDANCE

The impedance into the different ports within the oscillators is plotted with the following MATLAB script.

```
Freq = 10000000:10000:15*10^9;
55
Z1 = 2*pi()*j.*Freq*10^-9+20;
Z2 = 1./(j*2*pi().*Freq*40*10^-12);
Z3 = j.*2*pi().*Freq*10^-9*1.5+10;
Z4 = 1./(j.*Freq.*2*pi()*10^-12*0.005);
Z5 = 2*pi()*j.*Freq*10^-9;
Zin = abs(Z1+(Z4.^-1+(Z2.^-1+Z3.^-1)).^-1+Z5);
Cur=1./Zin.*(abs(Z2)./abs(Z3+Z2)).*abs(Z4./(Z4+(1./Z2+1./Z3).^-1));
plot((Freq),(abs(Z1)));
figure
plot(log10(Freq),20*log10(real(Cur)),'r-');
Freq = 10000000:100:10^9*5;
Zin = abs(j*2*pi.*Freq*10^-9+(1./(1./(j.*Freq*2*pi()*12*10^-
12)+1./(j*2*pi()*2.5*10^-9)+1/22).^(-1)));
plot(Zin);
```

A.2 SINGLE-PHASE SHOOTING BALANCE METHOD

The following MATLAB script iteratively searches for the oscillation frequency and amplitude, using a shooting balance routine.

```
f=0;
s=9800000;
k = 0;
j = 1;
format long
F = 0;
G = 1;
Ts = 1/5600000;
P= 0.8098;
DeltaX=Ts/800000;
R = 3000;
     C = 1*10^-12;
     L = 100*10^-9;

for iterations = 1:1:8
```

```
   g=s;
   T = Ts;
    f = P;
    F=1;
    G=0;
    H = 0;
    J = 1;
    DeltaX = Ts/18000000;
for k = 0:1:18000000
    f = f + DeltaX*g;
    g = g + DeltaX*(-1/C*(1/R-10^-5*exp(-12.85*f)+10^-12*exp(-37*f))*g-
1/L/C*f);
    F = F + DeltaX*G;
    G = G + DeltaX*(-1/C*(1/R-10^-5*exp(-12.85*F)+10^-12*exp(-37*F))*G-
1/L/C*F);
end;

    s = s-(f-P)/F;
  Ts = Ts - (f-P)/g;

end;
Ts

X = zeros(1,500001);
H = zeros(1,500001);
%Ts =1/96128;
x=0;
f=P;
g=s;
DeltaX = 5*Ts/499999;
for k = 0:1:500000
     f = f + DeltaX*g;
    g = g + DeltaX*(-1/C*(1/R-10^-5*exp(-12.85*f)+10^-12*exp(-37*f))*g-
1/L/C*f);
    i(k+1) = 10^-6*exp(-12.35*f)-10^-12*exp(-29*f);
   x = x + DeltaX;

   X(k+1)=x;
    H(k+1) = f;
    G(k+1) = g*Ts;
end;
plot(X,H);
hold on
plot(X,G);
hold on
plot(X,i);
```

A.3 COMPONENT SENSITIVITY ANALYSIS

The following MATLAB script investigates the oscillation frequency amplitude and phase noise as a function of the tank circuit components within the oscillator, and outputs the results to an MS-Excel file.

```
function sensitivity_analysis
```

```
 clc
 FILENAME = ['Inductor 1.xls';'Inductor 2.xls';'Inductor 3.xls';'Inductor
4.xls';'Inductor 5.xls';'Inductor 6.xls';'Inductor 7.xls'];
 FILENAMEPOINTER = 0;
 for Counter = 1:0.5:4
    FILENAMEPOINTER = FILENAMEPOINTER + 1;
 A = 0.000009;
 RES = 0.0000000005;
 t0 = 0:RES:A;
 L = A/RES;
 ZON = Counter;
 [t,x,ZON] = ode15s(@dfile,t0,[0.5;0;0.5;0.1;Counter]);
 figure
 plot(t,x(:,1),'r-');
[MAXX,I] = max((20*log10(abs(fft(RES/A.*x(:,1))))))
 hold on
  Fs = 0:1/RES:(A)/RES.^2;
   figure;
   Fs(I)*RES/A
  plot(Fs.*RES./A,(20*log10(abs(fft(x(:,1))))),'b-');
  XX =[transpose(Fs.*RES./A),20*log10(abs(fft(RES/A.*x(:,1)))),t,x(:,1)];

  inDistTOT = xlsread('TOTALCHANGINGL.xls');
  XXTOT =
[transpose(Fs.*RES./A),20*log10(abs(fft(RES/A.*x(:,1)))),t,x(:,1)];
  XXTOT = [inDistTOT, XXTOT];
  xlswrite('TOTALCHANGINGL.xls', XXTOT);
  xlswrite(FILENAME(FILENAMEPOINTER,:), XX);
inDist = xlsread('CHANGINGL.xls');
TT = [Fs(I)*RES/A,MAXX]
TT = [inDist; TT];
xlswrite('CHANGINGL.xls', TT);
hold on
 end
 function xprime= dfile(t,x)
 xprime = ones(5,1);
 xprime(1) = x(2);
 xprime(2) = (3.15*10^6*exp(-4*x(1))-exp(-40*x(1)))*x(2) -
x(5)*(10^15)*x(1);

function ColpitsFull
 clc
%% FILENAME = ['Inductor 1.xls';'Inductor 2.xls';'Inductor 3.xls';'Inductor
4.xls';'Inductor 5.xls';'Inductor 6.xls';'Inductor 7.xls'];
 %%FILENAMEPOINTER = 0;
%% for Counter = 1:0.5:4
 %%   FILENAMEPOINTER = FILENAMEPOINTER + 1;
 A = 0.000009;
 RES = 0.0000000005;
 t0 = 0:RES:A;
 ZON = 6;
 A = 0.000009;
 [t,x,ZON] = ode23(@dfile,[0,0.000002],[0.1;0.001;0.00003;1.2;0.1;0.95]);
 figure
 plot(x(:,4),'r-');
 figure
  plot(x(:,6),'r-');
  %figure
```

```
  %plot(x(:,5),'r-');
  figure
   plot(x(:,5),'r-');
[MAXX,I] = max((20*log10(abs(fft(RES/A.*x(:,1))))))
 hold on
 %% Fs = 0:1/RES:(A)/RES.^2;
 %  figure;
  % Fs(I)*RES/A
  %plot(Fs.*RES./A,(20*log10(abs(fft(x(:,1))))),'b-');
  %XX =[transpose(Fs.*RES./A),20*log10(abs(fft(RES/A.*x(:,1)))),t,x(:,1)];

%  inDistTOT = xlsread('TOTALCHANGINGL.xls');
 % XXTOT =
[transpose(Fs.*RES./A),20*log10(abs(fft(RES/A.*x(:,1)))),t,x(:,1)];
 % XXTOT = [inDistTOT, XXTOT];
%  xlswrite('TOTALCHANGINGL.xls', XXTOT);
%  xlswrite(FILENAME(FILENAMEPOINTER,:), XX);
%inDist = xlsread('CHANGINGL.xls');unh7 j
%TT = [Fs(I)*RES/A,MAXX]
%TT = [inDist; TT];
%xlswrite('CHANGINGL.xls', TT);
hold on
 end
 function xprime= dfile(t,x)
 Iss = 10^-17;
 xdel1 = zeros(1);
 xdel2 = zeros(1);
 format long
  Vt = 0.0258;
    R = 1588;
    Cb = 2000*10^-32;
   IBIAS = 12.8*10^-3;
 C1 = 100*10^-12;
 C2 = 350 *10^-12;
 L = 150 *10^-9;
 xprime = zeros(6,1);
  Beta = 500;

   Ib = Iss/Beta*(exp((x(6)-x(5))/Vt)-1)+Iss/20*(exp((x(6)-x(4))/Vt)-1)
 Ic = Iss*exp((x(6)-x(5))/Vt)-Iss*exp((x(6)-x(4))/Vt)-Iss/20*(exp((x(6)-
x(4))/Vt)-1);
 xprime(5) = (Ic + Ib)/(C1+C2)-IBIAS/(C1+C2)+C1* xdel2/(C1+C2);
 xprime(4) = xdel1-x(1)/C1+Ic/C1;
 xprime(1) = -1.2/L+x(4)/L-x(1)/15/L;
 xprime(6) = (-(x(6)-1.2)/R-Ib+Ib/100)/Cb;
 Vb = x(6)
 xdel1 = xprime(5);
 xdel2 = xprime(4);
 %Ve = x(5)
 vc = x(4)
 % Dif = C1*(xprime(5)-xprime(4))
 % tot = -x(1) + x(2) + Dif
 %Ic = Iss*exp((x(6)-x(5))/Vt)-Iss*exp((x(6)-x(4))/Vt)-Iss/20*(exp((x(6)-
x(4))/Vt)-1)

 %Iss/Beta*exp((x(6)-x(5))/Vt)+Iss/20*exp((x(6)-x(4))/Vt);
 %Iss*exp((x(6)-x(5))/Vt)-Iss/Beta*exp((x(6)-x(4))/Vt)
%Iss/Beta*exp((x(6)-x(5))/Vt)+Iss/Beta*exp((x(6)-x(4))/Vt)
```

```
end
```

A.4 MULTIPHASE OSCILLATOR SYSTEM ANALYSIS

The following MATLAB script investigates the oscillation frequency, amplitude, and phase noise for the multiphase oscillator. The output of the time domain oscillation is used as input to determine the trajectory of the oscillator to allow the phase noise projection to be calculated in order to predict phase noise performance.

```
figure
% hold on
dataset = csvread('C:\downloadFile\datafile.csv');
DeltaX =10^-12;
y1 = 0.000001;%1/dataset(1,end-1);
y2 = 1/dataset(2,end);
y3= -1/dataset(3,end);
y4= 1/dataset(4,end);

%300.5*(9500*10^1*0.5*cosh(12.8*x(1))-10^-5*cosh(-46*x(1)))*x(2)-
(10^20)*x(1)+3.5*10^9*(1-tanh(12.8*x(3))^2)*x(4);
hold on

for k = 19000:20000 % k =
floor(size(dataset(:,yl1),1)*0.7):1:size(dataset(:,1),1)*1

    y1 = y1 + DeltaX*y2;

    y2 = y2 +
DeltaX*(300.5*(9500*10^1*0.5*12.8*sinh(12.8*dataset(k,5))*dataset(k,6)-
46*dataset(k,6)*(10^-5*sinh(-46*dataset(k,5)))-(10^20)/300.5)*y1+...
                        (300.5*(9500*10^1*0.5*cosh(12.8*dataset(k,5))-10^-
5*cosh(-46*dataset(k,5))))*y2+...
                        (-
2*3.5*10^9*(dataset(k,8)*12.8*tanh(12.8*dataset(k,7))*(1-
tan(12.8*dataset(k,7)).^2)))*y3+...
                        (3.5*10^9*(1-tanh(12.8*dataset(k,7))^2)*y4));
    y3 = y3 + DeltaX*y4;
    y4 = y4 +
DeltaX*(300.5*(9500*10^1*0.5*12.8*sinh(12.8*dataset(k,7))*dataset(k,8)-
46*(10^-5*sinh(-46*dataset(k,7)))*dataset(k,8)-(10^20)/300.5)*y1+...
                        (300.5*(9500*10^1*0.5*cosh(12.8*dataset(k,7))-10^-
5*cosh(-46*dataset(k,7))))*y2+...

(2*3.5*10^9*(dataset(k,6)*12.8*tanh(12.8*dataset(k,5))*(-
1+tan(12.8*dataset(k,5)).^2)))*y3+...
                        (3.5*10^9*(-1+tanh(12.8*dataset(k,5))^2))*y4);
                  % if k > 4740001
                   if mod(k,10) == 1
```

```
%                       plot(k,dataset(k,5)+5,'b*');
                       %plot(k,y2,'b*');
                       plot(k,y1,'r*');
%                       plot(k,dataset(k,6),'c*');
                      plot(k,(300.5*(9500*10^1*0.5*cosh(12.8*dataset(k,5))-
10^-5*cosh(-46*dataset(k,5)))),'m*');

plot(k,300.5*(9500*10^1*0.5*12.8*sinh(12.8*dataset(k,5))*dataset(k,6)-
46*dataset(k,6)*(10^-5*sinh(-46*dataset(k,5)))-(10^20)/300.5),'c*');

plot(k,(2*3.5*10^9*(dataset(k,8)*12.8*tanh(12.8*dataset(k,7))*(1-
tan(12.8*dataset(k,7)).^2))),'k*');
                      plot(k,(3.5*10^9*(-1+tanh(12.8*dataset(k,5))^2)),'y*')
%
plot(k,(300.5*(9500*10^1*0.5*12.8*sinh(12.8*dataset(k,5))*dataset(k,6)-
46*dataset(k,6)*(10^-5*sinh(-46*dataset(k,5)))-(10^20)/300.5)+...
%                         (300.5*(9500*10^1*0.5*cosh(12.8*dataset(k,5))-10^-
5*cosh(-46*dataset(k,5))))+...
%                         (-
2*3.5*10^9*(dataset(k,8)*12.8*tanh(12.8*dataset(k,7))*(1-
tan(12.8*dataset(k,7)).^2)))+...
%                         (3.5*10^9*(1-tanh(12.8*dataset(k,7))^2))),'k*');
                    %
plot(k,(300.5*(9500*10^1*0.5*12.8*sinh(12.8*dataset(k,7))*dataset(k,8)-
46*(10^-5*sinh(-46*dataset(k,7)))*dataset(k,8)-(10^20)/300.5)+...
                   %     (300.5*(9500*10^1*0.5*cosh(12.8*dataset(k,7))-10^-
5*cosh(-46*dataset(k,7))))+...
                   %
(2*3.5*10^9*(dataset(k,6)*12.8*tanh(12.8*dataset(k,5))*(-
1+tan(12.8*dataset(k,5)).^2)))+...
                  %      (3.5*10^9*(-1+tanh(12.8*dataset(k,5))^2))),'y*')
%                       plot(k,dataset(k,5),'r*');
                     % ylim([-10 10]);
              %      end
                     end
end;
```

A.5 MULTIPHASE OSCILLATOR SYSTEM ANALYSIS

This MATLAB script generates the solutions required for the presented algorithm, (2.2.2.1), to calculate phase noise performance in a multiphase oscillator.

```
function  [matrixt matrixc] = multiphase_oscillator
%clc
%et(gca,'FontSize', 18);
 format long
 t1=1*10^-12;
 int=0.000005;
 t0 = 0:t1:int;
 %P = int/t1;
 [t,x] = ode113(@dfile,t0,[0.2;0;0.2;0;0.2;0;0.2;0]);
figure
hold on
 plot(t,x(:,1),'b-');
% plot(t,x(:,3),'r-');
```

```
 %figure
 zz =( 10^-18*(exp(2*37*(-x(:,1)/20))-0.01*exp(37*(-x(:,1)-
1.2)))*exp(37*0.72)).^2;
 zz = zz./max(zz);
 plot(t(floor(4/5*end):1:end),zz(floor(4/5*end):1:end),'color',[0,0,0]);

 figure

hold on

plot(t(floor(4/5*end):1:end),x((floor(4/5*end):1:end),5),'color',[0.6,0.6,0
.6]);
% plot(t,x(:,3),'r-');
 %figure
 zz = 10^-18*(exp(2*37*(-x(:,5)/20))-0.01*exp(37*(-x(:,5)-
1.2)))*exp(37*0.72);
 zz = zz./max(zz);
 plot(t(floor(4/5*end):1:end),zz(floor(4/5*end):1:end),'color',[0,0,0]);

 %plot(t(600000:end),x(600000:end,3),'r-')
 figure
 plot(x(2/3*end:end,1),x(2/3*end:end,2)*10*10^-12,'color',[0.6,0.6,0.6]);
 %hold on
 figure
 hold
 t;
 f = 1/t1*linspace(0,1,int/t1+1);
 size(f);
 point = max(size(x(2/3*end:end,1)));
% size(x((450000:50000)))
 t1 = 1/10^12;
% nois = sqrt(max(size(t))/2)*randn(size(t));
[pxx,f] =
periodogram(x(floor(9.5/10*end):end,1),blackmanharris(length(x(floor(9.5/10
*end):end,1))),length(x(floor(9.5/10*end):end,1)),1/t1,'ms');
matrixt = x(:,1);
matrixc = x(:,5);

[pwrest,idx] = max(pxx);
fprintf('The maximum power occurs at %3.1f Hz\n',f(idx));
fprintf('The power estimate is %2.2f\n',pwrest);
plot(f,20*log10(abs((pxx))),'color',[0,0,0]);
hold on

[pxx2,f2] =
periodogram(x(floor(9.5/10*end):end,5),blackmanharris(length(x(floor(9.5/10
*end):end,5))),length(x(floor(9.5/10*end):end,5)),1/t1,'ms');
[pwrest,idx] = max(pxx2);
fprintf('The maximum power occurs at %3.1f Hz\n',f(idx));
fprintf('The power estimate is %2.2f\n',pwrest);
plot(f2,20*log10(abs((pxx2))),'color',[0.6,0.6,0.6]);

size(f);
%ffted =fft(x(2/3*end:end,1));
%size(ffted(1:end/2+3/2))
%plot(f,20*log10(2/max(size(x(2/3*end:end,1)))*abs(ffted(1:end/2+3/2))))
```

```
%  %plot(t,(x(:,1)).^2+(x(:,3)).^2)
% plot(20*log10(abs(transpose(fft(x(:,1))))));
% hold on
% figure
% phase1 = unwrap(angle((fft(x(:,1)))));
% phase2 = unwrap(angle((fft(x(:,3)))));
% plot((phase1).*180./pi,'g-')
% hold on
%  plot((phase2).*180./pi,'r-')
% hold on
% % t0 = 0:0.00000001:0.00001;
% %  ll = interp1(t0,t,x(:,1));
% %  phase2 = unwrap(angle(transpose(fft(x(:,3)))));
% %  plot(phase*180/pi,'r-')
% %  hold on
% %  plot(10*log10(abs(transpose(fft(x(:,1))))),'r-');
% %  hold on
% figure;
%  plot((angle(transpose(fft(x(:,1))))),'b-');
%  hold on
 %plot((angle(transpose(fft(x(:,1))))./pi()*180),'r-');
 %title('y'''' + yy'' + y = 0, y(0) = 0, y''(0) = 1');
 xlabel('t'), ylabel('y'), grid

 figure;
 hold on

plot(t(floor(9.5/10*end):end),(0.5*x(floor(9.5/10*end):end,1).*x(floor(9.5/
10*end):end,2)*10^-9).^2,'r')
 plot(t(floor(9.5/10*end):end),(3.5*10^9*(1-
tanh(15*x(floor(9.5/10*end):end,3)).^2).*x(floor(9.5/10*end):end,4)*10^-
19).^2,'b')

plot(t(floor(4/5*end):1:end),x((floor(4/5*end):1:end),3).^2,'color',[0.6,0.
6,0.6]);
 xlabel('t'), ylabel('normalized noise currents and noise modulating
function'), grid
 csvwrite('C:\downloadFile\datafile.csv',x);
 csvwrite('C:\downloadFile\time.csv',t);

 function xprime = dfile(t,x)
 xprime = ones(8,1);
 xprime(1) = x(2) + 0*100000*x(1)+normrnd(0,sqrt(4*1.38*10^-
23*300*450))/10^-6;
 xprime(2) = 300.5*(9500*10^1*0.5*cosh(12.4*x(1))-10^-5*cosh(-
48*x(1)))*x(2)-(10^20)*x(1)+3.5*10^9*(1-tanh(12.4*x(3))^2)*x(4);
 xprime(3) = x(4)+ normrnd(0,sqrt(4*1.38*10^-23*300*450)/8.5)/100/10^-
12/10^-7;
 xprime(4) = 300.5*(9500*10^1*0.5*cosh(12.4*x(3))-10^-5*cosh(-
48*x(3)))*x(4)-(10^20)*x(3)+3.5*10^9*(tanh(12.4*x(1))^2-1)*x(2);
 xprime(5) = x(6)+ 0*normrnd(0,sqrt(4*1.38*10^-23*300*450000))/100/10^-
12/10^-8*0;
 xprime(6) = 300.5*(9500*10^1*0.5*cosh(12.4*x(5))-10^-5*cosh(-
48*x(5)))*x(6)-(10^20)*x(5)+3.5*10^9*(1-tanh(12.4*x(7))^2)*x(8) ;
 xprime(7) = x(8)+ 0*normrnd(0,sqrt(4*1.38*10^-23*300*450000))/100/10^-
13/10^-8;
 xprime(8) = 300.5*(9500*10^1*0.5*cosh(12.4*x(7))-10^-5*cosh(-
48*x(7)))*x(8)-(10^20)*x(7)+3.5*10^9*(tanh(12.4*x(5))^2-1)*x(6);
```

```
%   xprime(2) = -5.10*(2*tanh(10*x(1))^2-1)*x(2)-(10^4)*30.3*x(1)+0.10*(1-
tanh(10.0*x(3))^2)*x(4);
%  xprime(3) = x(4);
%  xprime(4) = -5.10*(2*tanh(10*x(3))^2-1)*x(4)-
(10^4)*30.3*x(3)+0.10*(tanh(10.0*x(1))^2-1)*x(2);
%
```